

Ebola Optimization Search Algorithm (EOSA): A new metaheuristic algorithm based on the propagation model of Ebola virus disease

Olaide N. Oyelade¹ and Absalom E. Ezugwu¹

¹School of Mathematics, Statistics, and Computer Science, University of KwaZulu-Natal, King Edward Avenue, Pietermaritzburg Campus, Pietermaritzburg, 3201, KwaZulu-Natal, South Africa

Corresponding authors: Olaide Oyelade (email: oyeladeo@ukzn.ac.za) and Absalom E. Ezugwu (email: ezugwua@ukzn.ac.za).

Abstract

Nature computing describes a field of computing which derives its computational operations from natural phenomenon. A subfield of nature-inspired computing is represented in bio-inspired algorithms, which have evolved with interesting, superior performance and powerful operations capable of solving complex real-world combinatorial optimization problems. These problems span across engineering, medical sciences, and sciences generally. The Ebola virus and the disease in effect tend to randomly move individuals in the population around susceptible, infected, quarantined, hospitalized, recovered, and dead sub-population. Motivated by the effectiveness in propagating the disease through the virus, a new bio-inspired and population-based optimization algorithm is proposed. This paper presents a novel metaheuristic algorithm named Ebola optimization algorithm (EOSA). To correctly achieve this, this study models the propagation mechanism of the Ebola virus disease, emphasising all consistent states of the propagation. The model was further represented using a mathematical model based on first-order differential equations. After that, the combined propagation and mathematical models were adapted for developing the new metaheuristic algorithm. To evaluate the proposed method's performance and capability compared with other optimization methods, the underlying propagation and mathematical models were first investigated to determine how they successfully simulate the EVD. Furthermore, two sets of benchmark functions consisting of forty-seven (47) classical and over thirty (30) constrained IEEE CEC-2017 benchmark functions are investigated numerically. The results indicate that the performance of the proposed algorithm is competitive with other state-of-the-art optimization methods based on scalability analysis, convergence analysis, and sensitivity analysis. Extensive simulation results indicate that the EOSA outperforms other state-of-the-art popular metaheuristic optimization algorithms such as the Particle Swarm Optimization Algorithm (PSO), Genetic Algorithm (GA), and Artificial Bee Colony Algorithm (ABC) on some shifted, high dimensional and large search range problems.

Keywords Ebola virus, Ebola disease, metaheuristic algorithm, optimization problems, constrained benchmark functions

1. Introduction

Ebola virus represents the virus causing the Ebola virus disease (EVD). The disease was first so named in the Democratic Congo Republic (DRC) in 1976. A widespread catastrophic outbreak was reported in late 2013 in the West African regions, including Sierra Leone, Liberia, Mali, Nigeria, and Senegal. It is widely reported that the virus made its entry into the human population through consumption or contact with infected animals such as fruit bat (Gumusova, Sunbul, & Leblebicioglu, 2015), (Osterholm, et al., 2015), (Kadanali & Karagoz, 2015). This animal-to-human infection led to person-to-person, hence becoming an epidemic across the West African region. Contrary to the novel corona virus (COVID-19), the EVD person-to-person transmission occurs only when the infected person exhibits some form of signs and symptoms associated with Ebola. This transmission is aided by contact with any form of body fluid of an infected person, and also when a healthy person comes in contact with infected objects since the Ebola virus can survive on dry surfaces, like doorknobs and countertops, for several hours (CDC, 2021), (Tanade, Pate, Paljug, Hoffman, & Wang, 2019). The haemorrhagic disease, known to be notoriously

fatal has been reported to have mortality rates ranging from 25% to 90%. An average of 50% is only due to fluid loss rather than blood loss (The Agent, 2020), (WHO, 2020). Although the experimental Ebola vaccine proved highly protective against EVD, the transmission rate from the infected to the susceptible population is alarming. The high survival rate of EBOV in body fluids, including breast milk, saliva, urine, semen, cerebrospinal fluid, and aqueous humor, in addition to blood and blood derivatives, and detected in amniotic fluid, tears, skin swabs and stool by reverse transcription (RT)-PCR, presents a very high infection and transmission rate. This then implies that a one-time entry of the virus into a susceptible population through a single individual has a high propagation rate among the population.

A closer study of the propagation strategy of the EVD and the resulting propagation model inspired the metaheuristic algorithm proposed in this study. Deriving computational solution from natural phenomena has promoted a field of computing referred to as nature-inspired computing. A broader view of this aspect of computing may well relate with the field of artificial intelligence (AI) and also computational intelligence (CI), where computational systems are designed by synthesizing behaviors of organisms or natural phenomenon (Marrow, 2000), (Wang, et al., 2017), (Siddique, 2015). Metaheuristic algorithms are nature-inspired optimization solutions with high performance and lower required computing capacity which has successfully solved complex real-life problems in Engineering, medical sciences and sciences, especially in areas concerning swarm intelligence based algorithms (XS, 2013), (Green, Aleti, & Garcia, 2017), (SwatiSwayamsiddha, 2020). These optimization algorithms are designed without specific to a particular problem and are often categorized by the ability to perform a local or global search, handle single-solution or whole population, use memory, adopt greedy or iterative search process. The techniques often achieve near-optimal solutions to large-scale optimization problems due to their highly flexible manner of operation and ability to learn quickly owing to their natural or biological systems from which their designs were inspired.

A subfield of natural computation consists of biology-inspired techniques which also referred to as bio-inspired algorithms or computational biology. These techniques are stochastic in nature, far from the design of deterministic heuristics (Ezugwu, Adeleke, Akinyelu, & Viriri, 2020). This feature has made it possible to represent the biological evolution of nature, hence capable of being used as a global optimization solution. Recently, bio-inspired optimization algorithms have helped support machine learning to address the optimal solutions of complex problems in science and engineering (Darwish, 2018). The bio-inspired algorithms combine biological concepts with mathematics and computer sciences and are broadly classified as evolutionary algorithms (EA), biology algorithms, and swarm intelligence (SI) algorithms. Although the last two categories are often combined and referred to as swarm intelligence, we found that not all bio-inspired algorithms have the swarm feature. Examples of the evolutionary algorithms are Genetic algorithms (GA) (Sivanandam & Deepa, 2008), Genetic programming (GP), differential evolution (DE), the evolution strategy (ES), Coral Reefs Optimization Algorithm (CRO) (Ezugwu, et al., 2021) and evolutionary programming (EP). Examples of SI-based algorithms are Food foraging behavior of honeybees Artificial Bee Colony (ABC), Echolocation ability Ant-lion optimizer (ALO), Luciferin induced glowing behavior Bees Algorithm (BAO), Bat Algorithm (BOA), , Hunting behavior Barnacles mating optimizer (BMO), Swarming around hive by honey bees Cuckoo optimization algorithm (COA), Echo-cancellation Cuckoo search (CSO), Hunting behavior & social hierarchy Dolphin echolocation (DEO), Social interaction and food foraging Dragonfly algorithm (DFA), Static and dynamic swarming behavior Deer hunting optimization (DHO), Pollination process of flowers Fire-fly algorithm (FFA), Food foraging behavior Hunting search (FFO), Bubble-net hunting Fruit fly optimization (FOA), Obligate brood parasitic behavior Flower-pollination algorithm (FPA), Navigation and foraging behaviors Grasshopper optimization algorithm (GOA), Spiral flying path of moth Glowworm Swarm Optimization (GSO), Cuckoos' survival efforts Grey wolf optimizer (GWO), Flashing light patterns Moth-flame optimization (MFO), Mating behavior Manta ray foraging optimizer (MRFO), Hunting behavior of humans SailFish optimizer (SFO), Group hunting behavior Salp swarm algorithm (SSA), and Hunting mechanism Whale optimization algorithm (WOA).

These EA and SI based algorithms have demonstrated good performance at solving real-world complex combinatorial problems, which are considered to be a fundamentally vital and critical task (Agushaka & Ezugwu, 2020), (Munien, et al., 2020), (Munien & Ezugwu, Metaheuristic algorithms for one-dimensional bin-packing problems: A survey of recent advances and applications, 2021), (Achary, et al., 2021), (Ezugwu, Adewumi, & Fríncu, 2017), (Ezugwu A. E., Enhanced symbiotic organisms search algorithm for unrelated parallel machines manufacturing scheduling with setup times, 2019), (Ezugwu & Prayogo, Symbiotic organisms search algorithm: theory, recent advances and applications, 2019). In addition, studies have shown their capability to efficiently scale up to handle large scale problems as opposed to traditional optimization methods, which are more effective for small-scale problems (Game, Vaze, & Emmanuel, 2020). Further research in bio-inspired computing areas will lead to achieving similar and better new optimization algorithms capable of solving modern-day optimization problems. Our study showed that exploring the propagation model of diseases with an endemic and pandemic nature may yield an outperforming optimization algorithm with interesting performance in solving real-world optimization problems. This study considers that the exploration and exploitation phases of optimization algorithms are practically coupled into the natural order and strategy of propagating these diseases. The study confirms that finding a good balance between exploitation and exploration of the problem search space for an optimization algorithm determines its ability to find a globally optimal solution (CREPINSEK, LIU, & MERNIK, 2012), (Cuevas, Echavarría, & Ramírez-Ortegón, 2014). The exploration phase often allows for finding candidate solutions that are not neighbor to the current solution, while exploitation maintains its search in the neighborhood. Hence, we found a balance of the two scenarios in the disease propagation model for escape from a local optimum with no neglect to good solutions in the neighborhood.

This study is motivated by the propagation strategy of the Ebola virus disease, and in general, the capability of bio-inspired algorithms to provide abundant inspiration for the design and implementation of intelligent algorithms that are powerful tools for solving real-life problems. We propose a novel metaheuristic algorithm, which is an optimization algorithm inspired by the Ebola virus disease and its propagation model. The proposed algorithm is referred to as the Ebola Optimization search algorithm (EOSA). The main advantage of this algorithm over similar optimization algorithms is that it presents a dynamic mechanism for profitably updating the population as they transit through susceptible, infection, quarantine, recovered, and hospitalized operations for a better fit. To quantitatively measure how fit a given solution is in solving the problem, giving intuitive results, discovering the best or worst candidate solution, the resulting optimization algorithm is investigated on about fifty (50) classical benchmark optimization functions (Jamil & Yang, 2013) and more than thirty (30) CEC functions (Cheng, et al., 2018). In summary, the main contributions of this research are as follows:

- i. A new nature-inspired metaheuristic algorithm called EOSA inspired by the propagation model of the Ebola virus disease is proposed.
- ii. Several experiments are conducted using over 89 mathematical optimization problems, including the classical benchmark functions and CEC'17 test suite, which are considered to be challenging test problems in the literature to evaluate the efficiency of the proposed EOSA. The results of these experiments may serve as important inputs for further research.
- iii. Validation of the obtained numerical results using statistical analysis test, which further support the superiority claim of the proposed EOSA optimization method over the existing state-of-the-art metaheuristic algorithms.

The rest of the paper is organized as follows. Section 2 provides an overview of the Ebola virus diseases. The proposed propagation model, mathematical model, and algorithmic design for the EOSA algorithm are given in Section 3. Section 4 details the benchmark functions applied to evaluate the performance of the proposed algorithm. Also, the section listed and discussed the parameterization and assignment of initial values used for experimentation. A discussion on results obtained is presented in Section 5, including numerical simulations that support the proposed propagation model. A detailed comparative analysis of the performance of EOSA and similar

algorithms are also presented in the section. In Section 6, we give concluding remarks on how our novel optimization algorithm fit in the literature, its real-life applicability, and perspectives for future works.

2. Overview of Ebola and Related Work

This section presents a summary of the Ebola virus disease, its propagation technique, and relevant SIR-based models that support the modeling presented in this study. Also, considering the nature of the optimization algorithm proposed in this study, which shares some biology principles, we review studies that have developed bio-inspired optimization algorithms. The phenomenon behind the resulting algorithms is briefly stated and reported performance or application of the algorithms is also expatiated.

2.1 The Ebola Virus (EBOV) and Ebola Virus Diseases (EVD): The Propagation Mechanism

Ebola viruses result in what is known as the Ebola virus disease (EVD) once they successfully infect the host in a manner suggesting victimization of the host. They are classified among the family of Filoviridae viruses, which are recognized by their different shapes of short or elongated branched filaments sizing up to 14,000 nanometers in length (The Agent, 2020). About six different species of the EBOV have been reported to exist. These are the Bundibugyo Ebola virus, Ebola-Zaire virus, Tai Forest Ebola virus, and Sudan Ebola virus account for large flare-ups or outbreaks in Africa.

Exposure of a human individual to the virus through pathogenic agents or contaminated environment initiates a population-based infection and thereafter propels the spread or propagation of the disease. Direct contact with infected individual spur the propagation and spread of the virus. This contact relies on broken skin or mucous membranes in the eyes, nose, mouth, or other openings. It is assumed that such openings in the human body allow for body fluids (e.g. urine, saliva, sweat, faeces, vomit, breast milk, amniotic fluid, blood and semen) bearing the virus to be transmitted to other susceptible individuals. Another host to the Ebola virus, which may transmit the disease to a healthy or susceptible individual is a contaminated environment. An environment, such as medical equipment's, clothes, beddings and other related utensils, is considered to be contaminated if the body fluid of an infected individual has been spilt within such environment or object. Whereas an infected individual and a contaminated environment appear to have enhanced the propagation of EVD, infected animals consumed by humans have also shown to propagate the disease (Rewar & Mirdha, 2014). These animals include bats, chimpanzees, fruit bats, and forest antelope, which are often hunted for food. Another propagative mechanism of the EBOV culturally driven is burial practices in the most affected population and regions. This is mainly transmitted through contact with infected dead bodies. Ebola virus is not propagated through the air.

Different strategies ranging from case-based management approach, surveillance and contact tracing, quarantine of infected cases, infection prevention and control practices, and safe burial rites have been adopted in reviving and surviving infected cases. However, infected cases remain positive while the virus remains in their blood. The EBOV infection and propagation rate presents an appealing computational solution to numerous problems and so motivated the design of the proposed metaheuristic algorithm. While it appears that the solutions for mitigating the spread of the virus are suggestive of scaling down the infection rate, we argue that some other factors are still contributory to the propagation model. For instance, it is widely reported that the time-scale from symptom onset to death is an average of 10 days in 50–90% of cases (Mobula, et al., 2018).

To formalize and apply the propagation model of EBOV, we review some susceptible-infection-recovery (SIR) models. This is necessary for mainstreaming the concept proposed in the study. An interesting SIR model, based on EBOV, combining agent-based and compartmental model, has been presented (Tanade, Pate, Paljug, Hoffman, & Wang, 2019). The authors suggested that the hybrid model can switch from one paradigm to another on a stochastic threshold. The agent-based model consists of Susceptible (S), Infected (I), Hospitalized (H), Recovered (R), Funeral (F), and Dead (D). In the compartmental model, the Exposed (E) item was added to make up seven compartments. The SIR-based model was proposed to model the movement of individuals in a population from one compartment to another in both paradigms. For instance, individuals may move from Susceptible (S), Infected (I), Hospitalized (H), based on pre-existing computed rates. One external compartment considered in the literature is the influence of EBOV carrying animals like bats. The assumption made was that since these animals can infect the human population without them (the animals) becoming ill, they present a reservoir-like mechanism for the virus in the SIR model. Furthermore, the authors assumed that rate of infection and hospitalization between infected individuals who will recover or die is the same, deceased individual is buried in unsafe practices, and that recovered individual are

removed from the system. This SIR model presents a foundation for the modeling and implementation of the optimization algorithm proposed in this study. We considered that the compartments defined by the work of Tanade *et al.* demonstrates the possibility to monitor and simulating the EBOV propagation model for the optimization task in our study.

In related work, Berge *et al.*, also modeled the propagation model of EBOV using the SIR-type model. The study's novelty was the addition of the role of the indirect environmental transmission on the dynamics of EVD and to assess the effect of such a feature on the long run of the disease (Berge, Lubuma, Moremedi, Morris, & Kondera-Shava, 2017). The authors showed that factoring direct and indirect transmission of EBOV into a SIR model promotes a system where the virus always exists in a population, increasing the propagation rate. Taking a cue from the novelty of this work in addition to that of Tanade *et al.*, we adapt the model proposed in this study to support the concept of direct and indirect transmission promoted by Berge *et al.* both studies supported their SIR models with mathematical models and further simulation for validating the performance of their model. Similarly, Yet (2019) successfully represented the basic interactions between EBOV and wild-type Vero cells in vitro (Yet, 2019). Rafiq *et al.* also proposed the SEIR model, which the mathematical model supported demonstrating the dynamics and illustrating the Ebola virus's stability pattern in the human population. We found that their mathematical model which is of the form couple linear differential equation. The authors applied their SEIR model to study the disease-free equilibrium (DFE) and endemic equilibrium (EE) and thereafter report on the stability of the model. In another study that investigated the spread of EVD in India, the authors (Sau, 2017) investigated EBOV transmission in the region through an SEIR model they proposed. Using ordinary differential equations, the study represented the SEIR model as a mathematical model and further simulated it using a spatiotemporal epidemiology modeler (STEM). Rachah and Torres also applied a mathematical model for the study of the outbreak of EBOV and eventually the EVD (Rachah & Torres, 2015). The novelty of this study is the addition of the use of vaccination to the proposed model. We found this appealing considering the role of the vaccine in stemming the tide of the infected population. Whereas most SIER approaches have often adopt the stochastic method for the simulation of the model, Okyere *et al.*, considered the use of a deterministic scheme for designing models and studying the infection rate of EBOV (Okyere, Ankamah, Hunkpe, & Mensah, 2020). As an improvement to the work of Rachah and Torres, which factored in vaccination, the study also captured treatment and educational campaign as time-dependent control functions in the SEIR model proposed.

Considering the review presented above, this study developed an SEIR-based model which added more compartments. The proposed SEIR model factored in the notion of quarantine, which we found to play a role in curtailing EBOV propagation. In addition, we modeled the SEIR model to allow for the inclusion of the influence of vaccine in the pace of the growth of infection among a given population. The SEIR model was then formulated using an ordinary differential equation. This presented a good understanding of the design of the proposed metaheuristic algorithm. We found this necessary due to the importance of all the compartments of the SIER model in achieving a population that successfully translates between S-I. The resulting model is detailed in Section 3 and its supporting mathematical model. Having considered the biological perspective of the inspiration of the proposed algorithm, the following sub-section presents a review of some related metaheuristic algorithms motivated by nature-biology behavioral patterns.

2.2 Metaheuristic optimization algorithms: Bioinspired-Based Algorithms

Bio-inspired optimization algorithm represents a class of metaheuristic algorithms whose principles are inspired by a biology-nature phenomenon and have been successfully applied to solve different problems (Oliveira, Pires, Boaventura-Cunha, & Martins, 2020). This category of algorithms exploits the basic process of nature and then translates them into rules or procedures, which are then model computational for solving complex real-life problems. The mostly population-based algorithms and examples of such are Satin Bowerbird Optimizer (SBO), Earthworm Optimisation Algorithm (EOA), Wildebeest Herd Optimization (WHO), Virus Colony Search (VCS), Slime Mould Algorithm (SMA), Invasive weed colonization optimization (IWO), Biogeography-based optimization (BBO), Coronavirus optimization algorithm (COA), emperor penguin and salp swarm algorithm (ESA). Although evolutionary-based algorithms like GA and DE and swarm-based algorithms like PSO, WOA, and ABC share some characteristics of a biology-inspired algorithm, we have chosen to limit our review to those mentioned earlier.

ESA is a hybrid of two phenomena drawn from the Salp swarm algorithm and emperor penguin. The behaviour of the two creatures is modelled to achieve ESA. Comparing the proposed algorithm with similar metaheuristic algorithms, authors (Dhiman, 2019) revealed that the algorithm demonstrated good performance based on

sensitivity, scalability, and convergence analyses. Coronavirus optimization algorithm (COA) based on its propagation strategy, and another variant namely Coronavirus herd immunity optimizer (CHIO) based on human immunity, have been proposed. The COA proposed in (Martínez-Álvarez, et al., 2020) and CHIO in (Al-Betar, Alyasseri, Awadallah, & Doush, 2020) leverages on herd infection and herd immunity, respectively. The effectiveness of COA was evaluated by applying it to the problem of the design of a convolutional neural network (CNN), while CHIO proved robust at real-world engineering problems. Earthworm Optimisation Algorithm (EOA), also referred to as EWA, is a metaheuristic algorithm whose inspiration was drawn from the reproductive nature of the earthworm (Wang, Deb, & Coelho, 2018). The mechanism involves two reproduction strategies where the first strategy allows for a parent to reproduce only one offspring while the other allows for more than one offspring. This reproducibility is controlled by the Cauchy mutation approach allowing for crossover operators.

Biogeography-Based Optimization (BBO) solves its optimization problem by implementing the concept for geographical distribution and positioning of the biological organism (Simon, 2008). Although BBO's features are similar to those of GAs, the authors drew inspiration from the original mathematical model of the biogeography of organisms to derive BBO. Experimentation shows that BBO successfully solved real-world sensor selection problems for detection of the status of aircraft engines and a selection of 14 benchmark optimization functions. Invasive Weed Optimization (IWO) is an optimization algorithm that has been widely applied to numerous problems and is based on a numerical stochastic optimization algorithm learned from the invasive nature of weeds (Mehrabian & Lucas, 2006). The aggressive invasive nature of weeds allows for colonizing the environment against other economically viable plants. Knowing that this is a disadvantage agricultural-wise, the concept has benefited the task of solving optimization problems. The resulting optimization algorithm was successfully applied to engineering problems, namely, optimizing and tuning the robust controller and well-known benchmark functions. Satin bowerbird optimization (SBO) is a biology-based optimization algorithm whose inspiration was drawn from the phenomenon of male satin bowerbird capable of attracting the female for breeding. (Zhang, Zhou, & Luo, 2019). The Satin Bowerbird Optimizer (SBO) optimization algorithm has been successfully applied to the problem of optimization in the estimation of efforts needed to develop software. Wildebeest Herd Optimization (WHO) is a bio-inspired metaheuristic algorithm rooted in wildebeest behaviour when searching for food (Amali, Bessie, & Dinakaran, 2019). The search is often guided by lookout for grazing land where there is a high density of vegetation. The WHO exploits the following natural characteristics of herds of wildebeest to achieve its performance: local search capability of wildebeest due to limited eyesight, look out for sparsely grazed region to avoid crowded grazing, exploitation of past experiences to explore regions with a high density of vegetation, starvation avoidance strategy deployed through a transition to new regions or location, and lastly, herd-based movement to avoid predators.

The propagation strategy of the virus in the host environment can sometimes be aggressive and often overwhelm the whole environment. Motivated by this mechanism, authors (DongLi, Zhao, Weng, & Han, 2016) proposed Virus Colony Search (VCS). The VCS exploration and exploitation phases leverage the propagation approach of the virus through diffusion or infection of the host environment. VCS has been successfully applied to the classic benchmark functions and the modern CEC2014 benchmark functions and real-life problem regarding energy consumption management (Jayasena, Li, Abd Elaziz, & Xiong, 2018). Slime Mould Algorithm (SMA) optimization algorithm is based on a fungus named slime mould inhabiting cold and humid places (Li, Chen, Wang, Heidari, & Mirjalili, 2020). The algorithm authors explored the nutritional stage, also referred to as plasmodium, of the organism for its design. They have a mechanism for multiple food sources at the same time to form a connected venous network so that they can even grow to more than 900 square centimetres depending on food availability. Using a mathematical model, authors were able to simulate the process of producing positive and negative feedback of the propagation wave of slime mould based on bio-oscillator to form the optimal path for connecting food with excellent exploratory ability and exploitation propensity. SMA was successfully applied to solve engineering problems, including cantilever, welded beam, and pressure vessel structure problems.

Although bio-inspired optimization algorithms are often classified into evolutionary and swarm intelligence-based approaches, we have presented a review of those we termed as biology-based. While we acknowledge that these are not exhaustive and many new optimization algorithms inspired by natural processes are developed day-by-day, they provide readers with a general understanding of the inspiration and principle behind such a class of algorithms.

3. EOSA: Methodology

Understanding how an SEIR-based model works in modeling the propagation of a disease is important to appeal to an optimization algorithm's design. Hence, this study proposes an improved SEIR-HDVQ model based on recent literature on EVD. Secondly, a presentation of the procedural flow of EOSA and the corresponding flow chart is designed and discussed. Lastly, to formalize the proposed optimisation algorithm, we represent it using a mathematical model and then design it. Therefore, this section is a detailed work on the methods applied to creating the new metaheuristic algorithm.

3.1 Model of EOSA

SEIR-based models designed for EVD have been proposed in the literature to monitor direct and indirect propagation of the disease in the selected population (Berge, Lubuma, Moremedi, Morris, & Kondera-Shava, 2017) and (Tanade, Pate, Paljug, Hoffman, & Wang, 2019). This study adopts and adapts two relevant models from the existing SEIR models by identifying and adding new compartments perceived to have been omitted. This study proposed adding the external agent or contaminated environment serving as a reservoir of the virus, vaccination, and quarantine, which PE, V represents, and Q, respectively. This became necessary considering that the Ebola virus and disease are not propagated among the human population except an individual is infected from the reservoir. Also, the roles played by vaccination and quarantining infected individuals have impacted the virus's propagation rate and disease. This perception is now reported in studies on the propagation of endemic or pandemic cases (Moghadas, et al., 2020), (BBC, 2021) (Mathebula, Ndwandwe, Pienaar, & Wiysonge, 2019), (Potluri, et al., 2020). This, therefore, necessitated the re-modeling of the propagation model, which now yielded the SEIR-HDVQ: Susceptible (S), exposed (E), Infected (I), Hospitalized (H), recovered (R), Death or death (D), Funeral (F), Vaccinated (V), and Quarantine (Q). Also, in designing the model, we considered that an insignificant number of recovered cases might still retain the virus in their body fluid, which has potency for infecting healthy cases (WHO, 2016), (UNCHC, 2017) (Thorson, et al., 2021). Since the interest of this study is to leverage the propagation model of the EVD for developing solving optimization algorithms, it became necessary to explore all factors supporting increased infection.

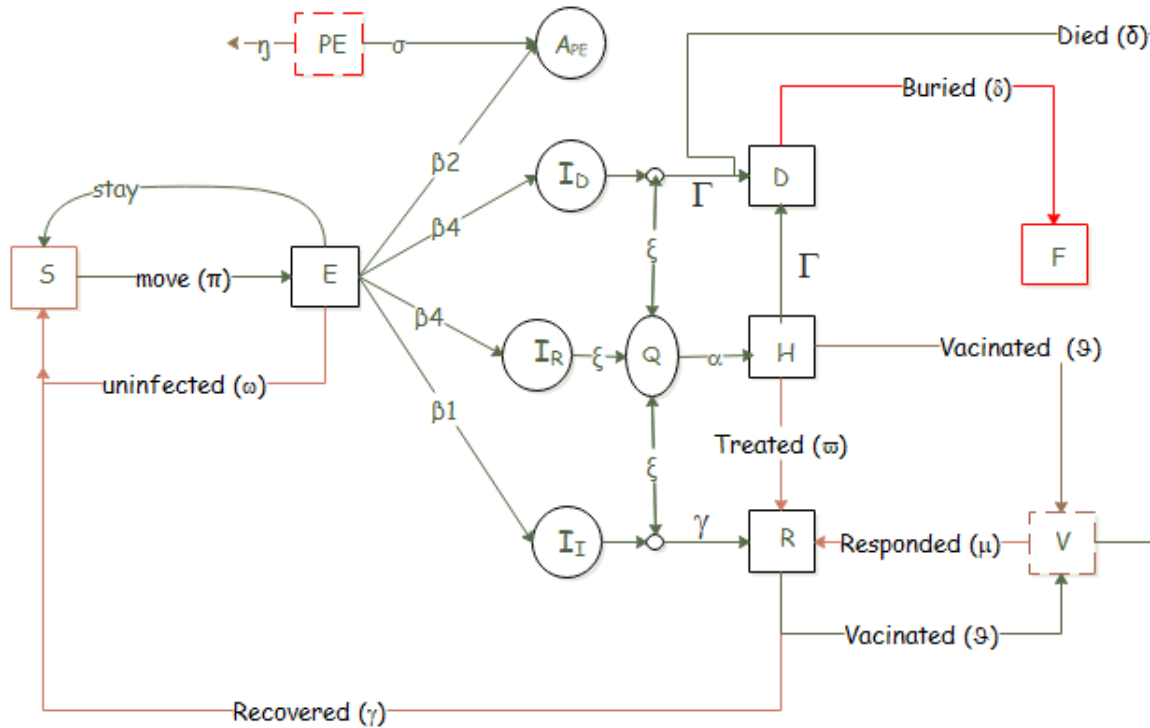


Figure 1: The SEIR-HDVQ propagation model of the proposed EOSA metaheuristic model

The model of the SEIR-HDVQ shown in Figure 1 and the listing of its parameters presented in Table 1. The propagation of EVD is assumed to provide a suitable manner for solving some optimization problems considering its aggressive mechanism overwhelming communities. The figure assumes a population of susceptible individuals whose exposure could trigger generating the population of other subgroups, though the reverse could also hold. Exposed individuals or contaminated environment or agent reservoirs can randomly draw arbitrary individuals from the susceptible into the categories of infected, which may be due to exposure to any individual from the subgroups of the infected. Subgroups of infected individuals are infected from the dead individual, infection from an infected individual who is alive, and infection from a recovered individual and infected from contaminated environment or agent-reservoir. We show that the virus has the potential of decaying in its contaminated environment. Furthermore, the propagation model shows that the infected cases could die without going to a hospital and may as well recover without hospitalization. An assumption made in this study is classifying every vaccinated case as hospitalized. Also, we assumed that both the hospitalized (H) and non-hospitalized cases could transit into the dead (D). At the same time, those recovered (R) from vaccination (V) are returned to the susceptible (S).

Table 1: Notations and description for variables and parameters for SEIR-HDVQ

Symbols	Data Type	Descriptions
S	Vector	Susceptible individuals
E		Exposed individuals
I		Infected individuals
H		Hospitalized infected individuals
R		Recovered infected individuals
D		Diseased from infection individuals
V		Vaccinated infected individuals
PE		Agents capable of infecting individuals
π	Scalar	Recruitment rate of susceptible human individuals
η		Decay rate of Ebola virus in the environment
α		Rate of hospitalization of infected individuals
Γ		Disease-induced death rate of human individuals
β_1		Contact rate of infectious human individuals
β_2		Contact rate of pathogen individuals/environment
β_3		Contact rate of deceased human individuals
β_4		Contact rate of recovered human individuals
γ		Recovery rate of human individuals
τ		Natural death rate of human individuals
δ		Rate of burial of deceased human individuals
ϑ		Rate of vaccination of individuals
ϖ		Rate of response to hospital treatment
μ		Rate response to vaccination
ξ		Rate of quarantine of infected individuals

The rates of change of variables or parameters applied in this study are summarized in Table 1. The values of most of these parameters are already predetermined by related studies on EVD, which this study simply leverages on their reported figures, as further discussed in Section 4.

3.2 Flowchart of EOSA

The SEIR-HDVQ propagation model presented in the last subsection motivated the design of the EOSA algorithm. This paper aims to adapt the propagation mechanism to the derivation and generation of potential search space for solving optimization problems using the proposed algorithm. The formalization of the EOSA algorithm is achieved from the following procedure:

1. Initialize all vector and scalar quantities which are individuals and parameters. Individuals in the sets: Susceptible (S), infected (I), recovered (R), dead (D), Vaccinated (V), Hospitalized (H), and Quarantine (Q) with their initial values.
2. Randomly generate the index case (I_1) from susceptible individuals.
3. Set the index case as the global best and current best, and compute the fitness value of the index case.
4. While the number of iteration is not exhausted and there exists at least an infected individual, then
 - a. For each susceptible individual, generate and update their position based on their displacement. Note that the further an infected case is displaced, the more the number of infections, so that short displacement describes exploitation, otherwise exploration.
 - i. Generate newly infected individuals (nI) base on (a).
 - ii. Add the newly generated cases to I
 - b. Compute the number of individuals to be added to H, D, R, B, V, and Q using their respective rates based on the size of I
 - c. Update S and I base on nI.
 - d. Select the current best from I and compare it with the global best.
 - e. If the condition for termination is not satisfied, go back to step 6.
5. Return global best solution and all solutions.

In Figure 2 below, the flow chart of the proposed EOSA metaheuristic algorithm is shown.

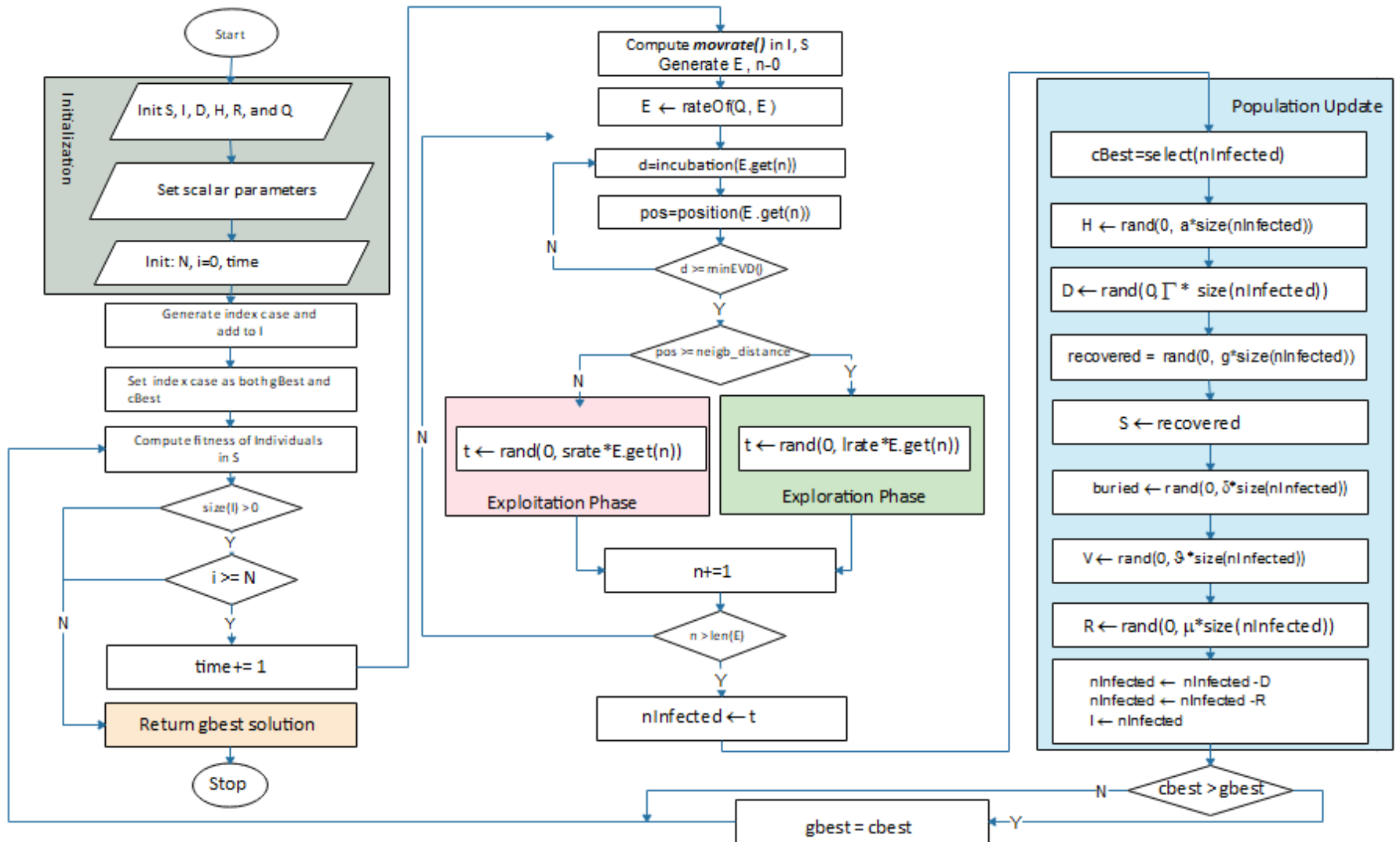


Figure 2: Flowchart of the proposed the EOSA metaheuristic algorithm

The flowchart presents a detailed flow of process and information as a build-up from the procedure described above. The detailing shows the various levels of initialization and conditional checking. Also, the computation leading to the exploration and exploitation stages of the proposed EOSA metaheuristic algorithm is detailed. Also, the procedure for update all subgroups are also identified. In the following subsection, the mathematical model applies to the flowchart of the algorithm presented and discussed.

3.3 Mathematical Model of EOSA

As earlier noted, we represent SEIR-HDVQ in this paper base on the definition of Susceptible (S), Infected (I), Hospitalized (H), Exposed (E), Recovered (R), Funeral (F), Dead (D), Vaccination (V), and Quarantine (Q). To update the positions of each exposed individual, Equation 1 applies:

$$mI_i^{t+1} = mI_i^t + \rho M(I) \quad (1)$$

where ρ represents the scale factor of displacement such individuals, mI_i^{t+1} and mI_i^t are respectively the updated and original position at time t, and t+1 is the current time. $M(I)$ is the movement rate made by individuals, which is further defined thus:

$$M(I) = srate * rand(0, 1) + M(Ind_{best}) \quad (2)$$

$$M(s) = lrate * rand(0, 1) + M(Ind_{best}) \quad (3)$$

The exploitation stage of the EOSA optimization algorithm assumes that the infected individual either stays within a distance of zero (0), or is displaced within a limit not exceeding *srate* denoting short distance movement. The exploration phase of the algorithm assumes that the infected individual has moved beyond the normal neighborhood range *lrate*. The consideration in this study is that the farther the displacement, the more the number of contacts exposed to the infection. Equations 2 and 3, therefore, ensure that the movement of each individual in consideration is appropriately assigned. Both *srate* and *lrate* are regulated by *neighborhood* parameter. If *neighborhood* is over 0.5, we assume the individual has moved beyond the *neighborhood* otherwise, remains within the *neighborhood*.

Initialization of Susceptible population: At the beginning, an initial population is generated by means of random number distribution whose initial positions are all zero (0), so that i^{th} individual is generated as shown in Equation 4. The function $rand(0, 1)$ generates uniformly distributed values, the variable i , and U_i and L_i denote the upper and lower bounds respectively for the i^{th} individual, ranges from 1,2,3...N, where is the population size.

$$individual_i = L_i + rand(0,1) * (U_i + L_i) \quad (4)$$

The selection of the current best is carried out on the set of infected individuals in time t. meanwhile, the selection of the global best is based on the following:

$$bestS = \begin{cases} gBest, & fitness(cBest) < fitness(gBest) \\ cBest, & fitness(cBest) \geq fitness(gBest) \end{cases} \quad (5)$$

where *bestS*, *gBest* and *cBest* all denotes the best solution, global best solution, and current best solution at time t; *fitness(.)* represents the objective function applied to the problem. We distinguish *gBest* and *cBest* as infected individuals who *Superspreader* and *Spreader* of the Ebola virus, respectively.

Update of Susceptible (S), Infected (I), Hospitalized (H), Exposed (E), Vaccinated (V), Recovered (R), Funeral (F), Quarantine (Q), and dead (D) uses a system of ordinary differential equations based on those in (Berge, Lubuma, Moremedi, Morris, & Kondera-Shava, 2017) (Tanade, Pate, Paljug, Hoffman, & Wang, 2019). Differential calculus

is a branch of calculus that is a branch in mathematics, where the former deals with the rate of change of one quantity concerning another, while the latter deals with finding different properties of integrals and derivatives. The application of differential calculus, in our case, intends to obtain the rates of change of quantities S, I, H, R, V D, and Q with respect to time t . Hence, the Equations 6, 7, 8, 9, 10, 11, 12 for S, I, H, R, V D, and Q respectively as follows:

$$\frac{\partial S(t)}{\partial t} = \pi - (\beta_1 I + \beta_3 D + \beta_4 R + \beta_2 (PE)\eta)S - (\tau S + \Gamma I) \quad (6)$$

$$\frac{\partial I(t)}{\partial t} = (\beta_1 I + \beta_3 D + \beta_4 R + \beta_2 (PE)\lambda)S - (\Gamma + \gamma)I - (\tau)S \quad (7)$$

$$\frac{\partial H(t)}{\partial t} = \alpha I - (\gamma + \varpi)H \quad (8)$$

$$\frac{\partial R(t)}{\partial t} = \gamma I - \Gamma R \quad (9)$$

$$\frac{\partial V(t)}{\partial t} = \gamma I - (\mu + \vartheta)V \quad (10)$$

$$\frac{\partial D(t)}{\partial t} = (\tau S + \Gamma I) - \delta D \quad (11)$$

$$\frac{\partial Q(t)}{\partial t} = (\pi I - (\gamma R + \Gamma D)) - \xi Q \quad (12)$$

We shall first assume that each of Equations (6 -11) is a *scalar function*, meaning that it has one number as a value, which can be represented as a real value. This is not far removed from some common scalar differential equations and their corresponding f functions, which include exponential growth of money or populations governed by scalar differential equations: $u'=au$, where u is the growth rate.

We determine the rate of change of the population of susceptible individuals and then apply it to the current size of the susceptible vector to obtain the number of susceptible individuals at time t . The same procedure is applied to compute the set of individuals in vectors I, H, R, V, D, and Q using rates described in Table 1. This study assumes the initial conditions $S(0) = S_0$, $I(0) = I_0$, $R(0) = R_0$, $D(0) = D_0$, $P(0) = P_0$, and $Q(0) = Q_0$ where our t follows after the epoch, and δ in Equation (11) is for the burial rate. Equation (12) models the rate of quarantine of infected cases of Ebola.

3.4 Algorithm Design of EOSA

The pseudo-code of the proposed EOSA metaheuristic algorithm is shown in Algorithm 1. Lines 1-7 of the algorithm show the initialization phase of parameters used in subsequent lines.

Algorithm 1: Algorithm of the EbOA metaheuristic algorithm

Result: Best solution
Input: objfunc, lb, ub, epoch, psize, evdincub
Output: solution, gbest

```
1  $S, E, I, H, R, V, Q, sols \leftarrow \emptyset$ ;  
2 Initialize S finite set  $S = \{ind_1, ind_2, \dots, ind_n\}$  ;  
3  $S \leftarrow createSusceptibleIndvd(psize, S), Eq.4$ ;  
4  $time \leftarrow 0$ ;  
5  $icase \leftarrow generatedIndexCase()$ ;  
6  $gbest, cbest \leftarrow icase$ ;  
7 while  $e \leq epoch \wedge len(I) > 0$  do  
8    $Q \leftarrow rand(0, Eq.12 \times I)$ ;  
9    $fracI = I - Q$ ;  
10  for  $i \leftarrow 1$  to  $len(fracI)$  do  
11     $pos_i \leftarrow movrate()$  using Eq.1;  
12     $d_i \leftarrow rand()$ ;  
13    if  $d_i > evdincub$  then  
14       $neighborhood \leftarrow prob(pos_i)$ ;  
15      if  $neighborhood < 0.5$  then  
16         $tmp \leftarrow rand(0, Eq.7 \times I \times srate)$ ;  
17      end  
18      else  
19         $tmp \leftarrow rand(0, Eq.7 \times I \times lrte)$ ;  
20      end  
21       $newI+ \leftarrow tmp$ ;  
22    end  
23     $I+ \leftarrow newI$ ;  
24  end  
25   $h \leftarrow rand(0, Eq.8 \times I)$ ,  $H+ \leftarrow h$ ;  
26   $r \leftarrow rand(0, Eq.9 \times I)$ ,  $R+ \leftarrow r$ ;  
27   $v \leftarrow rand(0, Eq.10 \times h)$ ,  $V+ \leftarrow v$ ;  
28   $d \leftarrow rand(0, Eq.11 \times I)$ ,  $D+ \leftarrow d$ ;  
29   $I+ \leftarrow I - add(r, d)$ ;  
30   $S+ \leftarrow r$ ;  
31   $S- \leftarrow d$ ;  
32   $cbest = fitness(objfunc, I)$ ;  
33  if  $cbest > gbest$  then  
34     $gbest = cbest$ ;  
35     $sols \leftarrow gbest$ ;  
36  end  
37 end  
38 return  $gbest, sols$ ;
```

To demonstrate that not all infected cases have the potency for recruiting new infected individuals, Line 8 shows that a sample is drawn into quarantine so that the remaining fraction of I infect the S population. On Lines 10-24, new infections are generated from S and then added to I. Since R, V, H, and V are only derivable from I, Lines 25-29 of Algorithm 1 generate their individuals using the appropriate equations. Logically, recovered and dead cases need to be removed from I before the next period. Also, recovered cases are added back to S while dead individuals are replaced in S with new cases. These are all model in Lines 29-31. Finally, the best solution is computed, the termination criterion is checked so that when it is satisfied, the algorithm terminates otherwise return to Line 7.

The overview of the proposed metaheuristic algorithm, EOSA, has been defined and designed in this Section. To demonstrate its practicability, we follow in the next Section for experimental setup, configurations, and parameter definition. These parameters provide details on those used in Algorithm 1.

4. Parameter Settings and Experimental Setup

This section is focused on reporting the environment for carrying out very detailed experimentation of the EOSA algorithm. First, we show control parameter settings and variable assignment, then list the benchmark functions applied to the algorithm, and then finally detail the evaluation criteria.

4.1 Configuration of experimental setup

Exhaustive experimentation for evaluating the proposed EOSA described in Algorithm 1 was carried out in a workstation environment with the following configurations: Intel (R) Core i5-7500 CPU 3.40GHz, 3.41GHz; RAM of 16 GB; 64-bit Windows 10 OS for each configuration of the system on the network. A total of ten (10) existing metaheuristic algorithms were compared with the proposed EOSA algorithm. To ensure that there is fairness in the execution of each algorithm, this study executed each algorithm twenty (20) times. Also, a total of five hundred (500) epochs were covered in each run of 20 for each algorithm. The runs of 20 for each algorithm allow computing the average values for all metrics in each 500 epoch.

4.2 Parameters of EOSA metaheuristic algorithm

The design and selection of EOSA's parameters and their corresponding values assumed the natural definitions generated from those reported by WHO. This study adopted the rates reported in studies that have carried out an extensive evaluation of the SEIR models they proposed. These studies relied on the WHO data for the evaluation of their models. All these parameters have been described and applied in Sections 3.1, 3.2, and 3.3, where the SEIR-HDVQ model was discussed.

Table 2: Notations and description for variables and parameters for SEIR-HDVQ

Symbols	Descriptions	Range
π	Recruitment rate of susceptible human individuals	Variable
η	Decay rate of Ebola virus in the environment	$(0, \infty)$
α	Rate of hospitalization of infected individuals	$(0, 1)$
Γ	Disease-induced death rate of human individuals	$[0.4, 0.9]$
β_1	Contact rate of infectious human individuals	Variable
β_2	Contact rate of pathogen individuals/environment	Variable
β_3	Contact rate of deceased human individuals	Variable
β_4	Contact rate of recovered human individuals	Variable
γ	Recovery rate of human individuals	$(0, 1)$
τ	Natural death rate of human individuals	$(0, 1)$
δ	Rate of burial of deceased human individuals	$(0, 1)$
ϑ	Rate of vaccination of individuals	$(0, 1)$
ω	Rate of response to hospital treatment	$(0, 1)$
μ	Rate response to vaccination	$(0, 1)$
ξ	Rate of quarantine of infected individuals	$(0, 1)$

In Table 2, the initial value for each parameter is defined. Considering the stochastic nature of EOSA, which is characteristic of biology-based optimization algorithms, some of the parameters assumed random values within the range of zero's (0) and 1's (1).

4.3 Benchmark functions

As an effort to evaluate the effectiveness of the proposed EOSA metaheuristic algorithm, this study curated forty-seven (47) standard and high dimensional functions for this purpose. These functions are listed in Table 3 and are subsequently used for observing the performance of EOSA with the hope of comparing its performance with those of a similar bioinspired metaheuristic algorithm. To give a proper presentation of the functions, we curated the names with the mathematical model representation of the functions alongside their range. These classical functions were also combined with the CEC'2010 and CEC'2017 benchmark functions to achieve very exhaustive experimentation.

Table 3: Standard benchmark functions used for the experimentation: Dimensions (D), Multimodal (M), non-separable (N), Unimodal (U), Separable (S)

ID	Function name	Range	Model of the function	D	Type	Min
F1	Ackley	[-32, 32]	$f(x) = -20e^{\left(-0.2\sqrt{\frac{1}{n}\sum_{i=1}^n x_i^2}\right)} - e^{\left(\frac{1}{n}\sum_{i=1}^n \cos(2\pi x_i)\right)} + 20 + e^{(1)}$	30	MN	0
F2	Alpine	[-10, 10]	$f(x) = \sum_{i=1}^n x_i \sin(x_i) + 0.1x_i $	N	MN	0
F3	Brown	[-1, 4]	$f(x) = \sum_{i=1}^{n-1} (x_i^2)^{(x_{i+1}^2+1)} + (x_{i+1}^2)^{(x_i^2+1)}$	N	UN	0
F4	Bent Cigar	[-100,100]	$f_{20}(x) = x_1^2 + 10^6 \sum_{i=2}^D x_i^2$	N	MS	0
F5	Composition1	[-100,100]	g1=Rosenbrock's Function F29 g2=High Conditioned Elliptic Function F15 g3=Rastrigin's Function F27	5		
F6	Composition2	[-100,100]	g1=Ackley's Function F1 g2=High Conditioned Elliptic Function F15 g3=Griewank Function F10 g4=Rastrigin's Function F27	3		
F7	Dixon and Price	[-10, 10]	$f_{18}(x) = 10^6 x_1^2 \sum_{i=2}^D x_i^2$	30	UN	0
F8	Discus Function	[-100, 100]	$f(x) = (x_1 - 1)^2 + \sum_{i=2}^n i(2x_i^2 - x_{i-1})^2$	N	U	
F9	Fletcher-Powell	[-100, 100]	$f(x) = 100 \left\{ [x_3 - 10\theta(x_1, x_2)]^2 + \left(\sqrt{x_1^2 + x_2^2} - 1 \right)^2 \right\} + x_3^2$ Where $2\pi\theta(x_1, x_2) = \begin{cases} \tan^{-1} \frac{x_2}{x_1}, & \text{if } x_1 \geq 0 \\ \pi - \tan^{-1} \frac{x_2}{x_1}, & \text{otherwise} \end{cases}$	N	MN	0.0001
F10	Griewank	[-600, 600]	$f(x) = 1 + \sum_{i=1}^n \frac{x_i^2}{1400} - \prod_{i=1}^n \cos\left(\frac{x_i}{\sqrt{i}}\right)$	30	MN	0
F11	Generalized Penalized Function 1	[-50, 50]	$f(x) = \frac{\pi}{n} X \left\{ 10\sin^2(\pi y_i) + \sum_{i=1}^{n-1} (y_i - 1)^2 [1 + 10\sin^2(\pi y_{i+1})] + (y_n - 1)^2 \right\} + \sum_{i=1}^n u(x_i, a, k, m)$	n	M	0

			<p>Where $y_i = 1 + \frac{1}{4} (x_i + 1)$, $u(x_i, a, k, m) = \begin{cases} k(x_i - a)^m & \text{if } x_i > a \\ 0 & \text{if } -a \leq x_i \leq a \\ k(-x_i - a)^m & \text{if } x_i < -a \end{cases}$</p> <p>$a=10, k=100, m=4$</p>			
F12	Generalized Penalized Function 2	[-5.12, 5.12]	$f(x) = 0.1 X \left\{ \sin^2(3\pi x_1) + \sum_{i=1}^{n-1} (x_i - 1)^2 [1 + \sin^2(3\pi x_{i+1})] + (x_n - 1)^2 [1 + \sin^2(2\pi x_n)] \right\} + \sum_{i=1}^n u(x_i, a, k, m)$ <p>Where $u(x_i, a, k, m) = \begin{cases} k(x_i - a)^m & \text{if } x_i > a \\ 0 & \text{if } -a \leq x_i \leq a \\ k(-x_i - a)^m & \text{if } x_i < -a \end{cases}$</p> <p>$a=5, k=100, m=4$</p>	N	M	0
F13	Holzman 2 function	[-100,100]	$f(x) = \sum_{i=1}^n i x_i^4$	N		
F14	HGBat	[-100,100]	$f_{23}(x) = \left \left(\sum_{i=1}^D x_i^2 \right)^2 - \left(\sum_{i=1}^D x_i \right)^2 \right ^{1/2} + (0.5 \sum_{i=1}^D x_i^2 + \sum_{i=1}^D x_i) / D + 0.5$	30	M	
F15	High Conditioned Elliptic	[-100,100]	$f_{23}(x) = \sum_{i=1}^D (10^6)^{\frac{i-1}{D-1}} x_i^2$	N		
F16	Hybrid1	[-100,100]	<p>g1 : Zakharov Function F45 g2 : Rosenbrock Function F29 g3: Rastrigin's Function F27</p>	3	UN	0
F17	Hybrid2	[-100,100]	<p>g1 : High Conditioned Elliptic Function F15 g2 : Ackley's Function F1 g3: Rastrigin's Function F27 g4: HGBat Function F14 g4: Discus Function F8</p>	3	MN	0
F18	Inverted Cosine Mixture	[-1,1]	$f_{14}(x) = 0.1n - (0.1 \sum_{i=1}^n \cos(5\pi x_i) - \sum_{i=1}^n x_i^2)$	N	MS	- 0.1x(n)

F19	Lévy 3 function	[-10, 10]	$f(x) = \sum_{i=1}^{n-1} \left[0.5 + \frac{\sin^2(\sqrt{100x_i^2 + x_{i+1}^2}) - 0.5}{1 + 0.001(x_i^2 - 2x_i x_{i+1} + x_{i+1}^2)} \right]$	N		
F20	Levy	[-10, 10]	$f_{12}(x) = \sum_{i=1}^n (x_i - 1)^2 [\sin^2(3\pi x_{i+1})] + \sin^2(3\pi x_1) + x_n - 1 [1 + \sin^2(3\pi x_n)]$	2	MN	0
F21	Levy and Montalo	[-5, 5]	$f_{17}(x) = 0.1(\sin^2(3\pi x_1)) + \sum_{i=1}^n (x_i - 1)^2(1 + \sin^2(3\pi x_{i+1})) + (x_n - 1)^2(1 + \sin^2(2\pi x_n))$	N	MS	0
F22	Noise	[-1.28, 1.28]	$f_7(x) = \sum_{i=1}^n x_i^4 + \text{random}[0, 1)$	N		
F23	Pathological function	[-100, 100]	$f(x) = \sum_{i=1}^5 i \cos((i-1)x_1 + i) \sum_{j=1}^5 j \cos((j+1)x_1 + j)$	N	MN	0
F24	Perm	[-20, 20]	$f(x) = \sum_{k=1}^n \left[\sum_{i=1}^n (i_k + \beta) \left(\left(\frac{x_i}{i} \right)^k - 1 \right) \right]^2$	N	MN	0
F25	Powel	[-4, 5]	$f(x) = (x_1 + 10x_2)^2 + 5(x_3 + x_4)^2 + (x_2 - 2x_3)^4 + 10(x_1 - x_4)^4$	N	UN	0
F26	Quartic	[-128, 128]	$f_6(x) = \sum_{i=1}^n i x_i^4$	30	MS	0
F27	Rastrigin	[-5.12, 5.12]	$f_9(x) = \sum_{i=1}^n [x_i^2 - 10 \cos(2\pi x_i) + 10]$	30	MN	0
F28	Rotated hyperellipsoid	[-100, 100]	$f_3(x) = \sum_{i=1}^n \left(\sum_{j=1}^i x_j \right)$	N	U	0
F29	Rosenbrock	[-30, 30]	$f(x) = \sum_{i=1}^{n-1} [100(x_{i+1} - x_i^2)^2 + (x_i - 1)^2]$	30	UN	0
F30	Schwefel 2.26	[-500, 500]	$f(x) = \sum_{i=1}^n [-x_i \sin(\sqrt{ x_i })]$	N	MS	-418.983
F31	Schwefel 1.2	[-100, 100]	$f(x) = \sum_{i=1}^n \left(\sum_{j=1}^i x_j \right)^2$	30	UN	0

F32	Schwefel 2.22	[-100, 100]		$f(x) = \sum_{i=1}^n x_i + \prod_{i=1}^n x_i $	30	UN	0
F33	Schwefel 2.21	[-100, 100]		$f(x) = \max\{ x_i , 1 \leq i \leq n\}$	N	US	0
F34	Sphere	[-100, 100]		$f_1(x) = \sum_{i=1}^n x_i^2$	30	US	0
F35	Step	[-100, 100]		$f(x) = \sum_{i=1}^n (\text{floor}(x_i) + 0.5)^2$	30	US	0
F36	Sum/SumSquares Function	[-10, 10]		$f(x) = \sum_{i=1}^n ix_i^2$	30	US	0
F37	Sum-Power	[-1, 1]		$f_8(x) = \sum_{i=1}^n x_i ^2$	N	US	0
F38	Sum of Different Power	[-100,100]		$f_{21}(x) = \sum_{i=1}^d x_i ^{i+1}$	N	US	0
F39	SR-F4	[-100,100]	Shifted and Rotated Bent Cigar Function		N		
F40	SR-F38	[-100,100]	Shifted and Rotated Sum of Different Power Function		N		
F41	SR-F45	[-100,100]	Shifted and Rotated Zakharov Function		N		
F42	SR-F29	[-100,100]	Shifted and Rotated Rosenbrock's Function		N	MN	0
F43	SR-F27	[-100,100]	Shifted and Rotated Rastrigin's Function		N	MS	0
F44	Wavy 1	[-100,100]		$f(x) = \sum_{i=1}^n x_i^2 + (\sum_{i=1}^n 0.5ix_i)^2 + (\sum_{i=1}^n 0.5ix_i)^4$	2	MS	0
F45	Zakharov	[-5, 10]		$f(x) = \frac{1}{n} \sum_{i=1}^n 1 - \cos(10x_i) e^{-\frac{1}{2}x_i^2}$	10	UN	0
F46	Salomon	[-100, 100]		$f_{19}(x) = 1 - \cos\left(2\pi \sqrt{\sum_{i=1}^n x_i^2}\right) + 0.1 \sqrt{\sum_{i=1}^n x_i^2}$	N	MN	0
F47	Weierstrass Function	[-0.5, 0.5]		$f(x) = \sum_{i=1}^D (\sum_{k=0}^{20} [0.5^k \cos(2\pi \cdot 3^k (x_i + 0.5))])$	50	MN	0

The list of common standard literature benchmark functions outlined in Table 3 is used to test and evaluate the quality of the proposed EOSA algorithm. The literature provides a classification for each of these functions to demonstrate the expected performance they are to show. Whereas many test functions are continuous, they are further categorized into four (4). In the first class are test functions characterized by unimodal, convex, and multidimensional forms. They represent a class of test functions with interesting functions with cases capable of slowing down convergence or even yielding a poor convergence. The resulting convergence trails from such a slow pace to a single global extremum. The second class consists of test functions of type multimodal, two-dimensional with a small number of local extremes. This category of test functions appeals to situations where we intend to test the quality of standard optimization procedures in an anticipated hostile environment. This hostile environment describes problem domains with only a few local extremes with a single global one.

The third and fourth classes collect a list of test functions known as multimodal, two-dimensional with a huge number of local extremes, and multimodal, multidimensional, with a huge number of local extremes, respectively. It has been shown that these test functions work well for situations where the quality of intelligent and resistant optimization algorithms are tested (Jamil & Yang, 2013), (Yang, 2010), (Molga & Smutnicki, 2020), (Digalakis & Margariti, 2014), (Hussain, Salleh, Cheng, & Naseem, 2017). The proposed EOSA method was also tested on 30 benchmark functions from IEEE CEC.

4.4 Evaluation Method

The following criteria are considered in the performance evaluation: mean, median, standard deviation, maximum values, minimum or worst values, average values, overall convergence time, and average execution time. In addition to these, we applied the outcome of the proposed EOSA and related optimization algorithms to statistical tests to evaluate their performance in terms of convergence to determine algorithms capable of generating similar final solutions. These metrics provide an unbiased platform for the comparison of algorithms discussed.

5. Result and Discussion

A detailed performance evaluation of the experiment's outcome carried out in Section 4 is presented and discussed in this Section. First, we study the performance of the proposed SEIR-HDVQ model to determine how effectively the model was able to describe the natural phenomenon associated with it. Thereafter, the performance of EOSA was compared with all selected metaheuristic algorithms experimented with. Performance evaluation is done using the values obtained while applying the optimization algorithms to the test functions discussed earlier. Finally, a discussion on the findings and suitability of the proposed EOSA algorithm is presented.

5.1 Simulation of EVD Propagation Based on SEIR-HDVQ model

This subsection presents the result of simulating the proposed SEIR-HDVQ model with the same randomly generated data applied to the experimentation of EOSA. This result is reported to investigate the rate at which the SEIR-HDVQ model represents corresponding curves obtained in the real-life propagation model for the EVD and EBOV.

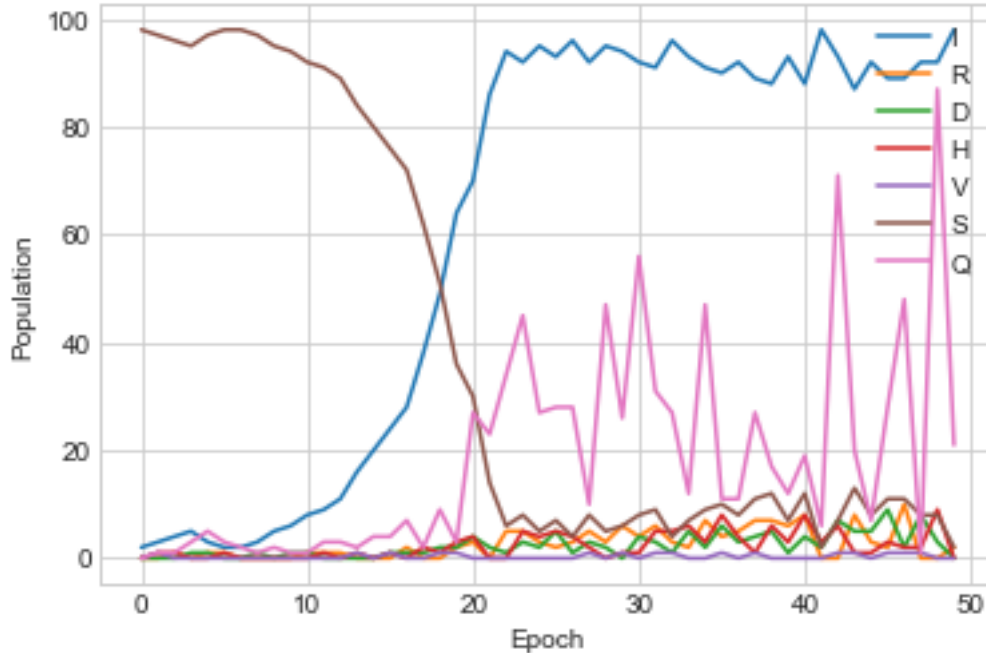


Figure 3: An estimated Ebola virus and disease propagation curve based on the simulation with randomly generated data while experimenting with the EOSA optimization algorithm. The curve illustrates variations in the values of Susceptible (S), Infected (I), Recovered (R), Hospitalized (H), Dead (D), Vaccinated (V), and Quarantine (Q) using the SEIR-HDVQ model

In Figure 3, the curves for Susceptible (S), Infected (I), Recovered (R), Hospitalized (H), Dead (D), Vaccinated (V), and Quarantine (Q) are captured so that they show the rate at which each compartment rises and falls within a period of fifty (50) epochs. In the figure, we observed that in the early phase of the outbreak, the infection rate rose against the susceptible population. The figure also revealed the response to the rising infection through quarantine measure, such that as infection rose, the number of quarantine individuals also increased – a measure to stem the outbreak. Meanwhile, we noticed that recovery and death rate curves wobbled along the curve of infection and quarantine.

5.2 Performance of EOSA with Similar Metaheuristic Algorithms Using Classical Benchmark functions

The performance of EOSA was compared with seven (7) different optimization algorithms, namely Artificial Bee Colony (ABC), Whale Optimization Algorithm (WOA), Butterfly Optimization Algorithm (BOA), Particle Swarm Optimization (PSO), Differential Evolution (DE), *Genetic Algorithm* (GA), and Henry gas solubility optimization algorithm (HGSO). The experimentation, which was executed for five hundred (500) iterations and twenty (20) different runs, applied forty-seven (47) standard benchmark functions.

In Table 4, the outcome for the best, worst, mean, median, and standard deviation for each of the 47 functions are listed. An overview of the result showed that although EOSA outperformed most of the algorithms in most cases for the 47 functions, some interesting differences were noticed to group the outcome into two. Whereas EOSA demonstrated a very close performance compared with ABC, WOA, BOA, and PSO, we observed that EOSA's outcome compared with DE, GA, and HGSO was significantly better. For example, for F1-4, F6-7, F12, F14-15, F18, F20-23, F2, F29-30, F32-36, F38, F40-43, and F46-47, EOSA clearly achieved the best values in all cases. However, in F5, F9-11, F13, F16-17, F19, and F25-26, EOSA was outperformed based on WOA and BOA, ABC, WOA, and PSO, ABC, BOA and PSO, ABC and PSO, ABC, ABC, WOA, and BOA, respectively. Meanwhile, we found some situations for the 47 functions where there was no clear superiority of EOSA over similar algorithms, neither were the similar algorithms able to demonstrate clear superiority. These cases are found in F28, F31, F37, F39, F44, and F45, where we observed that EOSA was beaten by ABC and PSO, beaten by WOA, BOA and PSO, ABC, matching values in ABC and PSO, beaten by WOA, and beaten by ABC, WOA, and PSO respectively

The values obtained for the worst, as shown in Table 4 for the 47 functions, revealed that there is an intense competition between EOSA and ABC, WOA, BOA, and PSO. We discovered that only in the cases of F3, F6, F12, F18, F22-23, F27, F29, F28, and F40-41 was the values of EOSA better than those earlier listed and was also completely outperformed those same algorithms in the cases of F13, F21, F25, and F32. We, however, noticed that the discrepancies reported by these algorithms in comparison with EOSA were not significantly large. Meanwhile, DE, GA, and HGSO have maintained a significant variation in the values obtained for those of best and worst computations. This implied that the proposed EOSA algorithm and its competitive related algorithms (ABC, WOA, BOA, and PSO) all significantly performed well over DE, GA, and HGSO.

Table 4: Comparison of best, worst, mean, median, and standard deviation values for ABC, WOA, BOA PSO, DE, GA, and HGSO metaheuristic algorithms using the classical benchmark functions over 500 runs and 100 population size

		ABC	WOA	BOA	PSO	EOSA	DE	GA	HGSO
F1	best	0.046635003	0.046548228	0.046606998	0.046595289	0.046579079	19.96184399	9.834179892	4.44E-16
	worst	20.90485862	0.046548228	0.046606998	0.046595289	0.046590768	20.91052673	19.84903108	17.47294741
	mean	19.35207569	0.046548228	0.046606998	0.046595289	0.046579273	20.0105497	10.33766475	0.224608623
	median	19.21059815	0.046548228	0.046606998	0.046595289	0.046579079	19.96347193	10.09803718	4.44E-16
	sd	0.943908994	4.86E-18	5.20E-18	5.20E-18	1.24E-06	0.146978912	0.961561963	1.441674873
F2	best	0.002749312	0.002795749	0.002762226	0.002778424	0.002735207	202.2092691	39.09706932	1.15E-59
	worst	243.8707278	0.002795749	0.002762226	0.002778424	0.002786444	243.8368578	181.9837599	151.3617491
	mean	33.43141849	0.002795749	0.002762226	0.002778424	0.002735311	223.0877822	43.99604306	1.067724803
	median	7.44293501	0.002795749	0.002762226	0.002778424	0.002735207	219.8379837	41.29894943	1.70E-31
	sd	52.1262757	4.12E-19	3.90E-19	4.34E-19	2.29E-06	13.7309761	10.72063849	10.27440175
F3	best	0.000414246	0.000406423	0.00041358	0.00040821	0.000341339	506.4395978	923.2199937	200
	worst	1459.126847	0.000406423	0.00041358	0.00040821	0.000402738	1511.839293	1242.053574	937.124982
	mean	290.8930668	0.000406423	0.00041358	0.00040821	0.000341484	766.5204487	940.9341817	203.9456023
	median	202.646981	0.000406423	0.00041358	0.00040821	0.000341339	689.7884683	931.4994158	200
	sd	219.6111673	3.79E-20	6.23E-20	7.32E-20	2.87E-06	242.3395941	28.42301313	44.96951031
F4	best	2.47E-12	2.48E-12	2.50E-12	2.44E-12	2.44E-12	1.46E+11	4106464761	8.23E-104
	worst	2.60168E+11	2.48E-12	2.50E-12	2.44E-12	2.44E-12	2.58E+11	1.35E+11	1.07E+11
	mean	2.04696E+11	2.48E-12	2.50E-12	2.44E-12	2.44E-12	2.06E+11	5647478875	489880801.7
	median	2.00955E+11	2.48E-12	2.50E-12	2.44E-12	2.44E-12	2.09E+11	4340687923	1.73E-49
	sd	13029284872	4.24E-28	3.23E-28	3.43E-28	4.27E-17	39224298697	7415345765	5813315095
F5	best	1.26E-06	1.23E-06	1.23E-06	1.24E-06	1.24E-06	293464.1073	10387.08092	0
	worst	513842.7078	1.23E-06	1.23E-06	1.24E-06	1.24E-06	510854.4233	271266.3555	198959.4441
	mean	408834.0144	1.23E-06	1.23E-06	1.24E-06	1.24E-06	389379.6679	13319.70525	1007.87092
	median	401536.9082	1.23E-06	1.23E-06	1.24E-06	1.24E-06	370976.4288	10947.76684	0
	sd	25604.25205	1.16E-22	1.59E-22	1.16E-22	9.72E-11	70462.61054	14783.10391	11466.50545
F6	best	2.40E-18	2.44E-18	2.37E-18	2.44E-18	2.37E-18	1.49E+17	53323511.38	44.10261447
	worst	1.45E+17	2.44E-18	2.37E-18	2.44E-18	2.40E-18	1.49E+17	2.52E+16	1.04E+16
	mean	6.40E+16	2.44E-18	2.37E-18	2.44E-18	2.37E-18	1.49E+17	5.83E+13	3.01E+13
	median	5.70E+16	2.44E-18	2.37E-18	2.44E-18	2.37E-18	1.49E+17	1670980321	44.12595826

	sd	1.59E+16	2.31E-34	2.50E-34	3.85E-34	1.55E-21	19.2	1.14E+15	5.15E+14
F7	best	2.86E-12	2.82E-12	2.76E-12	2.86E-12	2.57E-12	2.71E-146	865.7595089	1.02E-241
	worst	100289061.5	2.82E-12	2.76E-12	2.86E-12	2.80E-12	24647958.47	652837.5949	54779492.97
	mean	256702.4063	2.82E-12	2.76E-12	2.86E-12	2.57E-12	85506.69928	26635.78996	114542.9249
	median	548.2299318	2.82E-12	2.76E-12	2.86E-12	2.57E-12	3.40E-69	5236.830702	1.47E-122
	sd	4643773.174	3.64E-28	2.83E-28	3.43E-28	1.06E-14	1297580.095	84911.8986	2464983.02
F8	best	1.01E-10	1.02E-10	1.02E-10	1.01E-10	1.01E-10	152250.3059	11996.3679	1.22E-109
	worst	2219235.401	1.02E-10	1.02E-10	1.01E-10	1.02E-10	1083569.996	242291.8529	1472206.755
	mean	260786.7052	1.02E-10	1.02E-10	1.01E-10	1.01E-10	225703.8591	23799.47495	5060.550052
	median	247109.3042	1.02E-10	1.02E-10	1.01E-10	1.01E-10	202596.2197	14016.66679	6.40E-57
	sd	113140.258	1.81E-26	1.23E-26	1.42E-26	3.63E-14	99559.98645	29724.76944	73338.7961
F9	best	1.08E-19	1.16E-19	1.13E-19	1.04E-19	9.62E-20	1.00E-24	911.4244623	0.15590465
	worst	18770598227	1.16E-19	1.13E-19	1.04E-19	9.90E-20	92699584231	1419691418	3.69E+11
	mean	59781217.28	1.16E-19	1.13E-19	1.04E-19	9.62E-20	238666361.4	540844.124	745438916.6
	median	1010.651298	1.16E-19	1.13E-19	1.04E-19	9.62E-20	4.31E-07	1084.6816	0.426743166
	sd	1012213432	1.44E-35	1.69E-35	1.87E-35	1.25E-22	4423166355	78721555.39	16495993498
F10	best	0.000268707	0.000271867	0.000271857	0.000272074	0.000271605	1305.148346	37.97271859	0
	worst	2365.081755	0.000271867	0.000271857	0.000272074	0.000271631	2333.501515	1211.67998	758.1933658
	mean	1944.545227	0.000271867	0.000271857	0.000272074	0.000271605	1869.057115	52.82688221	3.586552218
	median	1927.15985	0.000271867	0.000271857	0.000272074	0.000271605	1869.71041	42.05742491	0
	sd	118.8407645	4.34E-20	3.52E-20	4.07E-20	1.29E-09	346.0828863	66.89207141	41.44826606
F11	best	1.71E-10	1.76E-10	1.72E-10	1.73E-10	1.72E-10	2394966487	4.159217166	1.02650854
	worst	2594482104	1.76E-10	1.72E-10	1.73E-10	1.74E-10	2567488472	678040718.4	429173991.9
	mean	975017964	1.76E-10	1.72E-10	1.73E-10	1.72E-10	2524020304	1702811.703	1632585.894
	median	835513938.7	1.76E-10	1.72E-10	1.73E-10	1.72E-10	2558711648	7.277752467	1.102714822
	sd	310620202.2	2.46E-26	1.94E-26	1.55E-26	1.13E-13	63720410.11	30979999.46	22580371.19
F12	best	0.00537744	0.005388969	0.005480457	0.005391917	0.003344178	59.10789733	6.976934078	9.850801272
	worst	106.5810109	0.005388969	0.005480457	0.005391917	0.004373574	107.3461889	63.34963883	43.96722626
	mean	11.41374051	0.005388969	0.005480457	0.005391917	0.003346353	81.28584828	8.490634765	10.05723641
	median	3.041798449	0.005388969	0.005480457	0.005391917	0.003344178	76.95222037	7.556693713	9.888497941

	sd	19.1491529	6.94E-19	8.67E-19	6.51E-19	4.69E-05	15.49249829	3.739496644	1.893231338
F13	best	3.65E-10	3.74E-10	3.66E-10	3.73E-10	3.74E-10	985634985.2	17956.26097	4950
	worst	1384897512	3.74E-10	3.66E-10	3.73E-10	3.75E-10	1361818654	464120523.3	340835146.7
	mean	889078912.1	3.74E-10	3.66E-10	3.73E-10	3.74E-10	1254140695	1772015.04	1336939.589
	median	851795363.5	3.74E-10	3.66E-10	3.73E-10	3.74E-10	1307126803	58264.23368	4950
	sd	94316100.35	3.88E-26	5.17E-26	5.95E-26	5.34E-14	129934049.2	22235444.11	17687769.58
F14	best	2.45E-06	2.45E-06	2.44E-06	2.42E-06	2.43E-06	150745.5792	4173.394244	0.5
	worst	263287.4203	2.45E-06	2.44E-06	2.42E-06	2.44E-06	262848.6996	139559.2807	75064.78913
	mean	205450.4186	2.45E-06	2.44E-06	2.42E-06	2.43E-06	207583.4194	5816.112605	366.1429711
	median	201684.2779	2.45E-06	2.44E-06	2.42E-06	2.43E-06	207654.9189	4635.050797	0.5
	sd	12935.14014	2.33E-22	3.39E-22	2.33E-22	1.64E-09	39242.75828	7628.700089	4110.579697
F15	best	2.77E-11	2.80E-11	2.74E-11	2.62E-11	2.70E-11	1756599198	6640180.976	1.37E-109
	worst	10468218437	2.80E-11	2.74E-11	2.62E-11	2.73E-11	11188908118	5342156920	5205941788
	mean	5419343203	2.80E-11	2.74E-11	2.62E-11	2.70E-11	3873865217	64605838.05	25839038.24
	median	5089210478	2.80E-11	2.74E-11	2.62E-11	2.70E-11	3205180965	16145847.47	4.70E-55
	sd	849483013.5	5.49E-27	4.85E-27	4.20E-27	3.21E-14	2157772540	295281070.4	296296090.2
F16	best	0.313183449	0.313642786	0.313833832	0.313841468	0.313411811	2.953082635	2.813194614	0
	worst	3.06604621	0.313642786	0.313833832	0.313841468	0.313489127	3.058624131	3.049294965	3.039113132
	mean	2.874483091	0.313642786	0.313833832	0.313841468	0.313412095	2.979055804	2.837486143	0.048640529
	median	2.858339278	0.313642786	0.313833832	0.313841468	0.313411811	2.973774936	2.828083314	0
	sd	0.123478977	4.16E-17	4.16E-17	3.05E-17	4.61E-06	0.023765099	0.034795524	0.3529256
F17	best	2.74E-11	2.79E-11	2.77E-11	2.74E-11	2.78E-11	1682987744	8124313.895	5.04E-111
	worst	11088768702	2.79E-11	2.77E-11	2.74E-11	2.78E-11	10720727065	5046542229	5836543916
	mean	5418948553	2.79E-11	2.77E-11	2.74E-11	2.78E-11	3789413735	69537793.4	36392422.41
	median	5064658325	2.79E-11	2.77E-11	2.74E-11	2.78E-11	3014132286	18167648.55	4.49E-55
	sd	885758421.1	4.20E-27	4.36E-27	4.52E-27	3.39E-15	2163046329	295379702.5	357170953.9
F18	best	0.065264947	0.055534741	0.065630095	0.065272135	0.046648475	11.29812226	4.736804364	0
	worst	11.507642	0.065329978	0.065630095	0.065272135	0.058911739	11.44580276	10.09038934	8.480262936
	mean	2.862967765	0.057169632	0.065630095	0.065272135	0.046680024	11.40128365	5.190692848	0.114397103
	median	1.559911469	0.055534741	0.065630095	0.065272135	0.046648475	11.44302638	4.917419975	0
	sd	2.575656552	0.003463235	1.04E-17	7.63E-18	0.000605181	0.064592634	0.739157175	0.754170922
F19	best	0.018649694	0.018759907	0.018764486	0.018698899	0.018690559	45.32931639	42.22016808	0

	worst	46.70160803	0.018759907	0.018764486	0.018698899	0.018746242	46.47403905	45.65285146	46.27336925
	mean	35.5326682	0.018759907	0.018764486	0.018698899	0.018690719	45.65823826	42.34684559	1.694447863
	median	34.73786127	0.018759907	0.018764486	0.018698899	0.018690559	45.65811462	42.33630398	1.134235292
	sd	2.631279754	2.60E-18	2.26E-18	1.91E-18	2.87E-06	0.31817398	0.272793571	5.762532227
F20	best	0.000250786	0.000246696	0.000249866	0.000252195	0.000246298	13.25336872	40.41662168	11.51810893
	worst	1477.956124	0.000246696	0.000249866	0.000252195	0.000247986	1437.269586	820.6332779	669.1654077
	mean	106.6199225	0.000246696	0.000249866	0.000252195	0.000246305	225.3094727	57.42482498	29.56622817
	median	14.32225309	0.000246696	0.000249866	0.000252195	0.000246298	64.6037593	46.02516801	19.93840466
	sd	235.2224648	2.98E-20	4.61E-20	3.39E-20	1.05E-07	322.074818	49.11711471	42.50885548
F21	best	0.001479242	0.001517382	0.001515007	0.001483363	0.001456843	6.978693002	20.75932802	0.75338742
	worst	323.037448	0.001517382	0.001515007	0.001483363	0.001525863	315.7329145	185.6204308	148.4719403
	mean	20.33662271	0.001517382	0.001515007	0.001483363	0.001457027	57.82178336	25.69890585	1.674645626
	median	2.67861904	0.001517382	0.001515007	0.001483363	0.001456843	28.30660489	22.13469236	0.753953307
	sd	48.64424139	2.49E-19	1.73E-19	1.63E-19	3.40E-06	69.53001349	11.49308344	9.058474116
F22	best	0.000267348	0.000268108	0.000264328	0.000267984	0.000122824	978.4644232	0.098573292	4.79E-05
	worst	1681.083806	0.000268108	0.000264328	0.000267984	0.00019473	1747.934015	561.5855192	247.2965395
	mean	115.8899526	0.000268108	0.000264328	0.000267984	0.000122984	1447.842362	2.207505659	0.73019635
	median	2.416271301	0.000268108	0.000264328	0.000267984	0.000122824	1484.787158	0.135816598	8.23E-05
	sd	300.0316907	4.61E-20	3.39E-20	4.07E-20	3.33E-06	279.6249961	26.86476596	11.68303402
F23	best	-302.5008149	-262.1755865	-182.7543715	-294.1230158	-16.54091663	-295.6844661	-	-270.8437899
	worst	-2.431610245	-226.2954225	-172.0744886	-204.9868298	-2.618649088	-221.660774	-	-220.8575849
	mean	-295.8858845	-259.1191967	-182.7082986	-284.8981188	-16.45742878	-290.057282	-	-266.4443466
	median	-301.8715247	-260.0368176	-182.7543715	-292.770422	-16.54091663	-293.8833165	-	-268.0098591
	sd	19.05436824	4.240456788	0.678269937	15.03776577	1.074758903	9.805001586	-	6.182581047
F25	best	1.73E-05	2.02E-05	2.19E-05	1.99E-05	2.22E-05	2.05E-29	0.005818419	2.98E-112
	worst	24.75787505	2.02E-05	2.19E-05	1.99E-05	2.25E-05	15.6011816	5.764924377	14.05993536
	mean	0.336241769	2.02E-05	2.19E-05	1.99E-05	2.22E-05	0.128138027	0.035160231	0.036388951
	median	0.004759136	2.02E-05	2.19E-05	1.99E-05	2.22E-05	1.17E-14	0.007171468	4.30E-51
	sd	1.716830508	3.05E-21	4.07E-21	2.71E-21	5.48E-08	1.159489759	0.298540229	0.653830959
F26	best	1.37E-10	1.36E-10	1.39E-10	1.39E-10	1.38E-10	2908169157	36768.89195	2.36E-07
	worst	3850449321	1.36E-10	1.39E-10	1.39E-10	1.39E-10	3685252577	1215212126	526426653.9
	mean	2393795142	1.36E-10	1.39E-10	1.39E-10	1.38E-10	3376494490	4715971.794	1701158.819

	median	2309813185	1.36E-10	1.39E-10	1.39E-10	1.38E-10	3399311165	165504.1559	2.36E-07
	sd	243210513.4	1.42E-26	1.94E-26	1.42E-26	3.00E-14	300829422.2	58549154.5	25984261.2
F27	best	0.00047527	0.00047985	0.000471891	0.000473586	0.000448786	1347.380357	749.9920473	0
	worst	1603.785958	0.00047985	0.000471891	0.000473586	0.000470662	1602.675545	1280.232203	1184.58447
	mean	451.6267178	0.00047985	0.000471891	0.000473586	0.000448847	1440.929879	772.4357583	11.72060634
	median	323.4669501	0.00047985	0.000471891	0.000473586	0.000448786	1418.535827	759.7515676	0
	sd	270.0398663	8.40E-20	5.15E-20	5.96E-20	1.10E-06	79.40879312	44.56932118	99.55250013
F28	best	1.07E-08	9.70E-09	9.31E-09	1.00E-08	9.25E-09	466932.353	12844.73759	1.67E-114
	worst	1022160.738	9.70E-09	9.31E-09	1.00E-08	9.93E-09	1011320.133	495929.0155	884512.6177
	mean	373004.6264	9.70E-09	9.31E-09	1.00E-08	9.25E-09	561177.5755	20051.98473	5008.283742
	median	344810.3587	9.70E-09	9.31E-09	1.00E-08	9.25E-09	537590.8983	15053.61311	2.68E-54
	sd	81563.46341	1.24E-24	1.36E-24	1.82E-24	3.71E-11	106070.0836	28150.07853	49908.74417
F29	best	4.59E-10	4.56E-10	4.50E-10	4.62E-10	4.51E-10	921421360.4	16533.59328	98.86771563
	worst	1085749209	4.56E-10	4.50E-10	4.62E-10	4.57E-10	1105359990	365586773.6	237130959.5
	mean	391773892	4.56E-10	4.50E-10	4.62E-10	4.51E-10	1041990575	1472601.153	746936.1114
	median	327193480.7	4.56E-10	4.50E-10	4.62E-10	4.51E-10	1048794876	58273.67518	98.88822056
	sd	141540445.4	6.98E-26	6.98E-26	9.31E-26	3.24E-13	68984880.73	17684842.71	11579159.04
F30	best	-8836.361886	-41041.09361	-82.284136	-8.37E+13	-1.77E+23	-10720.24772	-	-19627.1811
	worst	-0.06884986	-14838.49714	-55.03621215	-4236.486476	-0.073719104	-5231.572209	-	-4632.384271
	mean	-8466.742315	-40720.29286	-82.15043677	-4.29E+13	-1.75E+23	-9668.267461	-	-15952.69912
	median	-8755.05295	-41028.05197	-82.284136	-5.09E+13	-1.77E+23	-9966.438769	-	-16808.49531
	sd	735.9984565	1938.702109	1.754877788	3.92E+13	1.76E+22	1097.48294	-	3447.147118
F31	best	9.28E-09	1.08E-08	1.06E-08	1.04E-08	8.71E-09	466276.9769	13040.44756	1.04E-116
	worst	1183271.593	1.08E-08	1.06E-08	1.04E-08	8.99E-09	1097796.317	507957.0629	922710.1499
	mean	403966.8473	1.08E-08	1.06E-08	1.04E-08	8.71E-09	568102.224	20382.15347	4580.700889
	median	369094.2037	1.08E-08	1.06E-08	1.04E-08	8.71E-09	547682.4572	15390.81415	6.64E-59
	sd	95470.2388	1.08E-24	1.74E-24	1.86E-24	1.61E-11	109961.5849	28563.43898	50858.65247
F32	best	7.03E-167	1.69E-166	3.43E-166	2.37E-165	1.07E-166	4.99E+133	445.0616521	1.73E-58
	worst	8.34E+147	1.69E-166	3.43E-166	2.37E-165	4.44E-166	2.60E+146	3.58E+143	4.82E+135
	mean	1.68E+145	1.69E-166	3.43E-166	2.37E-165	1.26E-166	6.15E+144	7.26E+140	9.64E+132
	median	1.40E+106	1.69E-166	3.43E-166	2.37E-165	1.07E-166	7.01E+138	447.2618729	6.20E-31
	sd	3.73E+146	0	0	0	0	3.61E+145	1.60E+142	2.15E+134

F33	best	0.010001246	0.010001466	0.010000903	0.010000615	0.009960159	94.68547115	17.33513207	1.52E-57
	worst	94.81833964	0.010001466	0.010000903	0.010000615	0.010001165	94.68547115	81.02072384	57.37997572
	mean	87.26062108	0.010001466	0.010000903	0.010000615	0.009960264	94.68547115	19.58660243	0.520898377
	median	86.78228412	0.010001466	0.010000903	0.010000615	0.009960159	94.68547115	18.15536627	4.91E-27
	sd	4.179693275	7.81E-19	7.81E-19	1.39E-18	1.95E-06	8.53E-15	5.107576845	4.002551529
F34	best	2.39E-06	2.43E-06	2.49E-06	2.44E-06	2.42E-06	146564.3791	4151.903716	2.56E-92
	worst	257895.3838	2.43E-06	2.49E-06	2.44E-06	2.43E-06	257656.427	134925.0854	88039.69375
	mean	208128.671	2.43E-06	2.49E-06	2.44E-06	2.42E-06	200833.5123	5709.442348	687.5080256
	median	204667.8202	2.43E-06	2.49E-06	2.44E-06	2.42E-06	204872.6698	4541.823055	4.43E-29
	sd	13021.70178	1.91E-22	3.39E-22	2.33E-22	1.87E-10	40515.11285	7456.617438	5515.873891
F35	best	2.47E-06	2.43E-06	2.45E-06	2.44E-06	2.43E-06	149354.2611	4296.604798	19.93229264
	worst	257643.1306	2.43E-06	2.45E-06	2.44E-06	2.44E-06	261762.2494	138652.6906	91297.1041
	mean	205778.2306	2.43E-06	2.45E-06	2.44E-06	2.43E-06	204473.9907	5798.078168	401.736332
	median	201888.0566	2.43E-06	2.45E-06	2.44E-06	2.43E-06	204296.1293	4439.333834	21.13665172
	sd	13031.29588	3.18E-22	3.18E-22	2.33E-22	5.73E-10	39642.75925	7590.203072	4823.963514
F36	best	4.66E-06	4.61E-06	4.71E-06	4.72E-06	4.61E-06	66187.97685	1582.956209	1.63E-119
	worst	125317.1139	4.61E-06	4.71E-06	4.72E-06	4.66E-06	124112.1235	66662.76425	39912.02993
	mean	27848.95235	4.61E-06	4.71E-06	4.72E-06	4.61E-06	92944.77725	2388.574257	153.7211311
	median	18307.7666	4.61E-06	4.71E-06	4.72E-06	4.61E-06	90158.00805	1737.54854	2.68E-60
	sd	20873.64614	4.24E-22	7.62E-22	5.93E-22	2.90E-09	20130.48263	3711.651491	2089.954545
F37	best	0.000305122	0.023335766	0.024544119	0.024575999	0.011110877	14.4645922	0.409466028	6.78E-122
	worst	25.8151169	0.024556773	0.024544119	0.024575999	0.016303029	25.64204569	13.6419851	11.58066632
	mean	3.086996871	0.023597731	0.024544119	0.024575999	0.011125287	19.72266104	0.56836581	0.060472667
	median	0.118511189	0.023335766	0.024544119	0.024575999	0.011110877	18.95500975	0.447697234	3.98E-60
	sd	5.923666804	0.000498763	3.64E-18	3.64E-18	0.000258258	3.843309197	0.757549897	0.658790887
F38	best	8.34E-200	4.53E-200	3.09E-200	2.58E-200	1.58E-200	1.03E+153	1.50E+61	2.11E-62
	worst	1.21E+178	4.53E-200	3.09E-200	2.58E-200	2.18E-200	2.36E+175	1.89E+172	4.92E+167
	mean	2.42E+175	4.53E-200	3.09E-200	2.58E-200	1.58E-200	1.34E+173	3.78E+169	9.84E+164
	median	1.22E+162	4.53E-200	3.09E-200	2.58E-200	1.58E-200	1.35E+160	3.27E+81	1.96E-34
	sd	0	0	0	0	0	0	0	0
F39	best	2.46E-12	2.48E-12	2.47E-12	2.46E-12	2.46E-12	1.49E+11	4087014600	78062850.06
	worst	2.60533E+11	2.48E-12	2.47E-12	2.46E-12	2.47E-12	2.61E+11	1.35E+11	75834606829

	mean	2.02724E+11	2.48E-12	2.47E-12	2.46E-12	2.46E-12	2.05E+11	5631425626	752360824.7
	median	1.99043E+11	2.48E-12	2.47E-12	2.46E-12	2.46E-12	2.00E+11	4422413197	83482644.88
	sd	12748137431	3.43E-28	3.23E-28	3.03E-28	2.02E-16	39244378992	7381450963	5182164328
F40	best	3.01E-70	3.60E-70	2.93E-70	2.61E-70	2.02E-70	8.61E+48	1200.2428	1200.00029
	worst	4.50E+54	3.60E-70	2.93E-70	2.61E-70	2.53E-70	7.42E+54	1.37E+51	2.72E+54
	mean	1.09E+52	3.60E-70	2.93E-70	2.61E-70	2.02E-70	5.52E+53	5.37E+48	1.08E+52
	median	3.36E+45	3.60E-70	2.93E-70	2.61E-70	2.02E-70	9.18E+50	1201.064629	1200.000481
	sd	2.07E+53	3.58E-86	6.64E-86	4.02E-86	2.66E-72	1.69E+54	8.19E+49	1.71E+53
F41	best	5.69E-28	5.72E-28	5.76E-28	5.76E-28	5.53E-28	3.91E+26	1.13E+27	5.69E+26
	worst	1.09E+27	5.72E-28	5.76E-28	5.76E-28	5.65E-28	1.04E+27	1.13E+27	9.89E+26
	mean	9.31E+26	5.72E-28	5.76E-28	5.76E-28	5.53E-28	5.32E+26	1.13E+27	6.56E+26
	median	9.26E+26	5.72E-28	5.76E-28	5.76E-28	5.53E-28	5.00E+26	1.13E+27	6.32E+26
	sd	5.15E+25	7.17E-44	7.17E-44	5.83E-44	5.93E-31	1.31E+26	1.61E+24	7.69E+25
F42	best	4.27E-06	4.29E-06	4.26E-06	4.16E-06	4.09E-06	31976.73516	1188.933345	421.3277663
	worst	108535.2566	4.29E-06	4.26E-06	4.16E-06	4.17E-06	108929.7038	48344.70056	32891.91673
	mean	62929.59696	4.29E-06	4.26E-06	4.16E-06	4.09E-06	61436.09831	1620.118778	559.237889
	median	60073.02152	4.29E-06	4.26E-06	4.16E-06	4.09E-06	57366.81193	1310.196265	421.5626519
	sd	7334.315184	5.08E-22	5.08E-22	4.24E-22	5.31E-09	25706.21856	2466.571014	1710.546195
F43	best	0.000330323	0.000332408	0.000333684	0.000333589	0.00033233	2266.842103	1643.429176	942.528339
	worst	2479.036365	0.000332408	0.000333684	0.000333589	0.000333577	2493.325685	2169.822427	2069.438537
	mean	1909.413375	0.000332408	0.000333684	0.000333589	0.000332333	2359.039142	1679.482761	964.0878109
	median	1848.634581	0.000332408	0.000333684	0.000333589	0.00033233	2344.668872	1670.803483	944.5733014

	sd	157.8611421	3.79E-20	4.88E-20	3.79E-20	5.80E-08	66.81285479	46.64354787	104.1875831
F44	best	2.09E-29	1.78E-29	1.89E-29	2.03E-29	1.79E-29	438320.8487	110941.4238	592240.2576
	worst	2.76E+24	1.78E-29	1.89E-29	2.03E-29	1.93E-29	1.10E+24	1.04E+24	1.92E+23
	mean	1.43E+22	1.78E-29	1.89E-29	2.03E-29	1.79E-29	3.47E+21	3.14E+21	6.82E+20
	median	4.57E+18	1.78E-29	1.89E-29	2.03E-29	1.79E-29	463752.3183	137938.6535	614132.7943
	sd	1.59E+23	2.24E-45	3.01E-45	2.59E-45	6.78E-32	5.64E+22	5.05E+22	1.03E+22
F45	best	0.305715386	0.276970281	0.308726297	0.305443053	0.30646382	2.713949275	2.704585339	0
	worst	2.834155251	0.307895716	0.308726297	0.305443053	0.307290867	2.830118506	2.794061234	2.6140882
	mean	1.740456859	0.281499603	0.308726297	0.305443053	0.306468731	2.735885851	2.704932219	0.045569177
	median	1.619931442	0.276970281	0.308726297	0.305443053	0.30646382	2.723019587	2.704585339	0
	sd	0.264814711	0.010094625	3.61E-17	3.61E-17	6.02E-05	0.029287729	0.005105112	0.286856855
F46	best	2.46E-05	2.46E-05	2.44E-05	2.43E-05	2.44E-05	14557.36666	409.0949855	8.28E-108
	worst	26682.39023	2.46E-05	2.44E-05	2.43E-05	2.44E-05	26064.68463	13842.05832	9942.048708
	mean	20454.91167	2.46E-05	2.44E-05	2.43E-05	2.44E-05	20192.37282	565.2503799	57.57076258
	median	20071.41036	2.46E-05	2.44E-05	2.43E-05	2.44E-05	19688.65321	451.293936	5.07E-48
	sd	1324.806232	2.71E-21	3.22E-21	3.22E-21	4.47E-09	3845.341638	751.0738746	599.829055
F47	best	0.005888844	0.00587983	0.005866289	0.005919446	0.005858814	99.71266277	14.12662111	0
	worst	131.4206624	0.00587983	0.005866289	0.005919446	0.005890008	129.9725436	98.5658473	68.10191817
	mean	31.30562957	0.00587983	0.005866289	0.005919446	0.005858927	115.3842895	16.63768708	0.393527918
	median	7.982565255	0.00587983	0.005866289	0.005919446	0.005858814	114.8670662	14.94988815	0
	Sd	39.53996915	6.07E-19	7.81E-19	5.64E-19	1.84E-06	10.10326971	6.603864967	4.244564029

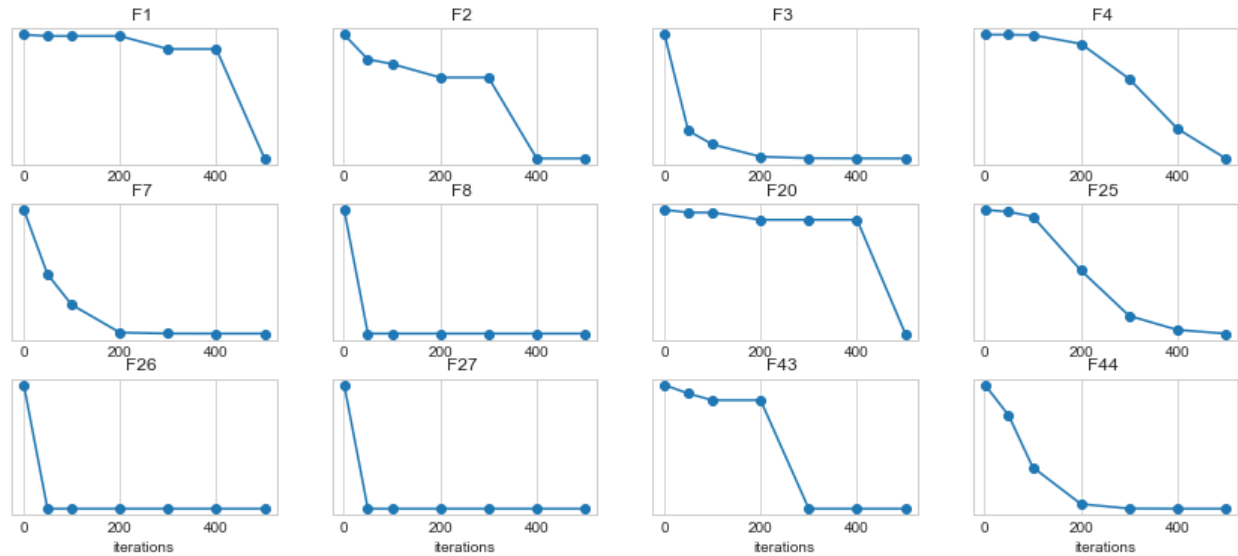


Figure 4: Convergent curves of EOSA on some selected standard benchmark functions over 1, 50, 100, 200, 300, 400, and 500 epochs

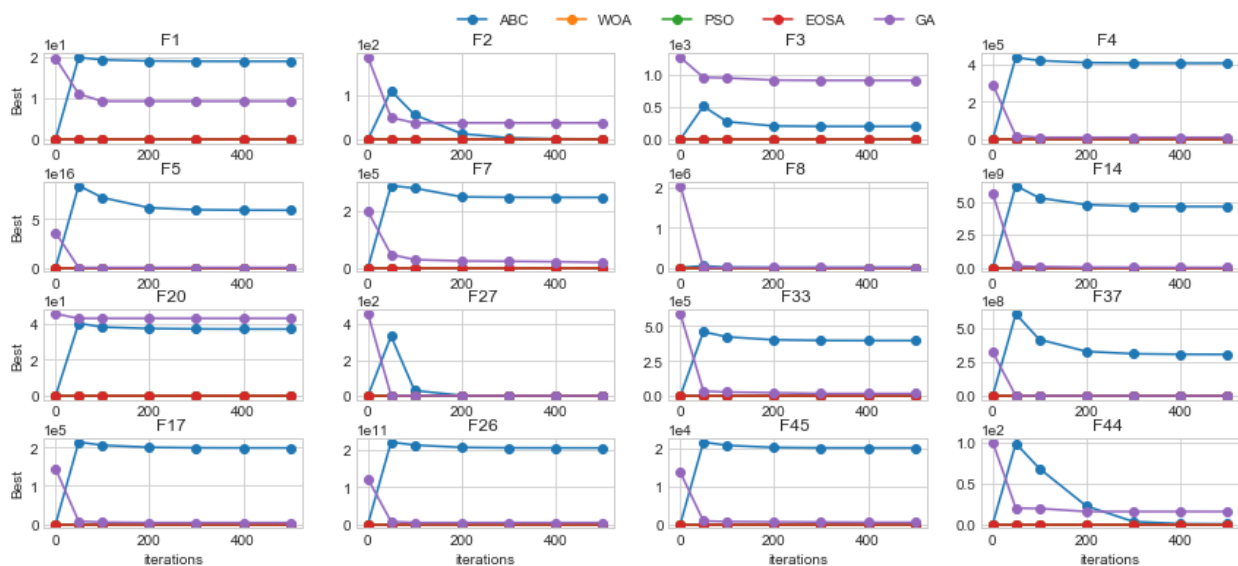


Figure 5: Convergent curves of EOSA and related optimization algorithms in some selected standard benchmark functions

To confirm the good performance and superiority of the EOSA, in Figure 4, the convergence curves of the history of solutions are graphed. The benchmark functions F1, F2, F3, F4, F7, F8, F20, F25, F26, F27, F43, and F45. We observed that in all cases, the curve of the plots descended appreciably. The implication is that the EOSA algorithm is a very competitive optimization algorithm that can discover optimum solutions both in the exploration and exploitation operations. To demonstrate the superiority of EOSA, when its convergence curve is plotted against those of state-of-the-art algorithms, we found that its solutions are significant.

The convergence of EOSA using the benchmark functions as compared ABC, WOA, PSO, and GA was graphed and illustrated in Figure 5. In most cases, the figures showed that the best values for all the algorithms were descending from their initial peak values to a lower value as the training improves over some epoch. The graphing was achieved by obtaining the best values for each case of EOSA, ABC, WOA, PSO, and GA at 1, 50, 100, 200, 300, 400, 500 iterations points. The figure confirms that the best values for GA are often larger than the others except in a few cases where ABC also has some large values. However, it is clear that ABC, WOA, PSO, and the proposed EOSA do not just have low value for the best cases but only drop in value for small fractions across all the iterations. This is

why their rise and fall in relation to their curves was not so pronounced in comparison with that of GA and sometimes ABC.

Perspective views, alongside the search history, of some selected functions, are shown in Figures 6 and 7. Again, to compare the performance of EOSA with other similar optimization algorithms, the illustrations in the figures were graphed with all the selected algorithms. The outcome for F1 function showed that EOSA appears to converge its points more closely compared with ABC while WOA showed only a point. However, in F3 and F34, PSO and GA respectively converged their point more closely than EOSA. Meanwhile, as in the F1 function, we found that EOSA converges its points more closely than BOA and ABC.

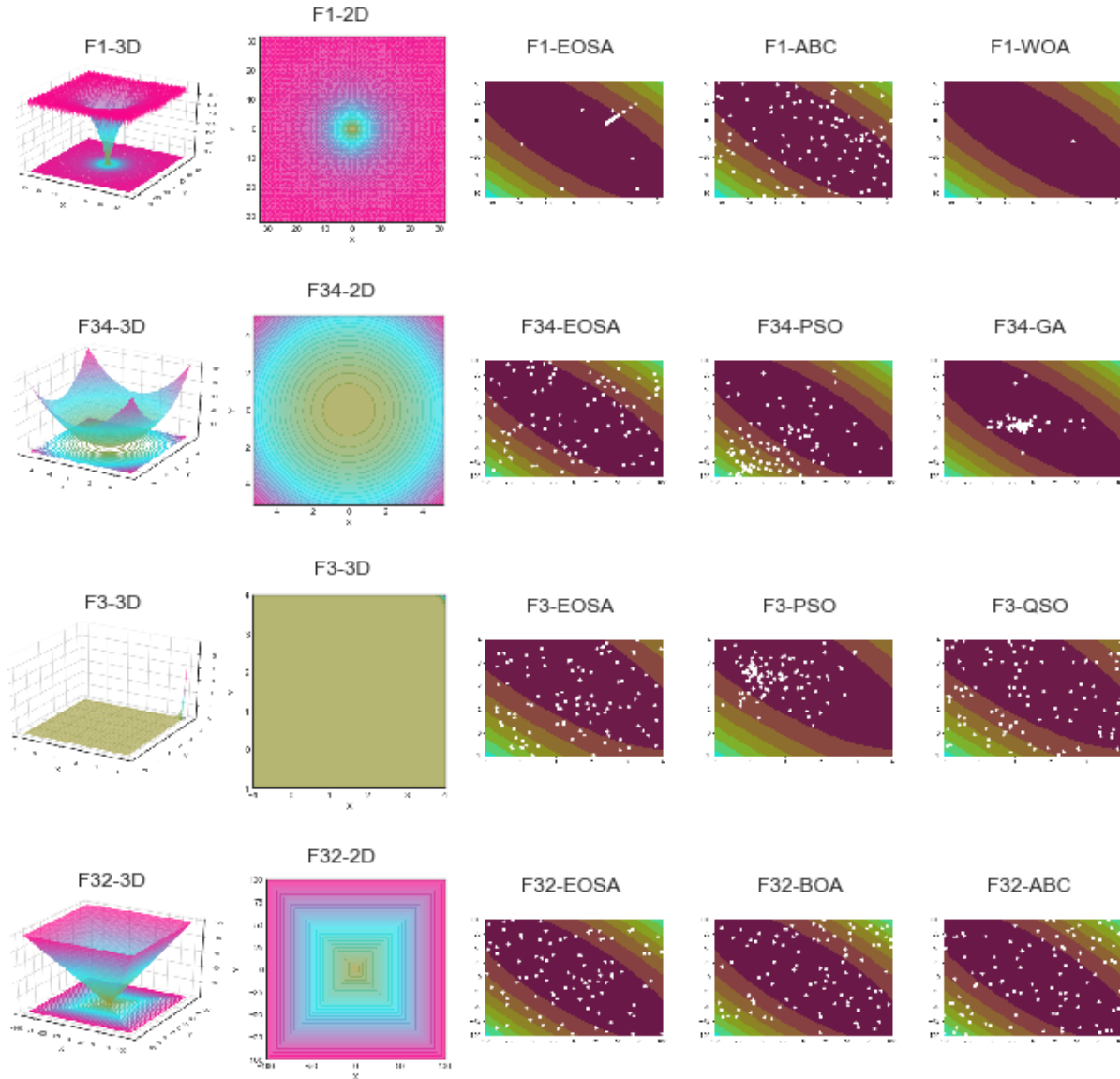


Figure 6: A 3D and 2D perspective view for functions F1, F3, F32, and F34 to 26 and their corresponding search history for EOSA and related optimization algorithms

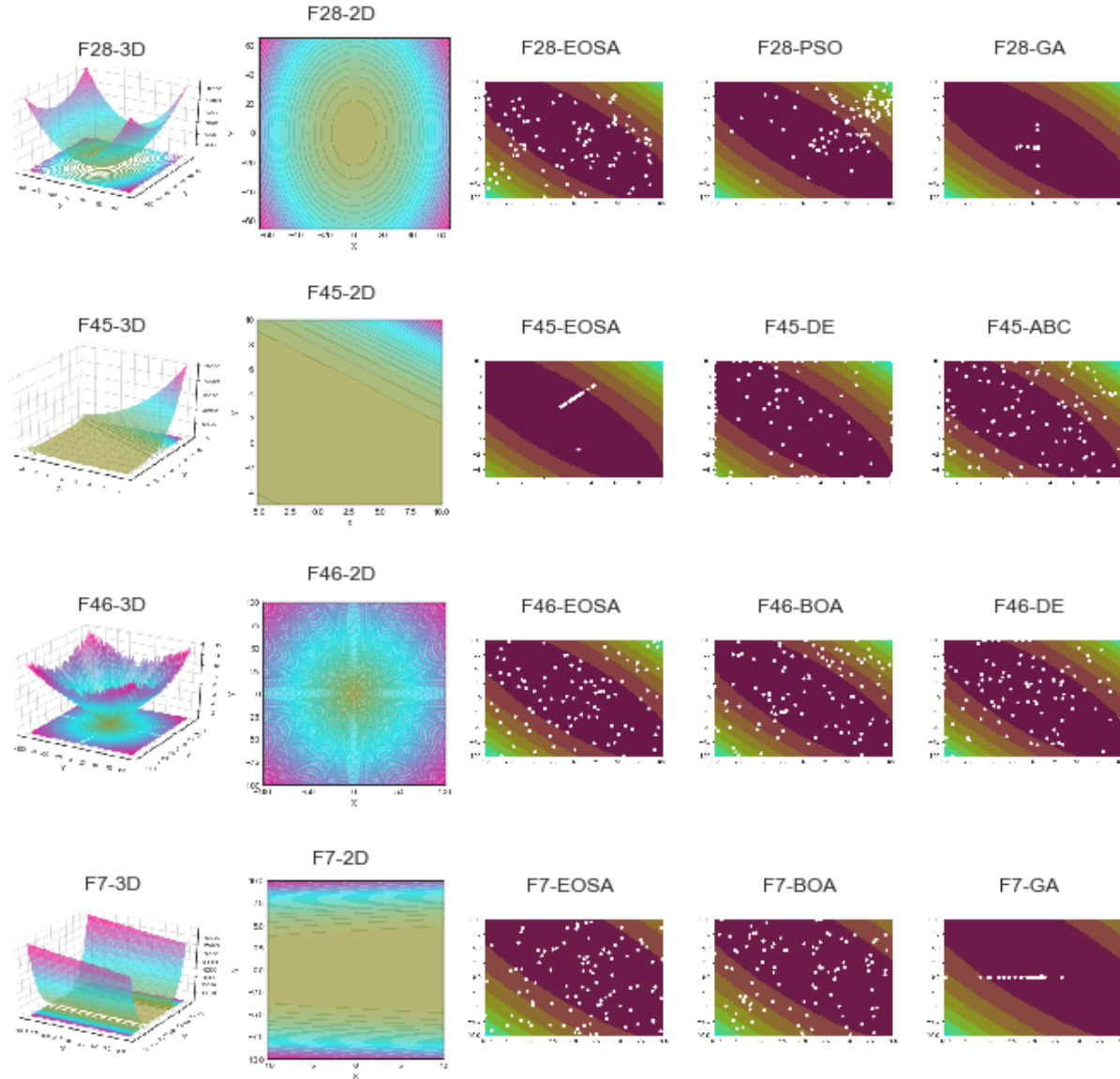


Figure 7: A 3D and 2D perspective view for functions F7, F28, F45, and F46 and their corresponding search history for EOSA and related optimization algorithms

The second illustration is shown in Figure 6 that only in F7 and F28 was GA able to cluster its points more closely compared with EOSA, PSO, BOA, DE, and ABC. While PSO attempts to achieve a clearer cluster in F28, EOSA also performs well in clustering of points or solutions in F7, F28, F45, and F46.

5.3 Evaluation of EOSA on Constrained CEC Benchmark functions

The result of experimentation with constrained functions of CEC was also collected and reported in this subsection. The CEC functions consist of fourteen (14) functions, and we further experimented with thirty (30) hybrids of the 14 CEC functions. The derivation for the hybrid functions is listed in Table 5. Functions C1-C8 and C10 are shifted versions of their corresponding CEC functions, while C9 and C11-C16 are shift-rotate versions of their corresponding CEC functions. Functions C17-C22 represent shift versions of a combination of some CEC functions, while those of C23-C30 are hybrids of predefined CEC hybrids. The total number of CEC-based functions used for the experiments is forty-four (44).

Table 5: Listing of thirty (30) hybrids of CEC functions applied to the proposed EOSA algorithm where shift is (S), and Shift rotate (SF)

Function	Hybrid CEC Functions	Function	Hybrid CEC Functions
C1	S CEC01	C16	SR CEC14
C2	S CEC02	C17	S [CEC09, CEC08, CEC01]
C3	S CEC03	C18	S [CEC02, CEC12, CEC08]
C4	S CEC04	C19	S [CEC07, CEC06,CEC04, CEC14]
C5	S CEC05	C20	S [CEC12, CEC03,CEC13, CEC08]
C6	S CEC06	C21	S [CEC14, CEC12,CEC04, CEC09, CEC01]
C7	S CEC07	C22	S [CEC10, CEC11,CEC13, CEC09, CEC05]
C8	S CEC08	C23	S(1,2,3,4,5) [C04, C01,C02, C03, C01]
C9	SR CEC08	C24	S(1,2,3) [C10, C09,C14]
C10	S CEC09	C25	S(1,2,3) [C11, C09,C01]
C11	SR CEC09	C26	S(1,2,3,4,5) [C11,C13,C01,C06, C07]
C12	SR CEC10	C27	S(1,2,3,4,5) [C14,C09,C11,C06, C01]
C13	SR CEC11	C28	S(1,2,3,4,5) [C15,C13,C13,C11, C16, C1]
C14	SR CEC12	C29	S(4,5,6) [C17,C18,C19]
C15	SR CEC13	C30	S(1,2,3) [C20,C21,C22]

Tables 6, 7, 8, 9 and 10 outline the outcome of experimenting with the forty-four (44) CEC functions regarding the best values, mean values, standard deviation, worst values, and median values, respectively. The results compare the performances of ABC, WOA, BOA PSO, DE, GA, and HGSO with EOSA based on the categories of outcome each table outlines. Regarding the best values, the result showed that EOSA outperformed all the related algorithms based on the CEC01, CEC03, CEC05-06, C3-4, C7-8, C15-16, C19-28, and C30 functions. Whereas it failed when compared with those related algorithms based on CEC07-CEC11, C2, C17-18, and C29 functions, we found out that it competed with the optimization algorithms based on CEC02 CEC04, CEC12-14, C1, C6, and C9-14functions.

Table 6: Comparison of best values for EOSA with ABC, WOA, BOA PSO, DE, GA, and HGSO metaheuristic algorithms using the CEC functions over 20 runs and 100 population size

	ABC	WOA	BOA	PSO	EOSA	DE	GA	HGSO
CEC_F1	2.78E-11	2.78E-11	2.75E-11	2.78E-11	2.75E-11	1.67E+09	6500451	1.22E-111
CEC_F2	2.49E-12	2.45E-12	2.48E-12	2.49E-12	2.48E-12	1.43E+11	4.17E+09	2.15E-104
CEC_F3	1.02E-10	1.02E-10	1.02E-10	1.03E-10	1.01E-10	150261.7	8666.065	2.06E-112
CEC_F4	3.68E-12	3.70E-12	3.73E-12	3.73E-12	3.71E-12	1.09E+11	1099091	98.82988
CEC_F5	0.045719	0.045711	0.045704	0.045704	0.045669	20.00005	18.25292	4.44E-16
CEC_F6	0.005831	0	0.005899	0.005873	0.005742	0	116.5891	0
CEC_F7	0.009643	0.009774	0.009701	0.009743	0.009735	41.81979	2.200358	0
CEC_F8	2.44E-06	2.40E-06	2.45E-06	2.44E-06	2.43E-06	136298.4	5267.792	0
CEC_F9	2.92E-05	2.91E-05	2.92E-05	2.94E-05	2.94E-05	14531.82	564.2694	0.001273
CEC_F10	0.002292	0	0.006114	0.006148	0.005866	0	41.94161	0
CEC_F11	0.00048	0.000473	0.000486	0.000486	0.000483	789.2033	31.14832	1.230663
CEC_F12	2.42E-06	2.43E-06	2.40E-06	2.41E-06	2.42E-06	149732	4302.336	0.499963
CEC_F13	2.35E-18	2.40E-18	2.44E-18	2.39E-18	2.37E-18	1.53E+17	33160379	43.51473
CEC_F14	0.019793	0.019827	0.019773	0.019808	0.019795	48.82636	45.96347	0
C_F1	2.73E-11	2.81E-11	2.77E-11	2.76E-11	2.76E-11	1.78E+09	6167884	1758730
C_F2	2.47E-12	2.45E-12	2.46E-12	2.46E-12	2.48E-12	1.49E+11	3.96E+09	79257090
C_F3	1.01E-10	1.01E-10	1.02E-10	1.02E-10	1.00E-10	154556.7	8413.72	511.0519
C_F4	4.25E-06	4.17E-06	4.26E-06	4.27E-06	4.22E-06	30378.79	1195.367	421.332
C_F5	0.001916	0.001916	0.001916	0.001916	0.001916	520	518.3289	503.618
C_F6	0.001302	0.001298	0.001298	0.001298	0.001299	698.3652	618.1048	600.2262
C_F7	0.000228	0.000227	0.000227	0.000226	0.000224	2044.892	761.7748	701.7483
C_F8	0.000345	0.000344	0.000344	0.000343	0.000343	2147.28	1557.367	843.4343

C_F9	0.00033	0.000334	0.000333	0.000332	0.000333	2255.36	1657.835	942.7569
C_F10	2.17E-05	2.19E-05	2.19E-05	2.18E-05	2.16E-05	34128.95	22425.71	1997.69
C_F11	2.19E-05	2.17E-05	2.17E-05	2.18E-05	2.17E-05	33964.55	22397.62	2114.091
C_F12	0.000734	0.000735	0.000733	0.000732	0.000734	1228.011	1241.808	1202.002
C_F13	0.000763	0.000763	0.000763	0.000763	0.000763	1305.976	1301.055	1301.188
C_F14	0.000411	0.000412	0.000414	0.000413	0.000412	1775.71	1417.828	1400.543
C_F15	2.50E-08	2.52E-08	2.49E-08	2.58E-08	2.44E-08	4632115	1589.511	1529.351
C_F16	0.000604	0.000604	0.000604	0.000604	0.0006	1642.558	1642.565	1633.591
C_F17	6.08E-11	6.27E-11	6.46E-11	6.51E-11	6.25E-11	31245659	972217.5	141272.7
C_F18	7.19E-12	7.38E-12	7.18E-12	7.31E-12	7.33E-12	1.64E+10	14568328	10901519
C_F19	1.02E-11	1.01E-11	1.04E-11	1.01E-11	1.01E-11	3.72E+09	31531.58	4856.103
C_F20	6.27E-18	6.13E-18	6.15E-18	6.31E-18	6.17E-18	1.57E+15	471768.5	3461.329
C_F21	1.33E-11	1.30E-11	1.34E-11	1.34E-11	1.27E-11	2.16E+09	755298.5	106452.7
C_F22	8.61E-18	8.51E-18	8.22E-18	8.94E-18	8.37E-18	4.65E+12	45227.98	2312.382
C_F23	4.36E-05	4.29E-05	4.27E-05	4.31E-05	4.23E-05	3614.32	2864.019	2427.505
C_F24	5.36E-05	5.35E-05	5.37E-05	5.37E-05	5.32E-05	13879.79	10012.92	3038.901
C_F25	0.000169	0.000168	0.000169	0.000169	0.000168	3201.834	3272.164	2719.248
C_F26	7.61E-05	7.58E-05	7.66E-05	7.61E-05	7.52E-05	7477.168	4168.648	2831.635
C_F27	4.39E-05	4.47E-05	4.40E-05	4.33E-05	4.34E-05	5538.155	5652.608	3297.419
C_F28	2.77E-05	2.77E-05	2.73E-05	2.77E-05	2.75E-05	12625.29	20133.18	3338.48
C_F29	1.01E-11	1.02E-11	1.04E-11	1.03E-11	1.02E-11	2.28E+10	19089355	4647940
C_F30	1.09E-17	1.10E-17	1.06E-17	1.11E-17	1.05E-17	1.09E-17	1615135	49862.93
AVG	2.07E-03	1.88E-03	2.15E-03	2.16E-03	2.15E-03	3.52E+15	1.87E+08	2.20E+06

Table 7: Comparison of mean values for EOSA with ABC, WOA, BOA PSO, DE, GA, and HGSO metaheuristic algorithms using the CEC functions over 20 runs and 100 population size

	ABC	WOA	BOA	PSO	EOSA	DE	GA	HGSO
CEC_F1	5.33E+09	2.78E-11	2.75E-11	2.78E-11	2.75E-11	3.83E+09	70517786	22571997
CEC_F2	2.06E+11	2.45E-12	2.48E-12	2.49E-12	2.48E-12	1.97E+11	5.72E+09	3.43E+08
CEC_F3	265756.9	1.02E-10	1.02E-10	1.03E-10	1.01E-10	229059.3	19263.3	5501.943
CEC_F4	8.86E+10	3.70E-12	3.73E-12	3.73E-12	3.71E-12	1.27E+11	1.78E+08	1.21E+08
CEC_F5	20.14394	0.045711	0.045704	0.045704	0.045669	20.04248	18.59328	0.538232
CEC_F6	18.67283	4.56E-05	0.005899	0.005873	0.005743	2.564157	118.74	0.236027
CEC_F7	53.29714	0.009774	0.009701	0.009743	0.009735	54.29449	2.550741	0.1217
CEC_F8	206645.9	2.40E-06	2.45E-06	2.44E-06	2.43E-06	201318.7	6854.159	555.4132
CEC_F9	19317.58	2.91E-05	2.92E-05	2.94E-05	2.94E-05	17770.2	743.7232	52.63696
CEC_F10	2.637136	8.98E-06	0.006114	0.006148	0.005868	0.005729	44.05648	0.000168
CEC_F11	1068.986	0.000473	0.000486	0.000486	0.000483	1073.152	39.1105	3.161078
CEC_F12	211335	2.43E-06	2.40E-06	2.41E-06	2.42E-06	207142.2	5722.981	404.0977
CEC_F13	6.38E+16	2.40E-18	2.44E-18	2.39E-18	2.37E-18	1.53E+17	5.95E+13	4.04E+13
CEC_F14	48.55728	0.019827	0.019773	0.019808	0.019795	49.02163	46.34748	1.215093
C_F1	5.17E+09	2.81E-11	2.77E-11	2.76E-11	2.76E-11	3.85E+09	68708917	35387699
C_F2	2.06E+11	2.45E-12	2.46E-12	2.46E-12	2.48E-12	2.07E+11	5.63E+09	4.76E+08
C_F3	264273.1	1.01E-10	1.02E-10	1.02E-10	1.00E-10	229257.4	18720.24	7385.135
C_F4	66642.05	4.17E-06	4.26E-06	4.27E-06	4.22E-06	60684.81	1629.658	601.2972
C_F5	519.1411	0.001916	0.001916	0.001916	0.001916	520.0447	518.6585	503.8836
C_F6	710.693	0.001298	0.001298	0.001298	0.001299	713.7333	620.3631	600.7176
C_F7	2558.992	0.000227	0.000227	0.000226	0.000224	2521.263	776.6596	707.6167
C_F8	1817.585	0.000344	0.000344	0.000343	0.000343	2229.991	1581.796	858.1452

C_F9	1918.445	0.000334	0.000333	0.000332	0.000333	2357.754	1683.917	954.2328
C_F10	23020	2.19E-05	2.19E-05	2.18E-05	2.16E-05	34606.45	23387.87	2446.736
C_F11	22642.04	2.17E-05	2.17E-05	2.18E-05	2.17E-05	34535.5	23444.82	2538.994
C_F12	1200.547	0.000735	0.000733	0.000732	0.000734	1231.839	1244.155	1203.938
C_F13	1304.738	0.000763	0.000763	0.000763	0.000763	1307.094	1301.152	1301.302
C_F14	1915.752	0.000412	0.000414	0.000413	0.000412	1909.953	1422.289	1401.656
C_F15	3991227	2.52E-08	2.49E-08	2.58E-08	2.44E-08	8250976	5798.619	2590.23
C_F16	1631.447	0.000604	0.000604	0.000604	0.0006	1642.966	1642.567	1635.098
C_F17	6.52E+08	6.27E-11	6.46E-11	6.51E-11	6.25E-11	2.35E+08	11945024	6293094
C_F18	3.41E+10	7.38E-12	7.18E-12	7.31E-12	7.34E-12	3.17E+10	3.32E+08	1.25E+08
C_F19	1.01E+10	1.01E-11	1.04E-11	1.01E-11	1.01E-11	1.07E+10	26262424	14398954
C_F20	3.09E+15	6.13E-18	6.15E-18	6.31E-18	6.17E-18	9.07E+15	3.96E+12	8.23E+12
C_F21	6.69E+09	1.30E-11	1.34E-11	1.34E-11	1.27E-11	5.96E+09	29193444	17906516
C_F22	5.71E+14	8.51E-18	8.22E-18	8.94E-18	8.37E-18	7.38E+14	7.24E+11	5.42E+12
C_F23	5648.371	4.29E-05	4.27E-05	4.31E-05	4.23E-05	4936.6	2915.359	2442.92
C_F24	10545.33	5.35E-05	5.37E-05	5.37E-05	5.32E-05	14160.14	10305.09	3177.754
C_F25	3470.654	0.000168	0.000169	0.000169	0.000168	3362.374	3294.278	2742.184
C_F26	8109.353	7.58E-05	7.66E-05	7.61E-05	7.52E-05	8290.179	4250.187	2857.924
C_F27	7333.635	4.47E-05	4.40E-05	4.33E-05	4.34E-05	6777.938	5851.102	3486.684
C_F28	17319.94	2.77E-05	2.73E-05	2.77E-05	2.75E-05	14334	20220.09	3719.304
C_F29	2.68E+10	1.02E-11	1.04E-11	1.03E-11	1.02E-11	3.07E+10	2.13E+08	93832603
C_F30	3.29E+14	1.10E-17	1.06E-17	1.11E-17	1.05E-17	1.09E+17	6.25E+11	8.25E+11
AVG	1.54E+15	1.89E-03	2.15E-03	2.16E-03	2.15E-03	3.71E+15	1.47E+12	1.25E+12

Table 8: Comparison of standard deviation values for EOSA with ABC, WOA, BOA PSO, DE, GA, and HGSO metaheuristic algorithms using the CEC functions over 20 runs and 100 population size

	ABC	WOA	BOA	PSO	EOSA	DE	GA	HGSO
CEC_F1	8.44E+08	3.39E-27	4.36E-27	3.88E-27	1.46E-15	2.13E+09	3.1E+08	2.43E+08
CEC_F2	1.3E+10	4.64E-28	3.03E-28	2.83E-28	9.11E-17	3.92E+10	7.53E+09	4.41E+09
CEC_F3	124317.8	1.36E-26	2.07E-26	2.13E-26	3.19E-14	80504.07	23773.8	94634.65
CEC_F4	9.64E+09	5.65E-28	6.26E-28	7.88E-28	1.35E-16	7.2E+09	2.26E+09	1.59E+09
CEC_F5	0.957905	5.90E-18	4.16E-18	5.90E-18	9.25E-07	0.146082	0.531952	2.67635
CEC_F6	28.93125	0.000486	1.08E-18	6.94E-19	8.98E-06	9.64147	2.394845	2.535846
CEC_F7	3.287874	9.54E-19	1.04E-18	1.13E-18	5.86E-07	9.165075	1.842338	1.222283
CEC_F8	13463.5	3.18E-22	3.81E-22	3.18E-22	7.16E-11	44270.92	7394.998	5414.126
CEC_F9	1125.511	4.91E-21	4.91E-21	4.57E-21	7.61E-09	2475.684	812.3379	525.8539
CEC_F10	8.081229	0.000189	9.54E-19	1.04E-18	1.80E-05	0.079924	3.439061	0.003118
CEC_F11	67.00617	7.59E-20	6.78E-20	8.13E-20	2.51E-08	203.6223	38.53338	22.77025
CEC_F12	13017.52	2.75E-22	2.12E-22	3.18E-22	7.17E-11	40966.34	7434.063	4920.48
CEC_F13	1.56E+16	3.08E-34	3.08E-34	3.27E-34	6.53E-22	16	1.16E+15	7.79E+14
CEC_F14	2.18245	2.26E-18	2.60E-18	2.26E-18	1.36E-06	0.160205	0.52921	7.091001
C_F1	9.38E+08	5.65E-27	4.04E-27	3.72E-27	1.54E-15	2.18E+09	3.19E+08	3.53E+08
C_F2	1.27E+10	3.84E-28	3.43E-28	2.63E-28	5.13E-17	3.91E+10	7.35E+09	5.18E+09
C_F3	97428.44	1.42E-26	1.42E-26	1.42E-26	3.41E-14	85524.47	21249.39	92545.77
C_F4	7311.002	6.56E-22	5.08E-22	7.41E-22	1.73E-09	25164.55	2379.42	1832.528
C_F5	23.24212	3.79E-19	2.93E-19	2.49E-19	7.25E-10	0.144908	0.504494	1.673248
C_F6	31.98589	1.52E-19	1.30E-19	1.63E-19	8.59E-09	10.84148	6.159877	4.5231
C_F7	141.8918	4.07E-20	3.39E-20	3.25E-20	7.57E-09	329.3684	66.00672	52.04919
C_F8	156.4804	3.79E-20	3.52E-20	3.52E-20	4.04E-08	78.9143	44.58426	95.90718

C_F9	158.7789	4.34E-20	3.25E-20	4.88E-20	1.49E-08	82.38662	45.19802	86.11494
C_F10	3268.026	2.20E-21	2.54E-21	1.86E-21	2.54E-09	423.4968	1633.723	2997.41
C_F11	3252.009	4.24E-21	3.05E-21	3.90E-21	1.13E-09	560.3687	1641.823	2811.823
C_F12	54.43402	1.03E-19	9.76E-20	1.03E-19	6.74E-08	4.051227	3.398669	5.949288
C_F13	58.4083	8.67E-20	1.03E-19	1.14E-19	9.74E-10	0.786165	0.315701	0.26207
C_F14	88.99855	7.05E-20	4.61E-20	6.51E-20	2.92E-09	91.06467	19.00835	10.87745
C_F15	989141.6	4.63E-24	2.98E-24	4.14E-24	3.48E-11	2442085	78999.93	20600.54
C_F16	73.05729	8.13E-20	4.34E-20	8.67E-20	2.35E-07	0.325375	0.037071	1.887207
C_F17	2E+08	9.37E-27	1.62E-26	9.69E-27	8.98E-15	3.7E+08	62967751	65905146
C_F18	4.48E+09	1.62E-27	1.29E-27	1.21E-27	1.91E-15	1.26E+10	1.79E+09	1.26E+09
C_F19	2.5E+09	1.13E-27	1.37E-27	1.37E-27	1.68E-15	6.61E+09	3.95E+08	2.2E+08
C_F20	2.2E+15	1.00E-33	1.16E-33	9.63E-34	2.07E-21	7.23E+15	8.15E+13	1.33E+14
C_F21	1.71E+09	1.94E-27	2.58E-27	2.02E-27	1.70E-15	4.08E+09	2.93E+08	2.81E+08
C_F22	6.8E+14	1.16E-33	1.39E-33	8.47E-34	2.69E-21	1.44E+15	1.49E+13	1.03E+14
C_F23	505.2743	6.10E-21	5.76E-21	6.10E-21	5.58E-09	1319.089	159.8902	144.9136
C_F24	1142.609	8.13E-21	8.13E-21	6.10E-21	7.63E-09	294.4141	523.598	873.6135
C_F25	172.4484	2.17E-20	2.57E-20	2.71E-20	1.41E-08	175.9663	26.39227	92.35979
C_F26	447.5749	8.81E-21	7.45E-21	8.81E-21	1.23E-08	609.1627	214.4841	201.5054
C_F27	555.7132	6.44E-21	5.08E-21	4.74E-21	9.68E-09	1223.351	231.5779	574.4783
C_F28	1546.707	3.73E-21	5.76E-21	4.07E-21	2.74E-09	1742.996	532.2733	2264.442
C_F29	2.8E+09	1.86E-27	1.62E-27	1.37E-27	1.54E-15	6.16E+09	1.15E+09	9.03E+08
C_F30	4.95E+14	1.54E-33	1.62E-33	1.39E-33	3.53E-21	1.05E-21	1.24E+13	1.7E+13
AVG	4.31E+14	1.54E-05	2.45E-19	2.74E-19	6.90E-07	1.97E+14	2.89E+13	2.34E+13

Table 9: Comparison of worst values for EOSA with ABC, WOA, BOA PSO, DE, GA, and HGSO metaheuristic algorithms using the CEC functions over 20 runs and 100 population size

	ABC	WOA	BOA	PSO	EOSA3	DE	GA	HGSO
CEC_F1	1.12E+10	2.78E-11	2.75E-11	2.78E-11	2.75E-11	1.04E+10	5.59E+09	4.16E+09
CEC_F2	2.59E+11	2.45E-12	2.48E-12	2.49E-12	2.48E-12	2.56E+11	1.38E+11	8.22E+10
CEC_F3	2687918	1.02E-10	1.02E-10	1.03E-10	1.02E-10	758263.8	210260.8	1949480
CEC_F4	1.36E+11	3.70E-12	3.73E-12	3.73E-12	3.71E-12	1.33E+11	4.71E+10	2.92E+10
CEC_F5	21.52029	0.045711	0.045704	0.045704	0.04568	21.17672	21.51461	20.26211
CEC_F6	131.4872	0.005909	0.005899	0.005873	0.005825	90.86362	129.6001	44.31723
CEC_F7	67.33259	0.009774	0.009701	0.009743	0.009748	66.20478	35.20829	21.53974
CEC_F8	262494.3	2.40E-06	2.45E-06	2.44E-06	2.43E-06	262963.7	136488.5	89507.12
CEC_F9	23595.96	2.91E-05	2.92E-05	2.94E-05	2.95E-05	23589.75	14244.41	8958.105
CEC_F10	63.28519	0.004209	0.006114	0.006148	0.006093	1.718978	64.79516	0.06861
CEC_F11	1327.766	0.000473	0.000486	0.000486	0.000484	1347.94	717.9246	422.4248
CEC_F12	262772.6	2.43E-06	2.40E-06	2.41E-06	2.42E-06	262112.5	134429.3	88298.64
CEC_F13	1.54E+17	2.40E-18	2.44E-18	2.39E-18	2.38E-18	1.53E+17	2.58E+16	1.71E+16
CEC_F14	49.52848	0.019827	0.019773	0.019808	0.019824	49.48733	49.33462	49.38548
C_F1	1.15E+10	2.81E-11	2.77E-11	2.76E-11	2.77E-11	1.11E+10	5.67E+09	6.19E+09
C_F2	2.58E+11	2.45E-12	2.46E-12	2.46E-12	2.48E-12	2.59E+11	1.33E+11	1.01E+11
C_F3	2103257	1.01E-10	1.02E-10	1.02E-10	1.01E-10	917649.9	250629.4	1908977
C_F4	105914.3	4.17E-06	4.26E-06	4.27E-06	4.26E-06	105781.7	46273.45	30893.76
C_F5	521.5171	0.001916	0.001916	0.001916	0.001916	521.1812	521.5299	519.7741
C_F6	730.2922	0.001298	0.001298	0.001298	0.001299	730.5756	696.6942	670.6866
C_F7	3079.45	0.000227	0.000227	0.000226	0.000224	3029.567	1923.113	1559.444
C_F8	2406.95	0.000344	0.000344	0.000343	0.000343	2400.625	2074.284	1962.092

C_F9	2506.628	0.000334	0.000333	0.000332	0.000334	2506.397	2177.013	2044.832
C_F10	36158.47	2.19E-05	2.19E-05	2.18E-05	2.17E-05	36205.08	34710.49	33711.3
C_F11	36240.38	2.17E-05	2.17E-05	2.18E-05	2.17E-05	36030.53	34829.66	33964.02
C_F12	1264.28	0.000735	0.000733	0.000732	0.000734	1254.941	1261.787	1254.078
C_F13	1308.329	0.000763	0.000763	0.000763	0.000763	1308.369	1306.122	1304.812
C_F14	2070.763	0.000412	0.000414	0.000413	0.000412	2042.449	1748.141	1589.229
C_F15	10490478	2.52E-08	2.49E-08	2.58E-08	2.51E-08	10914694	1748135	444906.5
C_F16	1643.261	0.000604	0.000604	0.000604	0.000604	1643.697	1643.287	1643.891
C_F17	2.25E+09	6.27E-11	6.46E-11	6.51E-11	6.27E-11	2.25E+09	1.17E+09	1.18E+09
C_F18	5.88E+10	7.38E-12	7.18E-12	7.31E-12	7.35E-12	6.01E+10	3.2E+10	2.18E+10
C_F19	2.73E+10	1.01E-11	1.04E-11	1.01E-11	1.01E-11	2.44E+10	8.51E+09	4.48E+09
C_F20	2.05E+16	6.13E-18	6.15E-18	6.31E-18	6.21E-18	2.19E+16	1.81E+15	2.51E+15
C_F21	1.81E+10	1.30E-11	1.34E-11	1.34E-11	1.27E-11	1.79E+10	6.09E+09	5.93E+09
C_F22	7.01E+15	8.51E-18	8.22E-18	8.94E-18	8.43E-18	6.17E+15	3.32E+14	2.19E+15
C_F23	8511.456	4.29E-05	4.27E-05	4.31E-05	4.24E-05	8622.02	5437.081	4831.978
C_F24	15051.17	5.35E-05	5.37E-05	5.37E-05	5.34E-05	15014.57	14393.9	13420.02
C_F25	3955.273	0.000168	0.000169	0.000169	0.000168	3923.978	3536.828	3525.063
C_F26	9478.512	7.58E-05	7.66E-05	7.61E-05	7.55E-05	9528.773	7271.734	6069.047
C_F27	10435.93	4.47E-05	4.40E-05	4.33E-05	4.35E-05	10466.53	7279.321	8191.818
C_F28	23982.63	2.77E-05	2.73E-05	2.77E-05	2.76E-05	22936.38	24198.69	23592.56
C_F29	4.24E+10	1.02E-11	1.04E-11	1.03E-11	1.02E-11	4.14E+10	2.11E+10	1.53E+10
C_F30	5.34E+15	1.10E-17	1.06E-17	1.11E-17	1.06E-17	1.09E+17	2.77E+14	3.76E+14
AVG	4.25E+15	2.11E-03	2.15E-03	2.16E-03	2.15E-03	4.12E+15	6.41E+14	5.04E+14

Table 10: Comparison of median values for EOSA with ABC, WOA, BOA PSO, DE, GA, and HGSO metaheuristic algorithms using the CEC functions over 20 runs and 100 population size

	ABC	WOA	BOA	PSO	EOSA	DE	GA	HGSO
CEC_F1	4.97E+09	2.78E-11	2.75E-11	2.78E-11	2.75E-11	3.16E+09	17405089	7.98E-53
CEC_F2	2.02E+11	2.45E-12	2.48E-12	2.49E-12	2.48E-12	1.95E+11	4.44E+09	1.11E-54
CEC_F3	251561	1.02E-10	1.02E-10	1.03E-10	1.01E-10	211966.5	12804.61	3.54E-59
CEC_F4	8.5E+10	3.70E-12	3.73E-12	3.73E-12	3.71E-12	1.3E+11	5359283	98.87237
CEC_F5	20.02451	0.045711	0.045704	0.045704	0.045669	20.00025	18.40464	6.22E-16
CEC_F6	4.21278	0	0.005899	0.005873	0.005742	0.000395	118.3358	0
CEC_F7	52.42071	0.009774	0.009701	0.009743	0.009735	54.26327	2.251702	0
CEC_F8	202970.3	2.40E-06	2.45E-06	2.44E-06	2.43E-06	193545.9	5656.178	0
CEC_F9	19028.6	2.91E-05	2.92E-05	2.94E-05	2.94E-05	17241.84	608.2115	0.001273
CEC_F10	0.15593	0	0.006114	0.006148	0.005866	3.57E-06	42.45588	0
CEC_F11	1050.116	0.000473	0.000486	0.000486	0.000483	1037.34	32.65625	1.305509
CEC_F12	208014.3	2.43E-06	2.40E-06	2.41E-06	2.42E-06	203259.8	4502.993	0.499963
CEC_F13	5.70E+16	2.40E-18	2.44E-18	2.39E-18	2.37E-18	1.53E+17	1.44E+09	43.7952
CEC_F14	48.56286	0.019827	0.019773	0.019808	0.019795	48.98768	46.16493	0
C_F1	4.81E+09	2.81E-11	2.77E-11	2.76E-11	2.76E-11	3.07E+09	15800257	2539288
C_F2	2.02E+11	2.45E-12	2.46E-12	2.46E-12	2.48E-12	2.07E+11	4.48E+09	83310110
C_F3	251898.3	1.01E-10	1.02E-10	1.02E-10	1.00E-10	207464.7	12286.88	569.2232
C_F4	63680.08	4.17E-06	4.26E-06	4.27E-06	4.22E-06	53106.6	1289.325	421.5314
C_F5	520.0264	0.001916	0.001916	0.001916	0.001916	520	518.4432	503.6196
C_F6	710.5576	0.001298	0.001298	0.001298	0.001299	713.8983	619.0061	600.2345
C_F7	2526.215	0.000227	0.000227	0.000226	0.000224	2476.466	766.6583	701.7771
C_F8	1756.355	0.000344	0.000344	0.000343	0.000343	2205.942	1567.959	844.6982
C_F9	1857.348	0.000334	0.000333	0.000332	0.000333	2351.115	1671.562	944.6468
C_F10	21565.89	2.19E-05	2.19E-05	2.18E-05	2.16E-05	34546.78	22826.18	2051.625
C_F11	21202.09	2.17E-05	2.17E-05	2.18E-05	2.17E-05	34411.18	23005.81	2162.177
C_F12	1200.098	0.000735	0.000733	0.000732	0.000734	1230.866	1243.101	1202.801
C_F13	1307.277	0.000763	0.000763	0.000763	0.000763	1306.991	1301.12	1301.257

C_F14	1908.945	0.000412	0.000414	0.000413	0.000412	1894.814	1419.233	1400.575
C_F15	3574560	2.52E-08	2.49E-08	2.58E-08	2.44E-08	8643243	1592.3	1529.579
C_F16	1633.813	0.000604	0.000604	0.000604	0.0006	1643.018	1642.565	1634.636
C_F17	5.76E+08	6.27E-11	6.46E-11	6.51E-11	6.25E-11	92363316	2870311	249692.2
C_F18	3.25E+10	7.38E-12	7.18E-12	7.31E-12	7.33E-12	2.81E+10	50256334	14649820
C_F19	9.14E+09	1.01E-11	1.04E-11	1.01E-11	1.01E-11	8.3E+09	218340.8	6335.723
C_F20	2.34E+15	6.13E-18	6.15E-18	6.31E-18	6.17E-18	7.03E+15	11716450	3736.184
C_F21	6.05E+09	1.30E-11	1.34E-11	1.34E-11	1.27E-11	4.54E+09	2438312	166857.2
C_F22	3.46E+14	8.51E-18	8.22E-18	8.94E-18	8.37E-18	8.57E+13	1945742	2390.839
C_F23	5473.74	4.29E-05	4.27E-05	4.31E-05	4.23E-05	4454.57	2878.711	2428.272
C_F24	10065.35	5.35E-05	5.37E-05	5.37E-05	5.32E-05	14042.95	10141.77	3059.551
C_F25	3444.507	0.000168	0.000169	0.000169	0.000168	3299.447	3287.133	2726.605
C_F26	8002.961	7.58E-05	7.66E-05	7.61E-05	7.52E-05	8208.712	4185.872	2835.785
C_F27	7171.65	4.47E-05	4.40E-05	4.33E-05	4.34E-05	6358.864	5809.833	3329.576
C_F28	16715.8	2.77E-05	2.73E-05	2.77E-05	2.75E-05	13773.55	20133.18	3352.717
C_F29	2.57E+10	1.02E-11	1.04E-11	1.03E-11	1.02E-11	3E+10	47619482	5734789
C_F30	1.85E+14	1.10E-17	1.06E-17	1.11E-17	1.05E-17	1.09E-17	25582427	76134.32
AVG	1.36E+15	1.88E-03	2.15E-03	2.16E-03	2.15E-03	3.65E+15	2.40E+08	2.43E+06

Similarly, the result for the worst values for the 44 functions, as shown in its corresponding table, also reveals an interesting performance for the proposed EOSA. We discovered that EOSA obtained the same values with WOA, BOA, and PSO using C5, C13, and C16 functions, whereas the corresponding values for ABC, DE, GA, and HGSO were significantly large. Also, EOSA leaped in-between in its values when compared with WOA, BOA, and PSO based on CEC_F1-4, CEC_F7-8, CEC_F10-12, CEC_F14, C1, C3, C8-9, C11-12, C14-15, C17-20, C22, C25, and C29-30 functions, whereas it records an overall good performance for CEC05-06, CEC13, C4, C7, C10, C21, C23-24, and C26-28.

Mean values for EOSA, ABC, WOA, BOA, and PSO demonstrated a very close outcome with no clear leading algorithm in the cases of CEC01-04, CEC06, CEC08-10, CEC12, CEC14, C1, C4, C8-9, C11-12, C14, C18-20, C22, C25, and C27-29 functions. But for the CEC05, CEC07, CEC11, CEC13, C3, C7, C10, C15-17, C21, C23-24, C26, and C30 functions, the mean values of EOSA outperformed all related algorithms including ABC, DE, GA, and HGSO, while it lags behind for the C2 and C6 functions. We also observed that the same values were obtained for EOSA, WOA, BOA, and PSO for the C5 and C13.

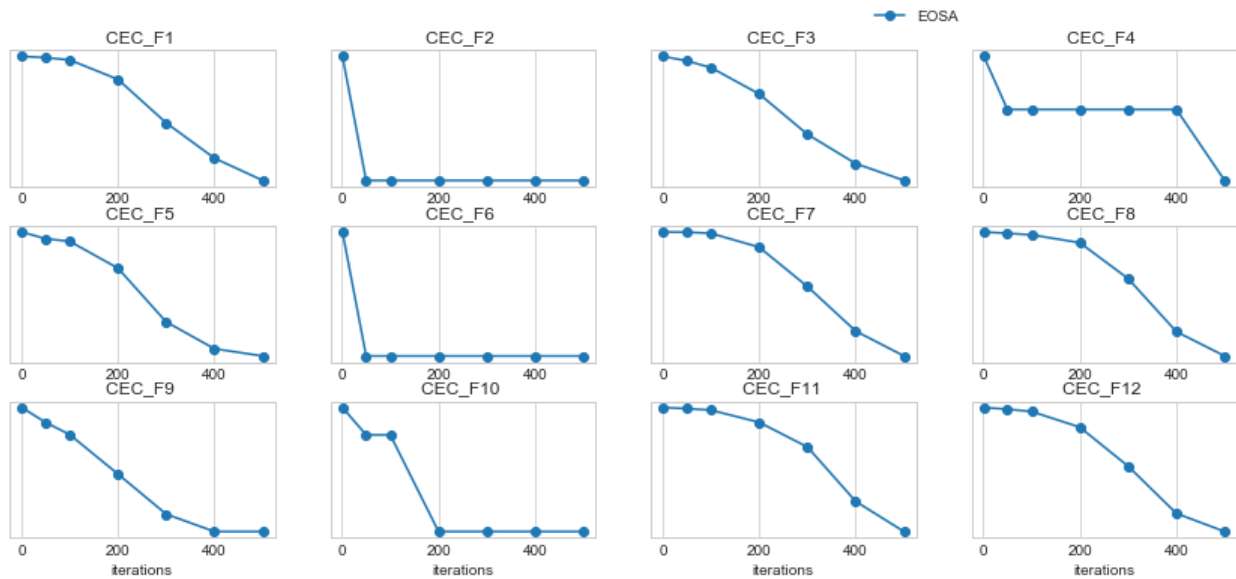


Figure 8: Convergent curves of EOSA on some selected CEC benchmark functions over 1, 50, 100, 200, 300, 400 and 500 epochs

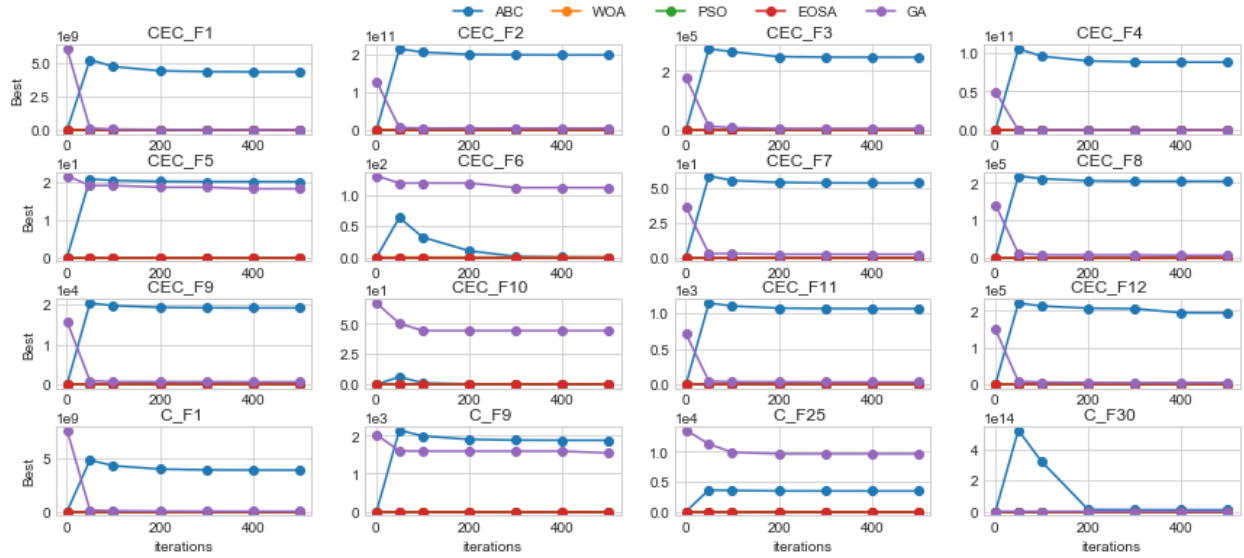


Figure 9: Convergent curves of EOSA and related optimization algorithms on some selected CEC functions

In Figure 8, the curves of the convergence of EOSA on the solutions of CEC benchmark functions are shown. We graphed the optimized solutions over 1, 50, 100, 200, 300, 400, and 500 epochs. To demonstrate this, we plot the curves of CEC_F1-14 and C_F1. The outcome of the pattern of the curves showed that the solutions were well optimized over the epochs. The convergence of the EOSA algorithm based on the best fit as compared with the best fits of ABC, WOA, BOA, PSO, DE, GA, and HGSO we plotted as shown in Figure 9. All the curves representing each optimisation algorithm showed a descent from high to low based on their best values. Although the curves of ABC and occasionally that of GA were often seen overshooting in values compared with others, we confirm that this is not unrelated to the significantly large values obtained by these algorithms (ABC and GA, with DE and HGSO inclusive). The curves of EOSA, WOA, BOA, and PSO appear to lie low, though with marginal descent overshadowed by ABC and GA continuously.

5.4 Computational requirement for EOSA and related algorithms on benchmark and CEC functions

The computational time required to run the optimization algorithms discussed in previous subsections was also recorded and reported in this subsection. We took an average of the computation time for all the forty-seven (47) standard benchmark functions and the forty-four (44) CEC-based functions. The outcome of these averages for ABC, WOA, BOA, PSO, DE, GA, and HGSO compared with EOSA are listed in Table 10. We discovered that the computational requirement of EOSA reports a minimal CPU time compared with other algorithms.

Table 10: Average computational requirements of ABC, WOA, BOA, PSO, QSO, DE, GA, and HGSO for forty-seven (47) benchmarks and forty-four (44) CEC for 500 runs and 100 population size

	ABC	WOA	BOA	PSO	EOSA	DE	GA	HGSO
Benchmark functions	450.9394	357.6453	418.0029	353.3408	132.1047	441.237	365.8788	442.8186
CEC	450.9394	357.6453	418.0029	353.3408	132.1047	441.237	365.8788	442.8186

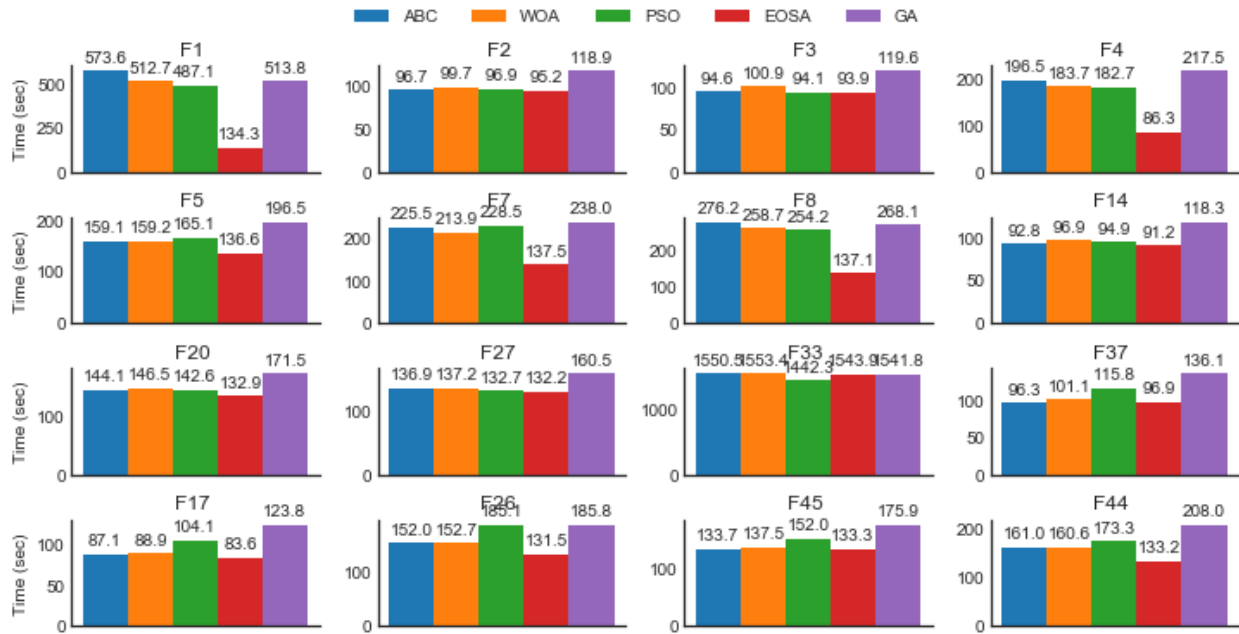


Figure 10: A graphical illustration of computational time required for the execution of EOSA compared with ABC, WOA, PSO, and GA for the standard benchmark functions

The computational requirement for executing all the algorithms on the standard benchmark functions was graphed as shown in Figure 10. We randomly selected some of these functions: F1, F2, F3, F4, F5, F7, F8, F14, F20, F27, F33, F37, F17, F26, D45, and F44. Although EOSA consumed the lowest CPU time in all cases, we noticed that the discrepancies in F27, F33, F2, and F14 were quite marginal. On the other hand, EOSA's computational requirements in F1, F4, and F8 were significantly low compared with related optimization algorithms.

Similarly, In Figure 11, the computational requirement for CEC-based functions was illustrated for some selected functions namely CEC01, CEC02, CEC03, CEC04, CEC05, CEC06, CEC07, CEC10, CEC11, CEC12, C1, C9, C25, and C30. In all cases, the CPU time for training EOSA showed to be lower than other related algorithms. While EOSA showed required less CPU time, GA and ABC were more demanding for this same computational resource. We note that the unusual computational time accounted for in some of the algorithms might not be unconnected with occasions when several algorithms experimented on the same system.

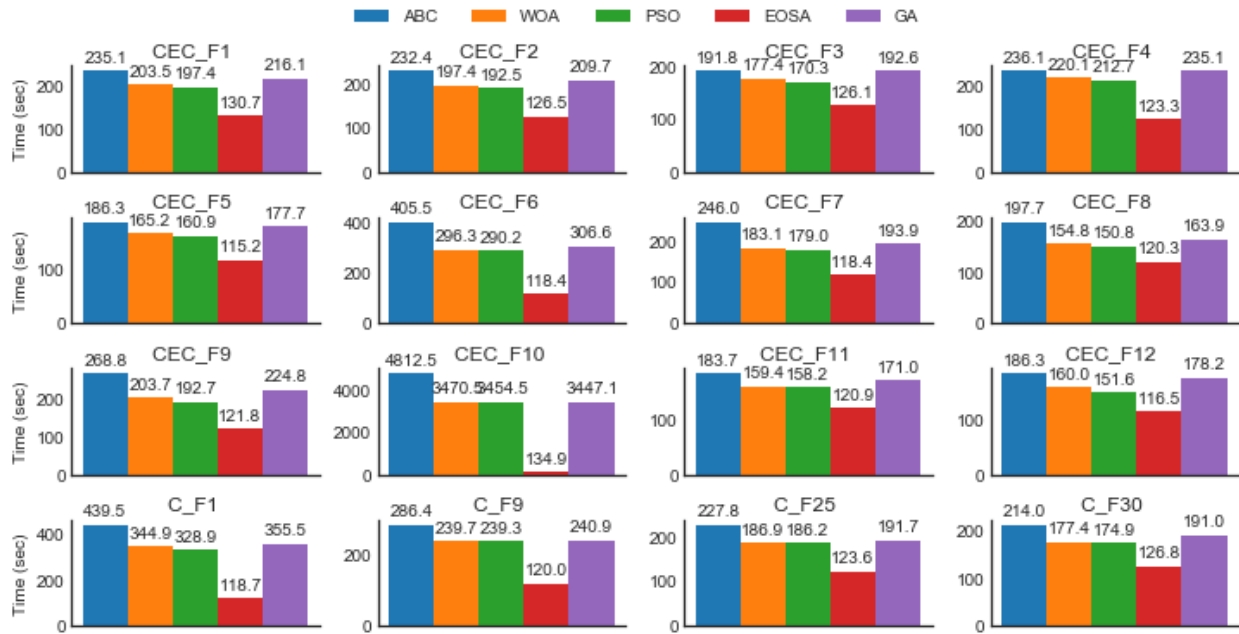


Figure 11: A graphical illustration of computational time required for the execution of EOSA compared with ABC, WOA, PSO, and GA for the CEC functions

5.5 Comparing the Performance of EOSA with Similar Methods Using Statistical Test

Using the results obtained from the forty-seven (47) standard benchmark functions, we validated the performance gain of EOSA as against those of ABC, WOA, BOA, PSO, DE, GA, and HGSO using statistical analysis. To achieve this, the Friedman mean the rank test was carried out, and the result obtained is as shown in Table 11. The results showed that the proposed EOSA method ranks best above all other methods by yielding the mean rank of 1.60. The PSO, WOA, and BOA trails after HGSO, GA, ABC, and DE follow in that order.

Table 11: Friedman mean Ranks test for EOSA compared with similar optimization algorithms

Algorithm	Mean rank
ABC	7.10
WOA	2.90
BOA	2.90
PSO	2.79
EOSA	1.60
DE	7.57
GA	6.12
HGSO	5.02

The test statistics (χ^2) result for the Friedman test revealed that there was an overall statistically significant difference between the mean ranks of the eight (8) methods: EOSA, ABC, WOA, BOA, PSO, GA, DE, and HGSO. The test statistics (χ^2) value of 249.847380 was obtained along with degrees of freedom (df) of 7 and significance level (Asymptotic Significance) of 0.001. We discovered a statistically significant difference in the performance of the eight (8) methods compared based on the values of $\chi^2(7) = 249.847380$, $p = 0.001$. The existence of this significant difference then necessitated the need for Wilcoxon signed-rank tests. Each method (optimization algorithm) was uniquely combined with EOSA to determine where the significance lies. Running the test, the results in Table 12 shows the post hoc output of the Wilcoxon signed-rank tests. The post hoc analysis confirms that there was a statistically significant reduction in perceived effort in the ABC-EOSA ($Z = -5.602$, $p = 0.001$), WOA-EOSA

($Z = -3.635$, $p = 0.001$), BOA-EOSA ($Z = -4.277$, $p = 0.001$), PSO-EOSA ($Z = -3.532$, $p = 0.001$), DE-EOSA ($Z = -5.613$, $p = 0.001$), GA-EOSA ($Z = -5.64$, $p = 0.001$), and HGSO-EOSA ($Z = -5.415$, $p = 0.001$).

Table 12: Wilcoxon Post hoc test of EOSA with each of the selected optimization methods

	ABC - EOSA	WOA - EOSA	BOA - EOSA	PSO - EOSA	DE - EOSA	GA - EOSA	HGSO - EOSA
Z	-5.602 ^b	-3.635 ^b	-4.277 ^b	-3.532 ^b	-5.613 ^b	-5.645 ^b	-5.415 ^b
Asymp. Sig. (2-tailed)	.000	.000	.000	.000	.000	.000	.000
a. Wilcoxon Signed Ranks Test							
b. Based on negative ranks.							

In summary, the argument that based on the outcome of the exhaustive experimentation done in this study, EOSA has shown to be a search algorithm capable of finding better solutions in a tight competition with state-of-the-art optimization algorithms. Also, that the proposed algorithm demonstrated that it could find far better solutions with fewer computational requirements compared with ABC, WOA, BOA, PSO, GA, DE, and HGSO methods.

6. Conclusion

This paper has presented a novel optimization algorithm, EOSA, based on the propagation model of the deadly Ebola virus and its associated disease. The study has shown how the bio-inspired algorithm derived its efficiency from the dynamic mechanism of moving individuals in the population through the susceptible, infected, quarantined, hospitalized, recovered, and dead sub-population. The study presented an improved version of the propagation model of the Ebola virus disease, which was further translated into a mathematical model. The resulting model was applied to the design of the design the novel optimization algorithm EOSA. We have applied EOSA to two sets of benchmark functions consisting of forty-seven (47) classical and over forty-four (44) constrained IEEE CEC-benchmark functions. The outcome of extensive experimentation to determine the algorithm's performance showed that it provides performance on a par with other population-based methods. Although the EOSA metaheuristic algorithm did not show superior performance in all cases, a significant outcome confirms it is very potent in handling optimization problems.

Moreover, considering the no-free lunch theorem, we safely conclude that the optimization fits into the body of recognized and viable optimization algorithms in the literature. A more interesting outcome of the proposed algorithm is the computational demand required for its performance. The result from the experimentation showed that the CPU time for the completion of the algorithm was substantially lower than some state-of-the-art optimization algorithm. This advantage will be more relevant and pronounced in applying the algorithm to real-world optimization problems, emphasizing time management. As future work, this study intends to investigate further strategies capable of maximizing greater balance between the exploration and exploitation phase of the algorithm. Also, the constraint of the new algorithm might be overcome using a hybridization solution with another optimization algorithm, demonstrating characteristics of eliminating the constraint.

Declaration of Competing Interest

The authors declare that they have no known competing financial interests or personal relationships that could have appeared to influence the work reported in this paper.

References

Association of Directors of Anatomic and Surgical Pathology. (2020, August 6). *Understanding Your Pathology Report: Breast Cancer*. Retrieved January 21, 2021, from American Cancer Society:

<https://www.cancer.org/treatment/understanding-your-diagnosis/tests/understanding-your-pathology-report/breast-pathology/breast-cancer-pathology.html>

- Abbas, A., Abdelsamea, M., & Gaber, M. (2020). Classification of COVID-19 in chest X-ray images using DeTraC deep convolutional neural network. *Applied Intelligence*, <https://doi.org/10.1007/s10489-020-01829-7>.
- Abdullayeva, A. (2019, September 11). *Clothes and color extraction with Generative Adversarial Network*. Retrieved March 16, 2020, from Towards Datascience: <https://towardsdatascience.com/clothes-and-color-extraction-with-generative-adversarial-network-80ba117e17e6>
- Achary, T., Pillay, S., Pillai, S. M., Mqadi, M., Genders, E., & Ezugwu, A. E. (2021). A performance study of meta-heuristic approaches for quadratic assignment problem. *Concurrency and Computation: Practice and Experience*, e6321.=.
- Adhikari, S. P., & Meng, S. (2020). Epidemiology, causes, clinical manifestation and diagnosis, prevention and control of coronavirus disease (COVID-19) during the early outbreak period: a scoping review . *Adhikari et al. Infectious Diseases of Poverty*.
- Agrebi, H. G., Bahri, A., & Bouaziz, R. (2009). Fuzzy Protégé for Fuzzy Ontology Models. *Conference: IPC'09*.
- Agushaka, O. J., & Ezugwu, A. E. (2020). Influence of Initializing Krill Herd Algorithm With Low-Discrepancy Sequences. *IEEE Access*, 8, 210886-210909.
- AI, MC. (2019, December 6). *How to fight mode collapse in GANs*. Retrieved March 30, 2020, from MC AI: <https://mc.ai/how-to-fight-mode-collapse-in-gans/>
- Al-antari, M. A., Hua, C.-H., & Lee, S. (2020). Fast Deep Learning Computer-Aided Diagnosis against the Novel COVID-19 pandemic from Digital Chest X-ray Images. *Applied Intelligence*, <https://doi.org/10.1007/s10489-020-02076-6>.
- Al-Betar, M., Alyasseri, Z., Awadallah, M., & Doush, I. A. (2020). Coronavirus herd immunity optimizer (CHIO). *Neural Computing and Applications*.
- Alexopoulos, P., & Mylonas, P. (2014). Towards vagueness-oriented quality assessment of ontologies. *Artificial Intelligent Methods and Application*, 8445(2014), 448-453.
- Alexopoulos, P., Wallace, M., Kafentzis, K., & Askounis, D. (2012). IKARUS-Onto: A methodology to develop fuzzy ontologies from crisp ones. *Knowledge and Information Systems*, 32(3), 667-695.
- Alphamoon. (2018, August 28). *Using GANs to dress up your photo*. Retrieved March 16, 2020, from Good Audience: <https://blog.goodaudience.com/using-gans-to-dress-up-your-photo-c300de7330ef>
- Alqahtani, H., Kavakli-Thorne, M., & Kumar, G. (2019). Applications of Generative Adversarial Networks (GANs): An Updated Review. *Archives of Computational Methods in Engineering*.
- Amali, D., Bessie, G., & Dinakaran, M. (2019). Wildebeest herd optimization: A new global optimization algorithm inspired by wildebeest herding behaviour. *Journal of Intelligent & Fuzzy Systems*, 37(6), 8063 – 8076.
- Ameur, S. T., Sellami, D., Wendling, L., & Cloppet, F. (2019). Breast Cancer Diagnosis System Based on Semantic Analysis and Choquet Integral Feature Selection for High Risk Subjects. *Big Data Cogn. Comput*, 3(41), 1-24.

- Amira, A., & Amel, G. T. (2015). An Extension of Protégé for an Automatic Fuzzy-Ontology Building Using Clustering and FCA. *International Journal of Computer Science & Information Technology (IJCSIT)*, 7(2), 13-20.
- Antipov, G., Baccouche, M., & Dugelay, J. L. (2017). Face Aging With Conditional Generative Adversarial Networks. *arXiv*.
- Apostolopoulos, I., & Mpesiana, T. (2020). Covid-19: automatic detection from x-ray images utilizing transfer learning with convolutional neural networks. *Physical and Engineering Sciences in Medicine*.
- Arjovsky, M., Chintala, S., & Bottou, L. (2017). Wasserstein GAN. *arXiv:1701.07875 [stat.ML]*.
- Armanious, K., Jiang, C., Fischer, M., Küstner, T., Hepp, T., Nikolaou, K., . . . Yang, B. (2020). MedGAN: Medical image translation using GANs. *Computerized Medical Imaging and Graphics*, 79.
- Asif, S., & Wenhui, Y. (2020). Automatic Detection of COVID-19 Using X-ray Images with Deep Convolutional Neural Networks and Machine Learning. *medRxiv*.
- Asif, S., Wenhui, Y., Jin, H., Tao, Y., & Jinhai, S. (2020). Classification of COVID-19 from Chest X-ray images using Deep Convolutional Neural Networks. *medRxiv*.
- Asma, D., & Zizette, B. (2014). Fuzzy Ontology Evolution: Classification of a New Individual. *JOURNAL OF EMERGING TECHNOLOGIES IN WEB INTELLIGENCE*, 6(1), 9-14.
- Bacanin, N., Bezdán, T., Tuba, E., Strumberger, I., & Tuba, M. (2020). Monarch Butterfly Optimization Based Convolutional Neural Network Design. *Mathematics*, 8(936), 1-32.
- BALANICĂ, V., DUMITRACHE, I., CARAMIHAI, M., RAE, W., & HERBST, C. (2011). EVALUATION OF BREAST CANCER RISK BY USING FUZZY LOGIC. *U.P.B. Sci. Bull., Series C*, 73(1), 53-64.
- Barstugan, M., Ozkaya, U., & Ozturk, S. (2020). Coronavirus (covid-19) classification using ct images by machine learning methods. *preprint arXiv:2003.09424*.
- BBC. (2021, February 3). *Covid-19: Study showing Oxford vaccine slows virus spread 'superb' - Hancock*. Retrieved February 24, 2021, from BBC: <https://www.bbc.com/news/uk-55913913>
- Berge, T., Lubuma, J., Moremedi, G., Morris, N., & Kondera-Shava, R. (2017). A simple mathematical model for Ebola in Africa. *Journal of Biological Dynamics*, 11, 2017(1), 42-74.
- Bobillo, F. (n.d.). *Fuzzy DL*. Retrieved January 20, 2021, from Fuzzy DL: <http://www.umbertostraccia.it/cs/software/fuzzyDL/fuzzyDL.html>
- Bobillo, F. (n.d.). *Fuzzy Ontology Representation using OWL 2*. Retrieved January 20, 2021, from Fuzzy Ontology Representation using OWL 2: <http://www.umbertostraccia.it/cs/software/FuzzyOWL/>
- Bobillo, F., & Straccia, U. (2016). The fuzzy ontology reasoner fuzzyDL. *Knowledge-Based Systems*, 12-34.
- Bobillo, F., Calvo-Flores, M. D., & Gómez-Romero, J. (2012). DeLorean: A reasoner for fuzzy OWL 2. *Expert Systems with Applications*, 39(1), 258-272. Retrieved January 20, 2021, from webdiis.unizar.es/~fbobillo/delorean
- Bobillo, F., & Straccia, U. (2011). Fuzzy ontology representation using OWL 2. *International Journal of Approximate Reasoning*, 52, 1073-1094.

- Brock, A., Donahue, J., & Simonyan, K. (2019). LARGE SCALE GAN TRAINING FOR HIGH FIDELITY NATURAL IMAGE SYNTHESIS. *arXiv:1809.11096v2 [cs.LG]*.
- CDC. (2021, January 14). *Ebola (Ebola Virus Disease)*. Retrieved February 19, 2021, from Centers for Disease Control and Prevention,: <https://www.cdc.gov/vhf/ebola/transmission/index.html>
- Changhee, H., Kohei, M., Shin'ichi, S., & Hideki, N. (2019). Learning More with Less: GAN-based Medical Image Augmentation. *MEDICAL IMAGING TECHNOLOGY*, 6.
- Chen, L., Lu, D., Zhu, M., Muzammal, M., Samuel, O. W., Huang, G., . . . Wu, H. (2019). OMDP: An ontology-based model for diagnosis and treatment of diabetes patients in remote healthcare systems. *International Journal of Distributed Sensor Networks*, 15(5), 1-15.
- Chen, T., Zhai, X., Ritter, M., Lucic, M., & Houlsby, N. (2019). Self-Supervised GANs via Auxiliary Rotation Loss. *arXiv:1811.11212 [cs.LG]*.
- Chen, X. (n.d.). *Image enhancement effect on the performance of convolutional neural networks*. Retrieved September 15, 2020, from Faculty of Computing Blekinge Institute of Technology SE-371 79 Karlskrona, Sweden.: <https://www.diva-portal.org/smash/get/diva2:1341096/FULLTEXT02>
- Chen, X., Duan, Y., Houthoof, R., Schulman, J., Sutskever, I., & Abbeel, P. (2016). InfoGAN: Interpretable Representation Learning by Information Maximizing Generative Adversarial Nets. *arXiv:1606.03657v1 [cs.LG]*.
- Cheng, R., Li, M., Tian, Y., Zhang, X., Yang, S., Jin, Y., & Yao, X. (2018). Benchmark Functions for the CEC'2018 Competition on Many-Objective Optimization. *Technical Report, University of Birmingham*.
- Chollet, F. (2016). Xception: Deep Learning with Depthwise Separable Convolutions. *arXiv:1610.02357 [cs.CV]*.
- Chowdhury, M., Rahman, T., Khandakar, A., Mazhar, R., Kadir, M., Mahbub, Z., . . . Islam, M. T. (2020). Can AI help in screening Viral and COVID-19 pneumonia? *IEEE Access*, 8(2020), 132665 - 132676.
- Cohen, J. P., Morrison, P., Dao, L., Roth, K., Duong, T. Q., & Ghassemi, M. (2020). COVID-19 Image Data Collection: Prospective Predictions Are the Future. *arXiv:2006.11988*, <https://github.com/ieee8023/covid-chestxray-dataset>.
- Costa, A., Oliveira, H., Catani, J., de Barros, N., Melo, C., & Vieira, M. (2020). Data augmentation for detection of architectural distortion in digital mammography using deep learning approach. . *Comput. Vis. Pattern Recognit. (2018)*. *arXiv:1807.03167*.
- COVIDNet. (n.d.). *COVIDNet*. Retrieved December 2, 2020, from COVIDNet: <https://github.com/iliaprc/COVIDNet>
- CREPINSEK, M., LIU, S.-H., & MERNIK, M. (2012). Exploration and Exploitation in Evolutionary Algorithms: A Survey. *ACM Comput. Survey*, 1-33.
- Cuevas, E., Echavarría, A., & Ramírez-Ortegón, M. (2014). An optimization algorithm inspired by the States of Matter that improves the balance between exploration and exploitation. *Applied Intelligence*, 40(2), 256-272.
- Darwish, A. (2018). Bio-inspired computing: Algorithms review, deep analysis, and the scope of applications. *Future Computing and Informatics Journal*, 3(2), 231-246.

- Dataset, A. C.-1.-r. (n.d.). Retrieved December 2, 2020, from <https://github.com/agchung/Actualmed-COVID-chestxray-dataset>
- Dataset, F. 1.-1.-r. (n.d.). Retrieved December 2, 2020, from <https://github.com/agchung/Figure1-COVID-chestxray-dataset>
- Demir, U., & Unal, G. (2018). Patch-Based Image Inpainting with Generative Adversarial Networks. *arXiv*.
- Dertat, A. (2017). *Applied Deep Learning - Part 4: Convolutional Neural Networks*. Retrieved March 13, 2020, from Towards Data Science: <https://towardsdatascience.com/applied-deep-learning-part-4-convolutional-neural-networks-584bc134c1e2>
- Dheebaa, J., N.Albert Singh, N., & S., T. S. (2014). Computer-aided detection of breast cancer on mammograms: A swarm intelligence optimized wavelet neural network approach. <https://doi.org/10.1016/j.jbi.2014.01.010>.
- Dhiman, G. (2019). ESA: a hybrid bio-inspired metaheuristic optimization approach for engineering problems. *Engineering with Computers*, 37(3).
- Dhingra, V., & Bhatia, K. K. (2015). Development of Ontology in Laptop Domain for Knowledge Representation. *Procedia Computer Science: International Conference on Information and Communication Technologies (ICICT 2014)*, 46(2015), 249 – 256.
- Digalakis, J., & Margariti, K. (2014). On benchmarking functions for genetic algorithms. *International Journal of Computer Mathematics*, 481-506.
- DINIS, B. (2017). OLD AND NEW APPROACHES TO THE SORITES PARADOX. *arXiv:1704.00450v1 [math.HO]*, 1-17.
- Disease Ontology. (n.d.). *Disease Ontology*. Retrieved January 20, 2021, from <https://disease-ontology.org/>
- Dong, E., Du, H., & Gardner, L. (2020). An interactive web-based dashboard to track COVID-19 in real time. *The Lancet infectious diseases*, 20(5), 533-534.
- DongLi, M., Zhao, H., Weng, X. W., & Han, T. (2016). A novel nature-inspired algorithm for optimization: Virus colony search. *Advances in Engineering Software*, 92, 65-88.
- Elhefny, M. A., Elmogy, M., & Elfetouh, A. A. (2017). Developing a fuzzy OWL ontology for obesity related cancer domain. *Int. J. Medical Engineering and Informatics*, 162-187.
- El-Sappagh, S., & Elmogy, M. (2017). A fuzzy ontology modeling for case base knowledge in diabetes mellitus domain. *Engineering Science and Technology, an International Journal*, 20(3), 1025-1040.
- Emami, H., Aliabadi, M. M., Dong, M., & Chinnam, R. B. (2019). SPA-GAN: Spatial Attention GAN for Image-to-Image Translation. *ArXiv, abs/1908.06616*.
- Eric, W., Kevin, W., David, C., & William, L. (2018). Conditional Infilling GANs for DataAugmentation in Mammogram Classification. *arXiv:1807.08093v2*.
- Ezugwu, A. E. (2019). Enhanced symbiotic organisms search algorithm for unrelated parallel machines manufacturing scheduling with setup times. *Knowledge-Based Systems*, 172, 15-32.
- Ezugwu, A. E., & Prayogo, D. (2019). Symbiotic organisms search algorithm: theory, recent advances and applications. *Expert systems with Applications*, 119, 184-209.

- Ezugwu, A. E., Adeleke, O. J., Akinyelu, A. A., & Viriri, S. (2020). A conceptual comparison of several metaheuristic algorithms on continuous optimisation problems. *Neural Computing and Applications*, 32(10), 6207-6251.
- Ezugwu, A. E., Adewumi, A. O., & Fr̄ncu, M. E. (2017). Simulated annealing based symbiotic organisms search optimization algorithm for traveling salesman problem. *Expert Systems with Applications*, 77, 189-210.
- Ezugwu, A. E., Shukla, A. K., Nath, R., Akinyelu, A. A., Agushaka, J. O., Chiroma, H., & Muhuri, P. K. (2021). Metaheuristics: a comprehensive overview and classification along with bibliometric analysis. *Artificial Intelligence Review*, 1-80.
- Fang, Y., Zhang, H., Xie, J., Lin, M., Ying, L., Pang, P., & Ji, W. (2020). Sensitivity of Chest CT for COVID-19: Comparison to RT-PCR. *Radiology*, <https://doi.org/10.1148/radiol.2020200432>, 296(2).
- Fermuller, C. G., & H`ajek, P. (2011). A Conversation About Fuzzy Logic and Vagueness. *A conversation*, 4015-416.
- Floyed Server. (n.d.). *Floyed*. Retrieved April 2, 2020, from Floyed: <https://www.floydhub.com/jobs>
- Fouda, H., Elmogy, M., Aboelfetoh, A., & Maat, A. R. (2015). Constructing Fuzzy Ontology for Cardiac Arrhythmias. *ICCES IEEE*, 402-409.
- Fukamizu, K., Kondo, M., & Sakamoto, R. (2019). Generation High resolution 3D model from natural language by Generative Adversarial Network. *arXiv*.
- Game, P., Vaze, V., & Emmanuel, M. (2020). Bio-inspired Optimization: metaheuristic algorithms for optimization. *National Conference on Emerging Trends, Challenges and Opportunities in Data Mining and Information Security (NTCOMIS-2020)*.
- Gedraite, E., & Hadad, M. (2011). Investigation on the effect of a Gaussian Blur in image filtering and segmentation. *Proceedings of ELMAR Conference*.
- Gerla, G. (2017). VAGUENESS AND FORMAL FUZZY LOGIC: SOME CRITICISMS. *Logic and Logical Philosophy*, 1-20.
- GHORBEL, H., BAHRI, A., & BOUAZIZ, R. (2010). Fuzzy Ontologies Building Method: Fuzzy OntoMethodology. *Conference Paper*, 1-9.
- Ghosh, A., Kulharia, V., Namboodiri, V., Torr, P. H., & Dokania, P. K. (2018). Multi-Agent Diverse Generative Adversarial Networks. *arXiv:1704.02906*.
- Godo, L´., & Gottwald, S. (2016). Fuzzy Sets and Formal Logics. *Fuzzy Sets and Systems*, 281, 44–60.
- Goodfellow, J. I., Pouget-Abadie, J., Mirza, M., Bing, X., Warde-Farley, D., Ozair, S., . . . Bengio, Y. (2014). Generative adversarial Network. *NIPS*.
- Google, D. (2020, 02 10). *Common Problems*. Retrieved March 17, 2020, from Generative Adversarial Networks: <https://developers.google.com/machine-learning/gan/problems>
- Green, D., Aleti, A., & Garcia, J. (2017). The Nature of Nature: Why Nature-Inspired Algorithms Work. *Modeling and Optimization in Science and Technologies*, https://doi.org/10.1007/978-3-319-50920-4_1, 10.

- Gu, H., Lv, H., Gao, J., & Shi, J. (2007). Towards a General Fuzzy Ontology and Its Construction. *College of Computer Science, Zhejiang University, Hangzhou*, 1-6.
- Guibas, J. T., Virdi, T. S., & Li, P. S. (2018). Synthetic Medical Images from Dual Generative Adversarial Networks. *arXiv:1709.01872v3 [cs.CV] 8 Jan 2018*, 9.
- Gulrajani, I., Ahmed, F., Arjovsky, M., Dumoulin, V., & Courville, A. (2017). Improved Training of Wasserstein GANs. *arXiv:1704.00028v3 [cs.LG]*.
- Gumusova, S., Sunbul, M., & Leblebicioglu, H. (2015). Ebola virus disease and the veterinary perspective. *Ann Clin Microbiol Antimicrob*, 14(30).
- Gurobi Optimizer. (n.d.). *Gurobi Optimizer*. Retrieved January 23, 2021, from Protege Wiki: https://protegewiki.stanford.edu/wiki/Gurobi_Optimizer
- Guruprasad, P. (2020). OVERVIEW OF DIFFERENT THRESHOLDING METHODS IN IMAGE PROCESSING. *TEQIP Sponsored 3rd National Conference on ETACC*.
- Hadjiiski, L., Sahiner, B., & Chan, H.-P. (2006). Advances in CAD for diagnosis of breast cancer. *Curr Opin Obstet Gynecol.*, 18(1), 64–70.
- Haldeman-Englert, C., Trevino, H., & Turley, K. (n.d.). *Albumin (Blood)*. Retrieved January 20, 2021, from University of Rochester Medical Center Health Encyclopedia: https://www.urmc.rochester.edu/encyclopedia/content.aspx?contenttypeid=167&contentid=albumin_blood
- Han Zhang, T. X., Zhang, S., Wang, X., Huang, X., & Metaxas, D. (2017). StackGAN: Text to Photo-realistic Image Synthesis with Stacked Generative Adversarial Networks. *arXiv*.
- Hashem, I. A., Ezugwu, A. E., Al-Garadi, M. A., Abdullahi, I. N., Otegbeye, O., Ahman, Q. O., & Chiroma, H. (2020). A Machine Learning Solution Framework for Combatting COVID-19 in Smart Cities from Multiple Dimensions. *medRxiv*.
- Heba, F., Mohammed, E., Ahmed, A., & Raziq, M. A. (2015). Constructing Fuzzy Ontology for Cardiac Arrhythmias. *Conference IEEE*, 402-409.
- Heinrich, G. (2017, April 20). *Photo Editing with Generative Adversarial Networks*. Retrieved March 16, 2020, from NVIDIA Developer: <https://devblogs.nvidia.com/photo-editing-generative-adversarial-networks-1/>
- Heras, S., Botti, V., & Juliana, V. (2013). A knowledge representation formalism for Case-Based-Reasoning. *Agreement Technol*, 105-119.
- Hu, S., Gao, Y., Niu, Z., Jiang, Y., Li, L., Xiao, X., & Ye, H. (2020). Weakly Supervised Deep Learning for COVID-19 Infection Detection and Classification from CT Images. *arXiv preprint arXiv:2004.06689*.
- Huang, R., Zhang, S., Li, T., & He, R. (2017). Beyond Face Rotation: Global and Local Perception GAN for Photorealistic and Identity Preserving Frontal View Synthesis. *arXiv*, 1-11.
- Hui, J. (2019, June 22). *GAN — Some cool applications of GAN*. Retrieved March 16, 2020, from Medium: https://medium.com/@jonathan_hui/gan-some-cool-applications-of-gans-4c9ecca35900
- Huikai, W., Shuai, Z., Junge, Z., & Kaiqi, H. (2017). GP-GAN: Towards Realistic High-Resolution Image Blending. *arXiv*.

- Hussain, K., Salleh, M. N., Cheng, S., & Naseem, R. (2017). Common Benchmark Functions for Metaheuristic Evaluation: A Review. *INTERNATIONAL JOURNAL ON INFORMATICS VISUALIZATION*, 218-223.
- Hyde, D. (2008). agueness, logic and ontology. *shgate new critical thinking in philosophy*.
- I., C. M., Amaral, I., Domingues, I., Cardoso, A., M., J. C., & J., S. C. (2012). INreast: Toward a full-field Digital Mammographic database. Faculdade de Medicina, Alameda Prof. Hernani. Monteiro, Universidade do Porto, doi:10.1016/j.acra.
- Ilya, T., Sylvain, G., Olivier, B., Carl-Johann, S.-G., & Bernhard, S. (2017). AdaGAN: Boosting Generative Models. *arXiv:1701.02386*.
- Ismoilov, N., & Jang, S.-B. (2018). A Comparison of Regularization Techniques in Deep Neural Networks. *Symmetry*, DOI: 10.3390/sym10110648., 10(11), 648.
- Isola, P., Zhu, J.-Y., Zhou, T., & Efros, A. A. (2016). Image-to-Image Translation with Conditional Adversarial Networks. *arXiv:1611.07004v1*.
- Isola, P., Zhu, J.-Y., Zhou, T., & Efros, A. A. (2017). Image-to-Image Translation with Conditional Adversarial Networks. *2017 IEEE Conference on Computer Vision and Pattern Recognition (CVPR)*, 5967-5976.
- Ivanova, T. I. (2008). A metric and approach for fuzzy ontology evaluation. in *Proceedings of International Scientific Conference Computer Science, 17th*, 822-827.
- J.A. Blake, M. D. (2012). Gene Ontology Annotations and Resources. *Nucleic Acids Research*, 41(D1), D530–535.
- Jaiswal, A., Gianchandani, N., Singh, D., Kumar, V., & Kaur, M. (2020). Classification of the COVID-19 infected patients using DenseNet201 based deep transfer learning. *Journal of Biomolecular Structure and Dynamics*, 1-8.
- Jamil, M., & Yang, X.-S. (2013). A literature survey of benchmark functions for. *Int. Journal of Mathematical Modelling and Numerical Optimisation*, 4(2), 150–194.
- Jang, Y., Kim, G., & Song, Y. (2018). Video Prediction with Appearance and Motion Conditions. *Proceedings of the 35 th International Conference on Machine*.
- Jayasena, K. P., Li, L., Abd Elaziz, M., & Xiong, S. (2018). Multi-objective Energy Efficient Resource Allocation Using Virus Colony Search (VCS) Algorithm. K. P. N. Jayasena, L. Li, M. Abd Elaziz and S. Xiong, "Multi-objective Energy Efficient Resource Allocation Using Virus Colony Search (VCS) Algorithm," *2018 IEEE 20th International Conference on High Performance Computing and Communications; IEEE 16th Int*, 766-773.
- Jonathan, H. (2018, June 21). *GAN — Why it is so hard to train Generative Adversarial Networks!* Retrieved March 17, 2020, from Medium: https://medium.com/@jonathan_hui/gan-why-it-is-so-hard-to-train-generative-advisory-networks-819a86b3750b
- Kadanali, A., & Karagoz, G. (2015). An overview of Ebola virus disease. *North Clin Istanbul*, 2(1), 81–86.
- Kashikar, P. (2019, February 26). *Reducing Mode Collapse in GANs using Guided Latent Spaces*. Retrieved March 30, 2020, from Medium: <https://medium.com/intel-student-ambassadors/reducing-mode-collapse-in-gans-using-guided-latent-spaces-36f52a08a668>

- Kauret, D., & Kaur, Y. (2014). Various Image Segmentation Techniques:A Review. *International Journal of Computer Science and Mobile Computing*, 3(5), 809-814.
- Kazemina, S., Baur, C., Kuijper, A., Ginneken, B. v., Navab, N., Albarqouni, S., & Mukhopadhyay, A. (2019). GANs for Medical Image Analysis. *arXiv:1809.06222*.
- Kazuhiro, K., Werner, R. A., Toriumi, F., Javadi, M. S., Pomper, M. G., Solnes, L. B., . . . Rowe, S. P. (2018). Generative Adversarial Networks for the Creation of Realistic Artificial Brain Magnetic Resonance Images. *Tomography*, 4(4), 159–163.
- Khan, A., Shah, J., & Bhat, M. (2020). Coronet: A deep neural network for detection and diagnosis of COVID-19 from chest x-ray images. *Computer Methods and Programs in Biomedicine*. doi:10.1016/j.cmpb.2020.105581.
- Ko, H., Chung, H., Kang, W., Kim, W., Shin, Y., Kang, S., . . . Lee, J. (2020). COVID-19 Pneumonia Diagnosis Using a Simple 2D Deep Learning Framework With a Single Chest CT Image: Model Development and Validation. *Journal of Medical Inter*.
- Korkinof, D., Rijken, T., O'Neill, M., & Yearsley, J. (2018). High-Resolution Mammogram Synthesis using Progressive Generative Adversarial Networks. *arXiv:1807.03401v1*.
- Korkinof, D., Rijken, T., O'Neill, M., Yearsley, J., Harvey, H., & Glocker, B. (2019). High-Resolution Mammogram Synthesis using Progressive Generative Adversarial Networks. *Medical Imaging with Deep Learning (MIDL) Workshops*.
- Krizhevsky, A., Sutskever, I., & Hinton, G. E. (2012). ImageNet Classification with Deep Convolutional Neural Networks. *Advances in Neural Information Processing Systems 25 (NIPS 2012)*.
- Kukačka, J., Golkov, V., Cremers, D., & Cremers, D. (2018). Regularization for Deep Learning: A Taxonomy. *Conference paper at ICLR*.
- Kumar, K., Pal, K., Sudeep, S., & Sudeep, K. S. (2016). Preprocessing for image classification by convolutional neural networks. *2016 IEEE International Conference on Recent Trends in Electronics, Information & Communication Technology (RTEICT)*.
- Kwon, Y.-H., & Park, M.-G. (2019). Predicting Future Frames using Retrospective Cycle GAN. *CVPR*, 11811-11820.
- L, W., & A., W. (2020). COVID-Net: A tailored deep convolutional neural network design for detection of COVID-19 cases from chest radiography images. *arXiv preprint arXiv:200309871*.
- Lalmuanawma, S., Hussain, J., & Chhakchuak, L. (2020). Applications of machine learning and artificial intelligence for Covid-19 (SARS-CoV-2) pandemic: A review. *Chaos, Solitons & Fractals*, 110059.
- Lars, M., Andreas, G., & Sebastian, N. (2018). Which Training Methods for GANs do actually Converge? *arXiv:1801.04406*.
- Lassiter, D. (2011). Vagueness as Probabilistic Linguistic Knowledge. *Vagueness in Communication*, Springer, 1-21.
- Ledig, C., Theis, L., Huszar, F., Caballero, J., Cunningham, A., Acosta, A., . . . Shi, W. (2017). Photo-Realistic Single Image Super-Resolution Using a Generative Adversarial Network. *CVPR*.

- Li, H., Zheng, Y., Wu, X., & Cai, Q. (2019). 3D Model Generation and Reconstruction Using Conditional Generative Adversarial Network. *International Journal of Computational Intelligence Systems*, 12(2), 697 - 705.
- Li, J., Liang, X., Wei, Y., Xu, T., Feng, J., & Yan, S. (2017). Perceptual Generative Adversarial Networks for Small Object Detection. *arXiv:1706.05274*.
- Li, S., Chen, H., Wang, M., Heidari, A. A., & Mirjalili, S. (2020). Slime mould algorithm: A new method for stochastic optimization. *Future Generation Computer Systems*, 111, 300-323.
- Liu, S., Sun, Y., Zhu, D., Bao, R., Wang, W., Shu, X., & Yan, S. (2017). Face Aging with Contextual Generative Adversarial Nets. *ACM - MM '17*.
- Lv, B., Liu, Y., Zhang, S., Zeng, H., & Zhu, G. (2018). Super Resolution with Generative Adversarial Networks. *Association for the Advancement of Artificial*.
- Maayan, F.-A., Idit, D., Eyal, K., Michal, A., Jacob, G., & Hayit, G. (2018). GAN-based Synthetic Medical Image Augmentation for increased CNN Performance in Liver Lesion Classification. *arXiv*.
- Mao, X., Li, Q., Xie, H., Lau, R. Y., Wang, Z., & Smolley, S. P. (2017). Least Squares Generative Adversarial Networks. *arXiv:1611.04076 [cs.CV]*.
- Marchesi, M. (2017). Megapixel Size Image Creation using Generative Adversarial Networks. *ArXiv, abs/1706.00082*.
- Marrow, P. (2000). Nature-Inspired Computing Technology and Applications. *BT Technology Journal* 18. <https://doi.org/10.1023/A:1026746406754>, 13–23.
- Martínez-Álvarez, F., G., A.-C., Torres, J. F., Gutiérrez-Avilés, D., Melgar-García, L., Pérez-Chacón, R., . . . Troncoso, A. (2020). Coronavirus Optimization Algorithm: A Bioinspired Metaheuristic Based on the COVID-19 Propagation Model. *Big Data*, doi: 10.1089/big.2020.0051. *Epub*, 8(4), 308-322.
- Mathebula, L., Ndwandwe, D. E., Pienaar, E., & Wiysonge, C. S. (2019). Effects of vaccines in protecting against Ebola virus disease: protocol for a systematic review. *BMJ Open*, e029617., 9(7).
- Mattila, J. K. (2012). Zadeh algebra as the basis of Łukasiewicz logics. *Conference: Fuzzy Information Processing Society (NAFIPS), 2012 Annual Meeting of the North American*.
- Mehrabian, A. R., & Lucas, C. (2006). A novel numerical optimization algorithm inspired from weed colonization. *ECOLOGICAL INFORMATICS* 1, 355 – 366.
- Mescheder, L., Geiger, A., & Nowozin, S. (n.d.). *Convergence and Stability of GAN training*. Retrieved March 31, 2020, from Autonomous Vision: <https://avg.is.tuebingen.mpg.de/projects/convergence-and-stability-of-gan-training>
- Mobula, L. M., MacDermott, N., Hoggart, C., Brantly, K., Plyler, W., Brown, J., . . . Fankhauser, J. (2018). Clinical Manifestations and Modes of Death among Patients with Ebola Virus Disease, Monrovia, Liberia, 2014. *Am J Trop Med Hyg.*, 98 (4), 1186–1193.
- Moghadas, S. M., Vilches, T. N., Zhang, K., Wells, C. R., Shoukat, A., Singer, B. H., . . . Galvani, A. P. (2020). The impact of vaccination on COVID-19 outbreaks in the United States. *medRxiv, Preprint, doi: 10.1101/2020.11.27.20240051*.

- Molga, M., & Smutnicki, C. (2020). Test functions for optimization needs. <https://www.robertmarks.org/Classes/ENGR5358/Papers/functions.pdf>.
- Muhic, I. (2013). Fuzzy Analysis of Breast Cancer Disease using Fuzzy c-means and Pattern Recognition. *SOUTHEAST EUROPE JOURNAL OF SOFT COMPUTING*, 50-55.
- Munien, C., & Ezugwu, A. E. (2021). Metaheuristic algorithms for one-dimensional bin-packing problems: A survey of recent advances and applications. *Journal of Intelligent Systems*, 30(1), 636-663.
- Munien, C., Mahabeer, S., Dzitiro, E., Singh, S., Zungu, S., & Ezugwu, A. E. (2020). Metaheuristic Approaches for One-Dimensional Bin Packing Problem: A Comparative Performance Study. *IEEE Access*, 8, 227438-227465.
- N., O. O., A., O. A., B., J. S., & Adewuyi, S. A. (2017). Patient symptoms elicitation process for breast cancer medical expert systems: A semanti web and natural language parsing approach. *Future Computing and Informatics Journal - Elsevier.*, 3(1), 72-81.
- Name, W. (2020). Synthesizing lesions using contextual GANs improves breast cancer classification on mammograms. *Proceedings of Machine Learning Research (MIDL) 2020 Conference*.
- National Kidney Foundation. (2017, April 21). *Tests to Measure Kidney Function, Damage and Detect Abnormalities*. Retrieved January 20, 2021, from National Kidney Foundation: <https://www.kidney.org/atoz/content/kidneytests>
- Neff, T. (2018). *Data Augmentation in Deep Learning using Generative Adversarial Networks*. Graz, Austria: Thesis: Graz University of Technology.
- Nguyen, A., Yosinski, J., Bengio, Y., Dosovitskiy, A., & Clune, J. (2016). Plug & Play Generative Networks: Conditional Iterative Generation of Images in Latent Space. *arXiv:1612.00005v1 [cs.CV]*.
- O.N.Oyelade, & Kana, A. F. (2019). OWL Formalization of Cases: An Improved Case-Based Reasoning in Diagnosing and Treatment of Breast Cancer. *International Journal of Information Security, Privacy and Digital Forensics (IJIS)*, 3(2), 92-105.
- Odena, A., Olah, C., & Shlens, J. (2017). Conditional Image Synthesis with Auxiliary Classifier GANs. *arXiv:1610.09585v4 [stat.ML]*.
- Okyere, E., Ankamah, J. D.-G., Hunkpe, A. K., & Mensah, D. (2020). Deterministic Epidemic Models for Ebola Infection with Time-Dependent Controls. *Discrete Dynamics of Nature and Society*.
- Olaide Oyelade, N., & Absalom Ezugwu, E. (2020). A deep learning model using data augmentation for detection of architectural distortion in whole and patches of images. *Biomedical Signal Processing and Control*, 65(2021), 1-17.
- Oliveira, P. M., Pires, E. S., Boaventura-Cunha, J., & Martins, T. (2020). Review of nature and biologically inspired metaheuristics for greenhouse environment control. *Transactions of the Institute of Measurement and Control*.doi:10.1177/0142331220909010, 42(12), 2338-2358.
- Osterholm, M. T., Moore, K. A., Kelley, N. S., Brosseau, L. M., Wong, G., Murphy, F. A., . . . E., J. (2015). Transmission of Ebola Viruses: What We Know and What We Do Not Know. *mBio*, 6(2), 137-15.

- Oyelade, O. N., & Ezugwu, A. E. (2020). A case-based reasoning framework for early detection and diagnosis of novel coronavirus. *Informatics in Medicine Unlocked*, 1-41.
- Oyelade, O. N., & Ezugwu, A. E. (2020). A case-based reasoning framework for early detection and diagnosis of novel coronavirus. *Informatics Medicine Unlock*. doi: 10.1016/j.imu.2020.100395, 20(100395).
- Oyelade, O., Obiniyi, A., Junaidu, S., & Adewuyi, S. (2018). ST-ONCODIAG: A semantic rule-base approach to diagnosing breast cancer base on Wisconsin datasets. *Informatics in Medicine Unlocked*, 117-125.
- Ozturk, T., Talo, M., Yildirim, E., Baloglu, U., Yildirim, O., & Acharya, U. (2020). Automated detection of COVID19 cases using deep neural networks with X-ray images. *Computers in Biology and Medicine*, 20(103792).
- Pan, J., Stamou, G., Stoilos, G., Thomas, E., & Taylor, S. (2008). Scalable querying service over fuzzy ontologies. *Proceedings of the 17th International World Wide Web Conference (WWW 2008)*, 575–584.
- Pana, J., Canton-Ferrerb, C., McGuinnessc, K., O’Connorc, N. E., Torresd, J., Sayrola, E., & XavierGiro-i-Nieto. (2017). SalGAN: visual saliency prediction with adversarial networks. *arXiv*.
- Pana, J., Canton-Ferrerb, C., McGuinnessc, K., O’Connorc, N. E., Torresd, J., Sayrola, E., & XavierGiro-i-Nieto. (2018). SalGAN: visual saliency prediction with adversarial networks. *Computer Vision and Image Understanding*, 1-9.
- Panwar, H., Gupta, P., Siddiqui, M., Morales-Menendez, R., & Singh, V. (2020). Application of deep learning for fast detection of COVID-19 in X-Rays using nCOVnet. *Chaos, Solitons, and Fractals*, DOI: 10.1016/j.chaos.2020.109944, 138(109944).
- Parry, D. (2004). A fuzzy ontology for medical document retrieval. *The Australasian Workshop on DataMining and Web Intelligence (DMWI2004)*, Dunedin, 1-6.
- Parry, D. T. (2005). Fuzzy ontology and intelligent systems for discovery of useful medical information. *A Doctoral Thesis Submitted to Auckland University of Technology*, 1-294.
- Potluri, R., Kumar, A., Maheshwari, V., Smith, C., Mathieu, V. O., Luhn, K., . . . Bhandari, H. (2020). Impact of prophylactic vaccination strategies on Ebola virus transmission: A modeling analysis. *Plos One*, <https://doi.org/10.1371/journal.pone.0230406>.
- PR., S., N., L., & E.Z., P. (2020). An Improved GAN Semantic Image Inpainting. *Advanced Concepts for Intelligent Vision Systems. ACIVS 2020. Lecture Notes in Computer Science*, 12002.
- Quach, K. (n.d.). *An AI system has just created the most realistic looking photos ever*. Retrieved March 16, 2020, from The Register: https://www.theregister.co.uk/2018/12/14/ai_created_photos/
- R., W. L., M., B. A., L., W., Byth, K., Burgemeister, F., Salisbury, E. L., . . . Balleine, R. L. (2005). Histopathologic indicators of breast cancer biology: insights from population mammographic screening. *Br Journal of Cancer*, 92(28), 1366–1371.
- Rachah, A., & Torres, D. F. (2015). Mathematical Modelling, Simulation, and Optimal Control of the 2014 Ebola Outbreak in West Africa. *Discrete Dynamics in Nature and Society*.
- Radhakrishnan, P. (2017, December 3). *GAN for Photo Editing*. Retrieved March 16, 2020, from BuzzRobot: <https://buzzrobot.com/photoshop-2-0-gan-for-photo-editing-3ba4eddcddd>

- Radpour, N. D., & Bheda, V. (2018). Conditional Generative Adversarial Networks for Emoji Synthesis with Word Embedding Manipulation. *arxiv*.
- Ramadan, S. Z. (2020). Methods Used in Computer-Aided Diagnosis for Breast Cancer Detection Using Mammograms: A Review. *Journal of Healthcare Engineering*, 1-21.
- Ramos-Soto, A., & Pereira-Fariña, M. (2017). On modeling vagueness and uncertainty in data-to-text systems through fuzzy sets. *Information Sciences*, 1-32.
- Rewar, S., & Mirdha, D. (2014). Transmission of Ebola Virus Disease: An Overview. *Annals of Global Health*, 80(6), 444-451.
- S., O., & K., M. (2019). Comparing data augmentation strategies for deep image classification. *IMVIP 2019: Irish Machine Vision & Image Processing, Technological University Dublin, Dublin, Ireland*.
- S.H., Y., H., G., T.L., C., S.K., Y., C., C. D., J., H., . . . H., L. (2020). Deep Learning-Based Decision-Tree Classifier for COVID-19 Diagnosis From Chest X-ray Imaging. *Front. Med.* 7:427. doi: 10.3389/fmed.2020.00427.
- Salcedo-Sanz, S., Del Ser, J., Landa-Torres, I., Gil-López, S., & Portilla-Figueras, J. A. (2014). The Coral Reefs Optimization Algorithm: A Novel Metaheuristic for Efficiently Solving Optimization Problems. *Scientific World Journal*, 1-15.
- Salimans, T., Goodfellow, I., Zaremba, W., Cheung, V., Radford, A., & Chen, X. (2016). Improved Techniques for Training GANs. *arXiv:1606.03498*.
- Samani, Z. R., & Shamsfard, M. (2017). The State of the Art in Developing Fuzzy Ontologies: A Survey . *Faculty of Computer Science and Engineering, Shahid Beheshti University*, 1-46.
- Sau, A. (2017). A Simulation Study on Hypothetical Ebola Virus Transmission in India Using Spatiotemporal Epidemiological Modeler (STEM): A Way towards Precision Public Health. *J Environ Public Health*.
- Schwartzman, A., Kagan, M., Mackey, L., Nachman, B., & DeOliveira, L. (2016). Image Processing, Computer Vision, and DeepLearning: new approaches to the analysis and physics interpretation of LHC events. *Journal of Physics: Conference Series*762.
- Sen, S., Patra, K., & Mondal, S. K. (2016). Fuzzy risk analysis in familial breast cancer using a similarity measure of interval-valued fuzzy numbers. *Pacific Science Review A: Natural Science and Engineering*, 18(2016), 203-221.
- Shaham, T. R., Dekel, T., & Michaeli, T. (2019). SinGAN: Learning a Generative Model from a Single Natural Image. *arXiv:1905.01164v2 [cs.CV]*.
- Shahinian, V. B., Bahl, A., Niepel, D., & Lorusso, V. (2017). Considering renal risk while managing cancer. *Cancer Management Res*, 9, 167-178.
- Shaker, E.-S., Mohammed, E., & Riad, A. (2015). A fuzzy-ontology oriented case-based reasoning framework for semantic diabetes diagnosis. *Artificial Intelligence in Medicine*, 1-30.
- Sharma, N. (2019, July 19). *My MangaGAN: Building My First Generative Adversarial Network*. Retrieved March 16, 2020, from Heart Beat: <https://heartbeat.fritz.ai/my-mangagan-building-my-first-generative-adversarial-network-2ec1920257e3>

- Sharma, P. (2020, Jan 13). *What are Generative Models and GANs? The Magic of Computer Vision*. Retrieved Feb 12, 2020, from Medium: <https://medium.com/analytics-vidhya/what-are-generative-models-and-gans-the-magic-of-computer-vision-86b813c4fac9>
- Shearer, R., Motik, B., & Horrocks, I. (2008). Hermit: A Highly-Efficient OWL Reasoner. *Proceedings of the 5th International Workshop on OWL: Experiences and Directions*.
- Shibly, K. H., KumarDey, S., Islam, M. T.-U., & Rahman, M. M. (n.d.). COVID faster R–CNN: A novel framework to Diagnose Novel Coronavirus Disease (COVID-19) in X-Ray images. *Informatics in Medicine Unlocked*, 20(100405).
- Shorten, C., & Khoshgoftaar, T. (2019). A survey on Image Data Augmentation for Deep Learning. *J Big Data*, <https://doi.org/10.1186/s40537-019-0197-0>, 6(60).
- Shorten, C., & Khoshgoftaar, T. M. (2020). A survey on Image Data Augmentation for Deep Learning. *Journal of Big Data*, 6(60).
- Siarohin, A., ere, S. L., Sangineto, E., & Sebe, N. (2015). Appearance and Pose-Conditioned Human Image Generation using Deformable GANs. *JOURNAL OF LATEX CLASS FILES*, 14(8), 1-16.
- Siarohin, A., Sangineto, E., ere, S. L., & Sebe, N. (2018). Deformable GANs for Pose-based Human Image Generation. *CVPR*, 3408-3416.
- Siddique, N. &. (2015). Nature Inspired Computing: An Overview and Some Future Directions. *Cognitive computation*, <https://doi.org/10.1007/s12559-015-9370-8>, 7(6), 706–714.
- Silva, V. T., Costalonga, E. C., Coelho, F. O., Caires, R. A., & Burdmann, a. E. (2018). Assessment of Kidney Function in Patients With Cancer. *Advances in Chronic Kidney Disease*, 25(1), 49-56.
- Simon, D. (2008). Biogeography-Based Optimization. *IEEE Transactions on Evolutionary Computation*, doi: 10.1109/TEVC.2008.919004, 12(6), 702-713.
- Simonyan, K., & Zisserman, A. (2014). Very Deep Convolutional Networks for Large-Scale Image Recognition. *arXiv:1409.1556 [cs.CV]*.
- Singh, D., Kumar, V., & Kaur, M. (2020). Classification of COVID-19 patients from chest CT images using multi-objective differential evolution–based convolutional neural networks. *European Journal of Clinical Microbiology & Infectious Diseases*, 1-11.
- Singh, D., Kumar, V., Yadav, V., & Kaur, M. (2020). Deep Neural Network-Based Screening Model for COVID-19-Infected Patients Using Chest X-Ray Images. *International Journal of Pattern Recognition and Artificial Intelligence*.
- Singh, N. K., & Raza, K. (2021). Medical Image Generation Using Generative Adversarial Networks: A Review. *In book: Health Informatics: A Computational Perspective in Healthcare*.
- Sirin, E., Parsia, B., Grau, B. C., Kalyanpur, A., & Katz, Y. (2007). Pellet: A practical OWL-DL reasoner. *Journal of Web Semantics*, 5(2), 51-53.
- Sivanandam, S., & Deepa, S. (2008). Introduction to genetic algorithms. *Springer, Berlin*.
- Skfuzzy2.0. (n.d.). *skfuzzy 0.2 docs*. Retrieved January 19, 2021, from Skfuzzy: <https://pythonhosted.org/scikit-fuzzy/>

- SMITH, N. J. (2006). Fuzzy Logic and Higher-Order Vagueness. *Department of Philosophy, Main Quadrangle, The University of Sydney*, 1-19.
- Stewart, M. (2019, July 9). *Simple Guide to Hyperparameter Tuning in Neural Networks*. Retrieved March 31, 2020, from Towards Data Science: <https://towardsdatascience.com/simple-guide-to-hyperparameter-tuning-in-neural-networks-3fe03dad8594>
- Stump-Sutliff, K., Cunningham, L., & Gersten, T. (n.d.). *Lab Tests for Cancer*. Retrieved January 20, 2021, from University of Rochester Medical Center: Health Encyclopedia: <https://www.urmc.rochester.edu/encyclopedia/content.aspx?contenttypeid=85&contentid=p07248>
- Surma, G. (2019, February 11). *Image Generator - Drawing Cartoons with Generative Adversarial Networks*. Retrieved March 16, 2020, from Towards Datascience: <https://towardsdatascience.com/image-generator-drawing-cartoons-with-generative-adversarial-networks-45e814ca9b6b>
- SwatiSwayamsiddha. (2020). Chapter 4 - Bio-inspired algorithms: principles, implementation, and applications to wireless communication. *Nature-Inspired Computation and Swarm Intelligence, Algorithms, Theory and Applications*, 49-63.
- Tanade, C., Pate, N., Paljug, E., Hoffman, R. A., & Wang, M. D. (2019). Hybrid Modeling of Ebola Propagation. *Proc IEEE Int Symp Bioinformatics Bioeng.*, 204–210.
- Tartaglione, E., Barbano, C. A., Berzovini, C., Calandri, M., & Grangetto, M. (2020). Unveiling COVID-19 from Chest X-ray with deep learning: a hurdles race with small data. *arXiv:2004.05405v1*.
- Team, O. (2020, July 22). *Liver Function Test (LFT)*. Retrieved January 20, 2021, from OncoLink: <https://www.oncolink.org/cancer-treatment/procedures-diagnostic-tests/blood-tests-tumor-diagnostic-tests/liver-function-test-lft>
- The Agent. (2020). *Ebola Virus*. Retrieved February 19, 2021, from Department of Molecular Virology and Microbiology, Baylor College of Medicine: <https://www.bcm.edu/departments/molecular-virology-and-microbiology/emerging-infections-and-biodefense/specific-agents/ebola-virus>
- Thorson, A., Deen, G. F., Bernstein, K. T., Liu, W. J., Yamba, F., Habib, N., . . . Singaravelu, S. (2021). Persistence of Ebola virus in semen among Ebola virus disease survivors in Sierra Leone: A cohort study of frequency, duration, and risk factors. *PLOS*, <https://doi.org/10.1371/journal.pmed.1003273>.
- Tian, Y., Peng, X., Zhao, L., Zhang, S., & Metaxas, D. N. (2018). CR-GAN: Learning Complete Representations for Multi-view Generation. *Proceedings of the Twenty-Seventh International Joint Conference on Artificial Intelligence (IJCAI-18)*, 942-948.
- Toll, C. D. (n.d.). *Coronavirus Death Toll*. Retrieved October 21, 2020, from WorldOMeter: <https://www.worldometers.info/coronavirus/coronavirus-death-toll/>
- Tolstikhin, I., Gelly, S., Bousquet, O., Simon-Gabriel, C.-J., & Schölkopf, B. (2017). AdaGAN: Boosting Generative Models. *arXiv:1701.02386 [stat.ML]*.
- Tsarkov, D., & Horrocks, I. (2006). FaCT++ Description Logic Reasoner: System Description. *Automated Reasoning. IJCAR 2006. Lecture Notes in Computer Science*, 4130.

- UNCHC. (2017, August 2). *Ebola detected in semen of survivors two years after infection: Researchers suggest updating WHO guidelines and exploring aging*. Retrieved February 24, 2021, from University of North Carolina Health Care: ScienceDaily: www.sciencedaily.com/releases/2017/08/170802152532.htm
- Vrandečić, V. (2010). *Ontology Evaluation. A Doctoral dissertation submitted to des Karlsruher Instituts für Technologie (KIT)*, 1-235.
- Wang, G.-G., Deb, S., & Coelho, L. (2018). Earthworm optimisation algorithm: A bio-inspired metaheuristic algorithm for global optimisation problems. *International Journal of Bio-Inspired Computation*, 12(1).
- Wang, M., Chen, H., Yang, B., Zhao, X., Hue, L., Cai, Z., . . . Tong, C. (2017). Toward an optimal kernel extreme learning machine using a chaotic moth-flame optimization strategy with applications in medical diagnoses. *Neurocomputing*, 267(6), 69-84.
- Wang, X., & Gupta, A. (2016). Generative Image Modeling using Style and Structure Adversarial Networks. *arXiv:1603.05631v2 [cs.CV]*.
- Wang, X., Peng, Y., Lu, L., Lu, Z., Bagheri, M., & Summers, R. (2017). ChestX-ray8: Hospital-scale Chest X-ray Database and Benchmarks on Weakly-Supervised Classification and Localization of Common Thorax Diseases. *IEEE CVPR*.
- Wang, X., Yu, K., Wu, S., Gu, J., Liu, Y., Dong, C., . . . Tang, X. (2018). ESRGAN: Enhanced Super-Resolution Generative Adversarial Networks. *ECCV 2018 workshop. Won Region 3 in the PIRM2018-SR Challenge. Won Region 3*.
- WANG, Z., SHE, Q., & WARD, T. E. (2020). Generative Adversarial Networks in Computer Vision: A Survey and Taxonomy. *arXiv*.
- WHO. (2016, January 16). *Interim advice on the sexual transmission of the Ebola virus disease*. Retrieved February 24, 2021, from WHO: Sexual and reproductive health : <https://www.who.int/reproductivehealth/topics/rtis/ebola-virus-semen/en/>
- WHO. (2020, February 10). *Ebola virus disease*. Retrieved February 19, 2021, from World Health Organization: <https://www.who.int/news-room/fact-sheets/detail/ebola-virus-disease>
- Wu, E., Wu, K., Cox, D., & Lotter, W. (2018). Conditional Infilling GANs for Data Augmentation in Mammogram Classification. *MICCAI 2018, Breast Image Analysis Workshop*.
- Wu, H., Zheng, S., Zhang, J., & Huang, K. (2019). GP-GAN: Towards Realistic High-Resolution Image Blending. *ACMMM 2019*.
- Wynants, L., Van Calster, B., Bonten, M. M., Collins, G. S., Debray, T. P., De Vos, M., & Schuit, E. (2020). Prediction models for diagnosis and prognosis of covid-19 infection: systematic review and critical appraisal. *BMJ*, 369.
- Xi, P., C., S., & R.A., G. (2018). Abnormality Detection in Mammography using Deep Convolutional Neural Networks. . *2018 IEEE International Symposium on Medical Measurements and Applications (MeMeA)*, 1-6.
- Xin, Y., Ekta, W., & Paul, B. (2019). Generative Adversarial Network in Medical Imaging: A Review. *arXiv:1809.07294*, 24.

- XS, Y. (2013). Metaheuristic Optimization: Nature-Inspired Algorithms and Applications. *Studies in Computational Intelligence*, https://doi.org/10.1007/978-3-642-29694-9_16, 427.
- Yang, X.-S. (2010). Firefly Algorithm, Stochastic Test Functions and Design Optimisation. *arXiv:1003.1409v1*, 1-12.
- Yet, N. N. (2019). Chapter 5 - Modeling Ebola Virus Infection. *Modeling and Control of Infectious Diseases in the Host, With MATLAB and R*, <https://doi.org/10.1016/B978-0-12-813052-0.00016-6>, 85-103.
- Yi, X., Walia, E., & Babyn, P. S. (2019). Generative Adversarial Network in Medical Imaging: A Review. *Medical Image Analysis* 58:101552.
- Zadeh, H. G., Pakdelazar, O., Haddadnia, J., Rezai-Rad, G., & Mohammad-Zadeh, M. (2012). Diagnosing Breast Cancer with the Aid of Fuzzy Logic Based on Data Mining of a Genetic Algorithm in Infrared Images. *Middle East Journal of Cancer*, 3(4), 119-129.
- Zhan, F., & Zhu, H. (2019). Spatial Fusion GAN for Image Synthesis. *CVPR*.
- Zhang, H., Sun, Y., Liu, L., & Xu, X. (2020). CascadeGAN: A category-supervised cascading generative adversarial network for clothes translation from the human body to tiled images. *Neuro Computing*, 382(21), 148-161.
- Zhang, H., Xu, T., Li, H., Zhang, S., Huang, X., Wang, X., & Metaxas, D. (2016). StackGAN: Text to Photo-realistic Image Synthesis with Stacked Generative Adversarial Networks. *arXiv:1612.03242v1 [cs.CV]*.
- Zhang, Q., Wang, H., Lu, H., Won, D., & Yoon, S. W. (2018). Medical Image Synthesis with Generative Adversarial Networks for Tissue Recognition. *2018 IEEE International Conference on Healthcare Informatics (ICHI)*, 10.1109/ICHI.2018.00030.
- Zhang, S., Zhou, Y., & Luo, Q. A. (2019). A complex-valued encoding satin bowerbird optimization algorithm for global optimization. *Evolving Systems*.
- Zhao L, W. J. (2020). GANsDTA: Predicting Drug-Target Binding Affinity Using GANs. *Front. Genet.* 10:1243. doi: 10.3389/fgene.2019.01243.
- Zheng, Q., Yang, M., Tian, X., Jiang, N., & Wang, D. (2020). A Full Stage Data Augmentation Method in Deep Convolutional Neural Network for Natural Image Classification. *Cognitive Modeling of Multimodal Data Intensive Systems for Applications in Nature and Society (COMDICS)*, 11.
- Zhu, J., Xie, J.-C., & Fang, Y. (2018). Learning Adversarial 3 D Model Generation with 2 D Image Enhancer. *In Conference Proceedings*.